Vesicular glutamate transporters possess multifunctional properties due to large pores

Inaugural-Dissertation

Zur Erlangung des Doktorgrades
der Mathematisch-Naturwissenschaftlichen Fakultät
der Heinrich-Heine-Universität Düsseldorf

vorgelegt von

Bettina Kolen geb. Mertens

aus Heinsberg

Jülich, April 2021

Vesikuläre Glutamat Transporter besitzen multifunktionale Eigenschaften aufgrund großer Poren

Inaugural-Dissertation

Zur Erlangung des Doktorgrades
der Mathematisch-Naturwissenschaftlichen Fakultät
der Heinrich-Heine-Universität Düsseldorf

vorgelegt von

Bettina Kolen geb. Mertens

aus Heinsberg

Jülich, April 2021

Aus dem Institut für Biologische Informationsprozesse (IBI-1)

Molekular- und Zellphysiologie

des Forschungszentrums Jülich

Gedruckt mit der Genehmigung der
Mathematisch-Naturwissenschaftlichen Fakultät der
Heinrich-Heine-Universität Düsseldorf

Berichterstatter:

1. Prof. Dr. Christoph Fahlke
2. Prof. Dr. Christine Rose

Tag der mündlichen Prüfung:

03. November 2021

Für Op(p)a, in ewiger Liebe ♥

I Table of Contents

II Abbreviations

Abbreviations	Description
AA	amino acid
AO	acridine orange
asp^-	aspartate
BNPI	brain-specific Na^+-dependent P_i cotransporter 1
CFTR	Cystic Fibrosis Transmembrane Conductance Regulator
CI	confidence interval
Cl^-	chloride
CNS	central nervous system
DgoT	D-galactonate transporter
DMEM	Dulbecco‘s Modified Eagle Medium
DNPI	differentiation-associated Na^+-dependent inorganic phosphate cotransporter
EAAT	excitatory amino acid transporter
EGTA	ethylene glycol-bis(-aminoethyl ether)-N,N,N',N'-tetraacetic acid
EPSP	excitatory postsynaptic potential
E_{rev}	reversal potential
FBS	fetal bovine serum
GABA	y-aminobutyric acid
GFP	green fluorescent protein
Gln^-	glutamine
GlpT	glycerol-3-phosphate transporter
$gluc^-$	gluconate
$glut^-$	glutamate
HA-tag	hemagglutinin-tag
HCO_3^-	bicarbonate
HEK293T	human embryonic kidney cells
HEPES	(4-(2-hydroxyethyl)-1-piperazineethanesulfonic acid)
IPSP	inhibitory postsynaptic potential
$iset^-$	isethionate
IV	current-voltage
LacY	lactose permease
MES	2-(N-Morpholino)ethanesulfonic acid
MFS	mayor facilitator family
MSA^-	Methanesulfonic acid
NHE	Na^+/H^+-exchanger
NPT	sodium-dependent inorganic phosphate transporters
PAG	Phosphate-activated glutaminase
PBS	phosphate buffered saline
P_i	inorganic phosphate
SD	standard deviation
SLC	solute carriers

Abbreviations	Description
SV	synaptic vesicle
TM	transmembrane
TMA	tetramethylammonium
VAChT	vesicular acetylcholine transporter
V-ATPase	vacuolar H^+ ATPase
VEAT	vesicular excitatory amino acid transporter
VGAT	vesicular GABA transporter
VGLUT	vesicular glutamate transporter
$VGLUT_{PM}$	plasma membrane inserted VGLUT
VMAT	vesicular monoamine transporter
VNUT	vesicular nucleotide transporter
VPAT	vesicular polyamine transporter
VRAC	volume regulated anion channel
WT	wild type
$\Delta\mu H^+$	electrochemical proton gradient
ΔpH	H^+ gradient
Δψ	membrane potential
[ ]	concentration

III List of figures

IV Supplementental Figures

V List of tables

1 Abstract

Vesicular glutamate transporters (VGLUTs) mediate the uptake of the excitatory neurotransmitter glutamate into synaptic vesicles and are thus crucially involved in the strength of excitatory synaptic transmission. They are not only of high physiological importance, but also functionally unique: VGLUTs are thought to be secondary active glutamate transporters, but can also function as anion channels or as Na^+-coupled phosphate transporters. Neither the mechanism nor the function are completely understood to date.

To characterize VGLUTs using electrophysiological patch clamp techniques, we used a VGLUT1 with mutations in targeting signals in the amino- and carboxy-terminal regions and heterologously expressed $VGLUT1_{PM}$ as a GFP fusion protein in the plasma membrane of HEK293T cells. We examined the function of the anion channel using a combination of whole cell patch clamp, noise analysis and fluorescence intensity measurements. We found that $VGLUT1_{PM}$ forms a strongly inward rectifying pH- and Cl^--dependent chloride channel with a lyotropic anion selectivity and a single channel amplitude of ~24 fA with Cl^- as permeant anion. We were also able to measure glutamate currents. Surprisingly, several large anions such as gluconate or aspartate were also permeable to $VGLUT1_{PM}$. In experiments with external chloride, gluconate and aspartate differ from glutamate in much more negative reversal potentials. Thus, VGLUT1 functions as a highly selective glutamate transporter or channel with a large pore within synaptic vesicles. By blocking the Cl^- channel with luminal or cytoplasmic glutamate, we showed that the binding of glutamate is stronger compared to Cl^- and that both ions share at least part, if not the same, permeation pathway.

A point mutation, H120A, which is thought to affect the transport of glutamate, showed altered channel gating in our measurements with markedly increased macroscopic current amplitudes due to a twofold higher single channel amplitude. In addition, we observed changes in anion selectivity and, most importantly, reduced glutamate permeability.

Our results demonstrate that VGLUT1 can function as an anion channel with a large pore that opens within multiple conformational changes and provide new insights into the different transport functions of vesicular glutamate transporters.

2 Zusammenfassung

Vesikuläre Glutamat Transporter (VGLUTs) vermitteln die Aufnahme des exzitatorischen Neurotransmitters Glutamat in synaptische Vesikel und sind damit maßgeblich an der Stärke exzitatorischer synaptischer Transmission beteiligt. Sie sind nicht nur von hoher physiologischer Bedeutung, sondern auch funktionell einzigartig: VGLUTs sollen sekundär aktive Glutamat Transporter sein, können aber auch als Anionenkanäle oder als Na^+-gekoppelte Phosphat-Transporter funktionieren. Weder der Mechanismus, noch die Funktion sind bis heute komplett verstanden.

Um VGLUTs mittels elektrophysiologischer Patch-Clamp-Techniken zu charakterisieren, verwendeten wir einen VGLUT1, der Mutationen in den Targeting-Signalen in den amino- und carboxy-terminalen Regionen trägt. Wir exprimierten $VGLUT1_{PM}$ heterolog als GFP-Fusionsprotein in HEK293T Zellen und untersuchten die Funktion des Anionenkanals mittels einer Kombination aus Ganzzell-Patch-Clamp, Rauschanalyse und Fluoreszenzintensitätsmessungen. Wir fanden heraus, dass $VGLUT1_{PM}$ einen stark einwärts rektifizierenden pH- und Cl^--abhängigen Chloridkanal mit einer lyotropen Anionenselektivität und einer Einzelkanalamplitude von ~24 fA mit Cl^- als permeables Anion formt. Wir konnten zudem Glutamat-Ströme messen. Überraschender Weise waren auch verschiedene große Anionen wie Gluconat oder Aspartat permeabel für $VGLUT1_{PM}$. In Experimenten mit externem Chlorid, haben sich Gluconat und Aspartat durch ein negativeres Umkehrpotential von Glutamat unterschieden. Somit fungiert VGLUT1 im synaptischen Vesikel als hoch selektiver Glutamat Transporter oder Kanal mit einer großen Pore. Durch den Block des Cl^--Kanals durch luminales oder zytoplasmatisches Glutamat konnten wir zeigen, dass die Bindung von Glutamat gegenüber Cl^- stärker ist und beide Ionen zumindest teilweise, wenn nicht sogar den gleichen Permeationsweg teilen.

Eine Punktmutation, H120A, die den Transport von Glutamat beeinflussen soll, zeigte in unseren Messungen ein verändertes Kanal-Gating mit deutlich erhöhten makroskopischen Stromamplituden, die durch eine verdoppelte Einzelkanalamplitude entstehen. Zudem konnten wir Änderungen in der Anionenselektivität und vor allem eine Reduzierung der Glutamat Permeabilität feststellen.

Unsere Ergebnisse demonstrieren, dass VGLUT als Anionenkanal mit einer großen Pore funktionieren kann, der in mehreren Konformationsänderungen öffnet. Damit geben wir neue Einblicke in die verschiedenen Transportfunktionen von vesikulären Glutamat Transportern.

3 Introduction

3.1 Glutamate in neurotransmission

In the central nervous system (CNS) signals are forwarded by a combination of electrical and chemical signal transmission. During synaptic transmission, an electrical signal is converted into a chemical signal. The depolarization of the presynaptic neuron opens voltage-activated Ca^{2+} channels and leads to a Ca^{2+} influx. Ca^{2+} triggers the fusion of neurotransmitter-filled vesicles with the presynaptic membrane and the release of neurotransmitters into the synaptic cleft, where they bind to postsynaptic receptors. Excitatory (glutamate and aspartate) or inhibitory (GABA or Glycine) neurotransmitters can be differentiated. Inhibitory neurotransmitters activate Cl^- selective ion channels. Cl^- influx into the postsynapse initiates an inhibitory postsynaptic potential (IPSP) and thus hyperpolarizes the neuron. However, excitatory neurotransmitters lead to an influx of cations that depolarize the postsynapse in an excitatory postsynaptic potential (EPSP). Besides this ionotropic activity, neurotransmitters can also activate a metabotropic pathway by involving G-protein coupled receptors (Figure 3.1).

Glutamate is the main excitatory neurotransmitter in the human CNS [1] and is involved in various cognitive processes e.g. learning and memory [2–4]. Different glutamate transporters are involved in the glutamatergic signalling pathway. Vesicular glutamate transporters (VGLUTs) transport glutamate into synaptic vesicles (SV) that are released into the synaptic cleft during synaptic transmission and bind to ionotropic (AMPA-, NMDA-, Kainat-receptors) or metabotropic (mGluR1-8) glutamate receptors. The physiological glutamate concentration in the extracellular space is very low [5] and overstimulation of the postsynaptic receptors leads to neurotoxicity [6]. Removal of glutamate from the synaptic cleft is therefore important for the termination of the chemical signal transduction. Excitatory amino acid transporters (EAATs) bind glutamate and transport the neurotransmitter into neighbouring glial cells and neurons and thus act as a buffer system for fast signal termination [7–9].

In glial cells, glutamate is metabolized to glutamine by the glutamine synthetase. Glutamine can be transported to excitatory neurons where the Phosphate-activated glutaminase (PAG) synthesizes glutamate which is then transported into SV by VGLUTs [10].

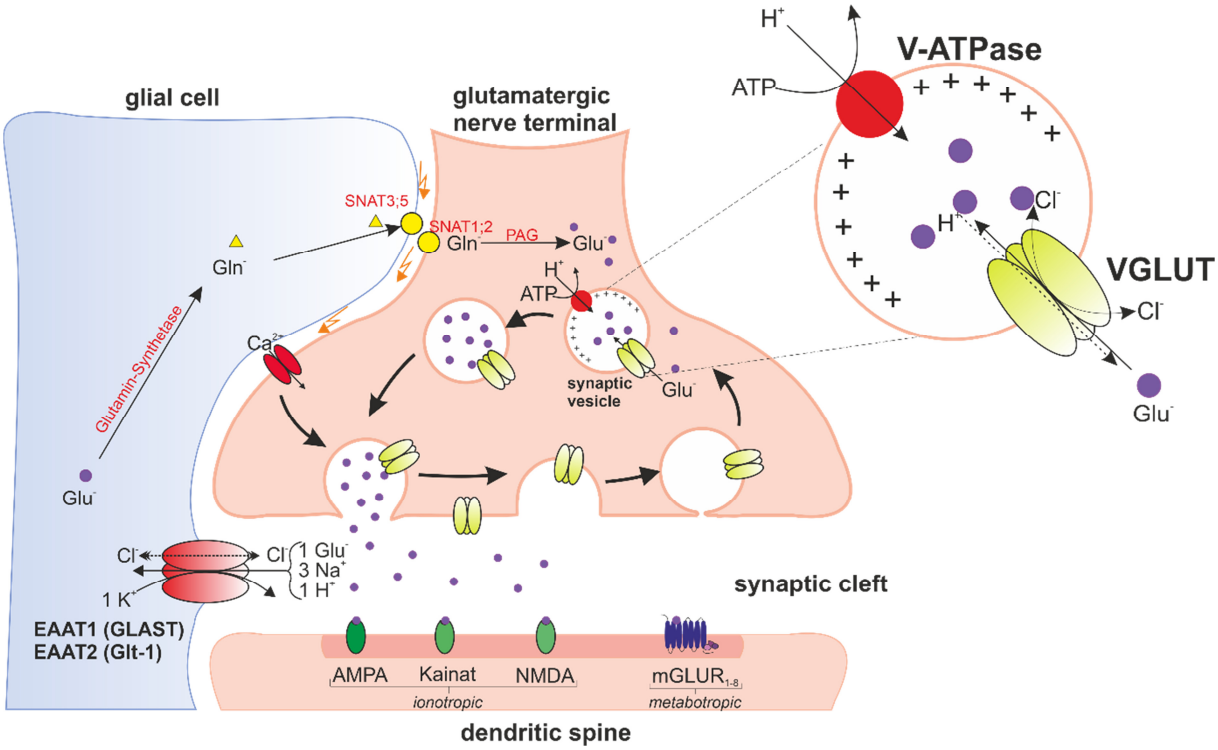

Figure 3.1 Excitatory synaptic transmission at a glutamatergic synapse. *Ca^{2+} influx triggers the fusion of synaptic vesicles with the presynaptic membrane, releasing glutamate into the synaptic cleft where it can bind to postsynaptic receptors. EAATs terminate the signal by transport of glutamate into neighboring glial cells where it is metabolized to Glutamine (Gln) and transported back to the neurons. Within neurons, glutamate can be synthesized from glucose or resynthesized from Gln by the phosphate-activated glutaminase (PAG). Synaptic vesicles are recycled and refilled with glutamate by VGLUTs, driven by the electrochemical proton gradient that is generated by the V-ATPase.*

3.2 The composition of synaptic vesicles

SVs are small, spherical organelles with a diameter of approximately 20-40 nm. Although the SV protein composition is studied best of all trafficking organelles, a detailed function of vesicular filling with neurotransmitter is not yet available. After exocytosis, SVs are mostly recycled through clathrin-dependent endocytosis [11]. Until now, 134 SV-resident proteins could be identified with proteomics including proteins for neurotransmitter filling, ion channels, trafficking proteins, and energy delivering proteins like the vacuolar H^+ ATPase (V-ATPase) [12–14] (Figure 3.2). Synaptophysin, synaptobrevin 2, synaptotagmin 1 and synapsin I are the most abundant proteins in SVs [13,15,16]. A typical SV contains an average number of 70 synaptobrevins, 32 synaptophysins, 9-14 neurotransmitter transporters, 10 Rav3As, 8 synapsins, 15 synaptotagmins and 1-2 V-ATPase [13].

With a volume of ~20 x 10^{21} l and a luminal glutamate concentration of 60-150 mM [13,17–19], one vesicle should be filled with 1800 glutamate molecules. The cytoplasmic glutamate concentration is ~5 mM, which implies that glutamate becomes concentrated up to 30 times [13,20]. The process of vesicle filling is therefore using energy in the form of ATP by the

V-ATPase. The electrogenic transport of H^+ by the V-ATPase simultaneously acidifies the vesicular lumen to ~pH 5.8 [21,22]. The vesicular membrane was reported to be ~4 nm thick with a high amount of cholesterol (~40%), a small amount of phosphatidylinositol, and a high proportion of phosphatidylethanolamine [13].

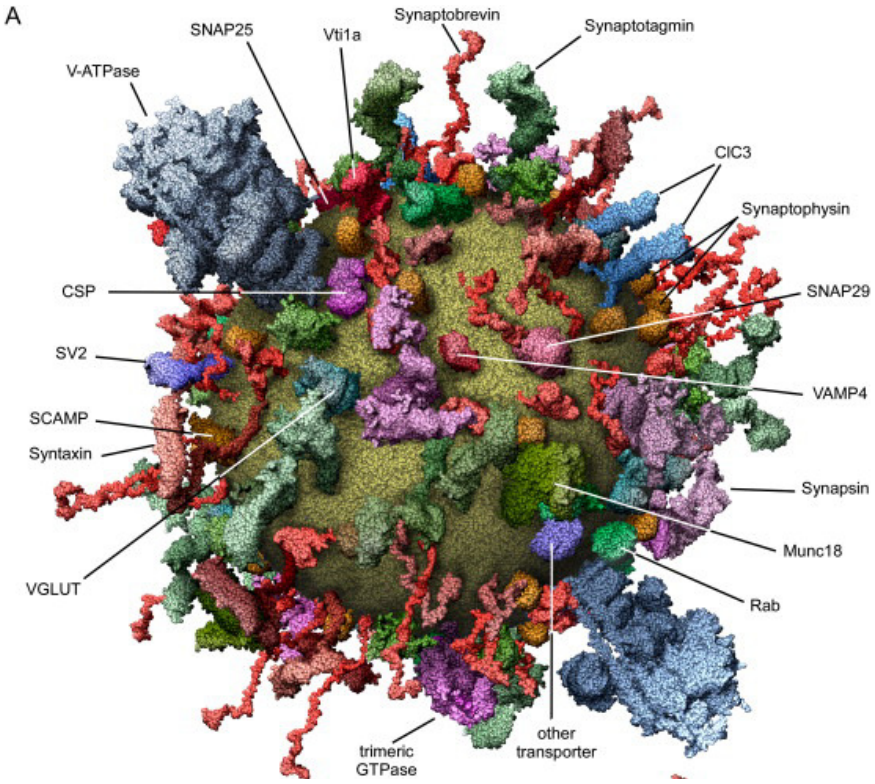

Figure 3.2 Protein content in a synaptic vesicle. *From Takamori et al., 2006.*

3.3 The solute carrier families: Vesicular neurotransmitter transporters

Vesicular neurotransmitter transporters accumulate neurotransmitters such as glutamate, aspartate, y-aminobutyric acid (GABA), glycine, nucleotides, and monoamines into secretory vesicles and are thus a major determinant in synaptic transmission. A total of ten different neurotransmitter transporters are identified by now. Besides their distribution in the CNS, they also differ in their amino acid sequence, preference of transported substrates, and inhibitors and blockers [23–25]. These transporters belong to the solute carriers (SLC) of membrane transport proteins that contain 55 families with 362 genes [26] and share 20-25% sequence identity to at least one other family member [27]. Neurotransmitter transporters can be classified into three families: SLC17, SLC18, and SLC32 (Figure 3.3). Members of the SLC17 family transport anionic neurotransmitters and are vesicular excitatory amino acid transporters (VEAT/sialin), vesicular glutamate transporters (VGLUT) and vesicular nucleotide transporters (VNUT). They contain 12 transmembrane helices and have similarities to other members of the major facilitator superfamily (MFS) like glycerol-3-phosphate transporters (GlpT) or D-galactonate transporters (DgoT). Next to the

neurotransmitter transporters, also four type 1 sodium-dependent inorganic phosphate transporters (NPTs) refer to the SLC17 family and cater for the removal of toxic organic anions from the liver and kidneys [28]. Members of the SLC17 family are thought to share a common Cl^- permeation pathway, although no structural basis for this has yet been found [18]. Vesicular monoamine transporters (VMAT), vesicular acetylcholine transporters (VAChT), and vesicular polyamine transporters (VPAT) belong to the SLC18 family and transport cationic neurotransmitters. The last family, SLC32, has only one member, the vesicular GABA transporter (VGAT) that transports electroneutral neurotransmitters like GABA, glycine, and ß-alanine.

The driving force for accumulating neurotransmitter into SVs is the electrochemical proton gradient $\Delta\mu H^+$ that results in the composition of a H^+ gradient (ΔpH) and luminal positive membrane potential ($\Delta\psi$). The $\Delta\psi$ was measured to be ~80 mV in hippocampal neurons and ~1.6 pH units [29]. There is evidence that VMAT, VACht, and VGAT are coupled to proton transport, with many inconsistencies in the literature for all neurotransmitter transporters [30–32].

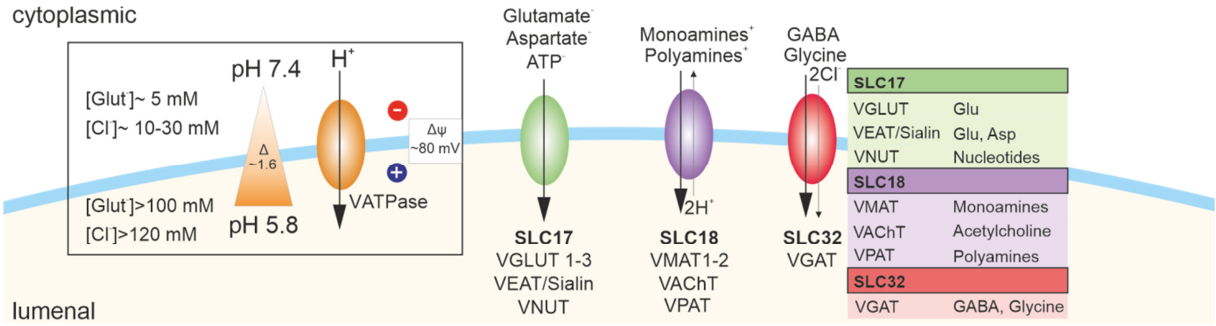

Figure 3.3 The solute carriers (SLC). *Members of the SLC are localized in the membrane of synaptic vesicles, loading them with neurotransmitters, with the electrochemical proton gradient $\Delta\mu^+$ generated by V-ATPase, serving as the driving force (Modified from Pietrancosta et al., 2020 (left) and Omote et al., 2016 (right)).*

3.4 Vesicular glutamate transporters

VGLUTs accumulate glutamate into SVs at the presynaptic nerve terminal. Three different isoforms have been identified by now: VGLUT1 (SLC17A7), VGLUT2 (SLC17A6), and VGLUT3 (SLC17A8) named in order of discovery [20,24,25,28,35], and sharing ~70-80% sequence identity with each other.

VGLUT1 was first discovered in 1994 in a screen for mRNA in cerebellar granule cells after NMDA treatment [36]. They showed ~32% sequence identity with Na^+-dependent P_i transporters in the kidney and were therefore named brain-specific Na^+-dependent P_i cotransporter 1 (BNPI). After heterologous expression of this newly discovered protein into *Xenopus* oocytes, the transport of phosphate was confirmed and it was suggested that the protein was responsible for the uptake of P_i into neurons. VGLUT2 was later found in rat

forebrain neurons and named differentiation-associated Na^+-dependent inorganic phosphate cotransporter (DNPI, Hisano et al., 2000). Shortly thereafter, the main function of the proteins was found to be the transport of glutamate into SVs under physiological conditions. [38–40]. This was also followed by the discovery of VGLUT3 [41–43].

3.4.1 VGLUT transport mechanisms and their bioenergetic properties

Glutamate

In contrast to EAATs, which are considered high affinity glutamate transporters with a KD of ~1 µM, VGLUTs have a very low affinity for their substrate glutamate (KD=2-4 mM), but are considered highly selective [20]. They have been reported to be insensitive to structurally similar molecules such as aspartate, glutamine or D-glutamate [44,45].

The transport mechanism of the VGLUTs is a secondary active transport, taking advantage of the proton gradient generated by the V-ATPase to transport glutamate against the gradient. Thus, cytoplasmic glutamate concentration ([$glut^-$]) is estimated to be ~ 5 mM and luminal [$glut^-$] ~150 mM [13,19], a factor of 30 against which glutamate has to be transported. In recent years, the weighting of Δψ or ΔpH for glutamate transport in VGLUTs has been very controversial. Some studies consider VGLUT as an H^+/$glutamate^-$ antiporter using the ΔpH of the V-ATPase, whereas the majority of publications consider Δψ as the main driving force [20,39,44–48]. Nevertheless, the luminal presence of protons seems to be essential for the allosteric activation of VGLUT, a mechanism that prevents the non-vesicular efflux of glutamate from VGLUT in the plasma membrane under physiological conditions [48–50].

Chloride also plays an important role in the transport of glutamate through VGLUT by binding as an allosteric modulator to a regulatory site that is distinct from the glutamate binding site. In this process, Cl^- can bind from the luminal and/or cytoplasmic side [51–54], and a biphasic modulation has already been shown for this process. The maximum activation of transport could be achieved with 4 mM Cl^-, which is within the physiological range of the cytosol, whereas concentrations >10 mM reduce the uptake of glutamate because the ions compete for the same binding site [54,55]. Another theory is that it is not a question of ion competition, but rather that a high [Cl^-] dissolves the membrane potential in proteoliposomes and thus the driving force for transport is absent [45,47]. The unusually strong cooperativity of Cl^- activation with a Hill coefficient of ~3 makes it possible that even small changes in [Cl^-] influence the activity of VGLUT [52]. The allosteric activation of VGLUT by Cl^- has the physiological purpose to turn the activity of VGLUT on and off like a switch and thus regulate glutamate release.

A coupled transport of glutamate together with H^+ or Cl^- has also often been discussed in recent years and has not yet been clarified. There are three different theories on how the

transport of glutamate could function: 1. as $Glut^-/H^+$ exchanger [19,54], 2. as $Glut^-/Cl^-$ exchanger [54,56] or 3. as an electrogenic $Glut^-$ uniporter [25].

Chloride

The influence of Cl^- ions in SVs provides a charge balance to the V-ATPase, which is needed to acidify the vesicles. If there was no compensation by anions, the influx of a few unbuffered protons could already generate a huge membrane potential. [55]. There are two main theories on how Cl^- is regulated in SVs: via the Cl^-/H^+ exchanger ClC-3 [57] or ClC-7 [58], or via VGLUT itself [54]. In 2000, the Cl^- conductance was postulated for the first time for VGLUT [39]. The weakly acidic dye Acridine Orange (AO) was used to measure acidification in synaptic vesicles. Less AO quenching was detected in VGLUT1 knock-out ($VGLUT1^{-/-}$), but not in $ClC\text{-}3^{-/-}$ neurons [39,53]. These results contrasted with experiments performed by Juge et al., (2010), who measured the uptake of radioactive Cl^- in proteoliposomes and performed fluorescence measurements with SPQ. They found that VGLUT2 does not transport Cl^- during glutamate transport but demonstrated that Cl^- is indispensable as an allosteric modulator to activate transport activity. However, the clear evidence of a Cl^--conductivity for VGLUT was first provided by the group of Edwards [49] by introducing heterologously expressed VGLUTs into the plasma membrane of *Xenopus* oocytes through mutations in N- and C-terminal regions and performing electrophysiological patch clamp experiments. They were able to measure a large inward rectifying Cl^- current in the absence of glutamate, which was allosterically activated by the binding of H^+ and Cl^-. Interestingly, this current could also be blocked by luminal glutamate, but not by aspartate, indicating a strong substrate specificity for VGLUT.

Phosphate

VGLUT was originally identified as a Na^+-P_i transporter [36]. In this transport, the distinction between localization in the SVs and in the plasma membrane is crucial, as has been found in several experiments. In the SVs, the phosphate transport by VGLUT was reported to occur via $\Delta\mu H^+$ as a driving force, whereas in the plasma membrane it is coupled to the co-transport of 2 sodium ions (Na^+) [50]. Probraschenski and colleagues (2018) demonstrated that both phosphate and glutamate compete for the same binding site with glutamate (K_m=1.09 mM) being preferred over phosphate (K_m=4.3 mM). This competence was later demonstrated in purified SVs where glutamate transport and glutamate-dependent acidification were inhibited by cytoplasmic phosphate with an IC_{50}=300 µM [50]. This shows that phosphate transport probably does not play a significant role in synaptic vesicles under physiological conditions. Also, in the orientation in the presynaptic membrane, the presence of 5-10 mM glutamate inhibits the transport of phosphate. On the other hand, no interaction between the transport modes of glutamate and phosphate could be detected with purified

VGLUTs in reconstituted liposomes by Juge et al. (2006). Two major differences from the transport of glutamate are that in both the plasma membrane and synaptic vesicles, the transport of phosphate appears to be independent of [Cl^-] and is not stimulated in the plasma membrane by the presence of H^+, which is why its physiological role is suspected here. Thus, VGLUT could transport phosphate under co-transport of Na^+ into the synapse, where it activates the PAG to regulate glutamate synthesis [59].

Potassium

The various transport mechanisms underlying VGLUT appear to be a complex mystery in SV filling with glutamate. In addition to glutamate, chloride, and phosphate, VGLUT has also been reported to have K^+/H^+ exchange activity in native synaptic vesicles [53]. The stoichiometry of the different ions can change during vesicle filling. The theory of Preobraschenski et al. (2014) states that when the buffer capacity in the vesicles is exhausted by the transport of glutamate, a second transport mode of VGLUT is activated in which luminal protons are exchanged for cytoplasmic potassium ions. Together with the Na^+/H^+-exchanger NHE6, which is also located in the vesicular membrane, VGLUT thus ensures the prevention of the over-acidification of the lumen by the transport of the V-ATPase [53,60]. Figure 3.4 shows the different transport mechanisms of VGLUT.

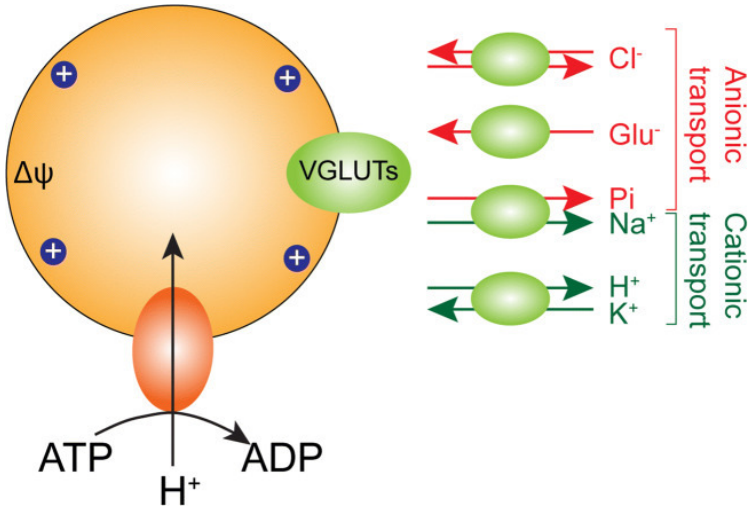

Figure 3.4 VGLUT transports various anions and cations. *In addition to their main role as glutamate transporters, VGLUTs can also transport Cl^-, P_i and K^+ in different modes, with Na^+/P_i cotransport probably taking place in the plasma membrane at the presynaptic nerve terminals. From Pietrancosta et al., 2020.*

3.4.2 Expression pattern of VGLUTs

VGLUTs are mainly expressed in presynaptic nerve terminals but can also be found in peripheral neurons and non-neuronal α-cells of the Langerhans islet, bone cells, cells of the

pineal gland, L-cells of the gastrointestinal tract, and testes [61–63]. In these non-neuronal cells they play a major role in storage of glutamate and function as a paracrine like modulator.

Although VGLUT1 and VGLUT2 are thought to be structurally and functionally similar, their expression pattern is different, suggesting different functional roles during development between the two transporters. While VGLUT1 is mainly expressed in the cortex, hippocampus, and cerebellar cortex, VGLUT2 can be found in the thalamus, brainstem, and cerebellar nuclei [64]. VGLUT2 is critical during developmental stages since targeted deletion of VGLUT2 leads to perinatal lethality [65]. In contrast to this, VGLUT3 is mainly found in caudate-putamen, olfactory tubercle, nucleus accumbens, hippocampus, raphe nuclei, and inner hair cells [64,66]. VGLUT3 knock-out mice appear to be deaf [67].

In general, the question arises whether VGLUT plays a role not only in the filling, but also in the release of SVs by interacting with other proteins [33]. VGLUT expression is also regulated by microRNAs (miR-1000) in presynaptic nerve terminals [68]. Whether VGLUT also interacts directly with other proteins or even forms multimeric proteins is to our knowledge not known, but also cannot be ruled out. VGLUT1-3 have similar glutamate transport probabilities despite their different expression patterns [13]. However, VGLUT1 is found in regions associated with a low release probability (olfactory bulb, neo-cortex, hippocampus, cerebellum), whereas VGLUT2 is found in regions with a high release probability (subcortical pathways of the thalamus and brainstem) [69].

3.4.3 Structure

VGLUT1-3 consist of 560-589 amino acids (AA) and share ~70-80% sequence similarity. They consist of 12 transmembrane domains (TM) that can be divided into two groups of 6, which are connected by a cytoplasmic flexible loop [70,71]. They form a hydrophilic, polar cavity in their center that favors the conductivity of negative substrates. The AAs that are probably responsible for substrate recognition or for modelling the transporter, are located within this central cavity. The N- and C-termini are located on the cytoplasmic side and contain dileucine-like motifs that are responsible for the transport pathway of VGLUT to the SVs [72]. These motifs have already been used by Eriksen et al. (2016) to change the localization of VGLUT.

Crystallography structure of the bacterial VGLUT homologs glycerol-3-phosphate transporter (GlpT, Huang et al., 2003), lactose permease (LacY, Abramson et al., 2003) and D-galactonate transporter (DgoT, Leano et al., 2019) have long demonstrated a uniform structure within the MFS-type transporters. Recently, the first rat VGLUT cryo-electron microscopy structure was published by Li et al. (2020), which largely confirms the acquired knowledge obtained by molecular dynamic simulations. The structure of VGLUT2 was

captured in the apo-state at pH 7.4, therefore in the inactive state. With this structure it was possible to identify a total of seven amino acids that are thought to be involved in the recognition of the different substrates (Figure 3.5, homolog AA in VGLUT1), which have been investigated in simulations [71], but also in uptake experiments [44] and in patch clamp measurements [49,75] using mutations (Figure 3.6).

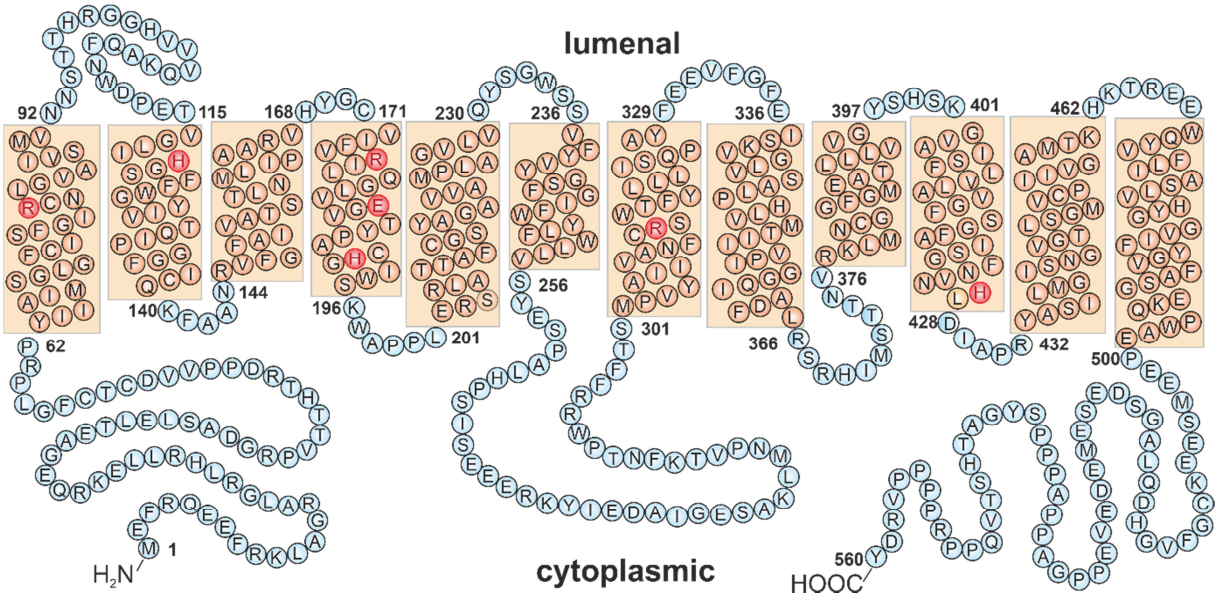

Figure 3.5 Transmembrane topology of rat VGLUT1. *VGLUT consists of 12 transmembrane regions (orange). The N- and C-termini are cytoplasmically localized. Seven amino acids (red) are thought to be involved in substrate recognition. Modified from Almqvist et al, 2007* [76].

Based on the structure and experimental results from the uptake experiments of Juge et al. 2006, Li et al. (2020) have developed a theory for the possible function of the seven amino acids: **R88**, which is oriented towards the binding site and conserved in the SLC17 family, is suggested to be involved in the anion recognition. **R322** is located at the opposite of R88 and presumably binds the second carboxyl group of glutamate. This amino acid is conserved only within the VGLUTs, but not within the SLC17 family. **E191**, localized in the TM4, which is highly conserved and when mutated, the transport activity is inhibited [44]. The equivalent AA E133 in DgoT is responsible for the symport of H^+ and is also present in the H^+-symporter Sialin (VEAT, Leano et al., 2019). It is suspected that E191 functions as a luminal proton sensor. Loss of H^+-transport activity prevents glutamate from exiting the vesicles, which is the reason why the AA is thought to play a role in allosteric H^+-activation. E191 is located deep in the transporter, which is probably why **H128** in TM2 in VGLUT2 acts as an initial H^+-acceptor. Moreover, this histidine is conserved in all VGLUTs, but not in the rest of the SLC17 family. One possible function of histidine through its negative charge could be the binding of glutamate. **R184** in TM4 could be responsible for allosteric activation by Cl^-, as a mutation shows the absence of Cl^- dependence [75]. This AA is uniformly conserved in the SLC17 family. R184 and H128 are located close to each other and are jointly responsible for

the activation of VGLUT. A neutral pH of 7.4 deprotonates H128 and thus inhibits the binding of Cl^- in the vicinity of H128 and R184 [71]. Mutation of the AAs reduces VGLUT activity [44]. A cytoplasmic gate for a channel is probably formed between **H199** at the N-domain and **H434** at the C-domain. These AA are called the two-His-gate and are specifically found in VGLUTs and sialin.

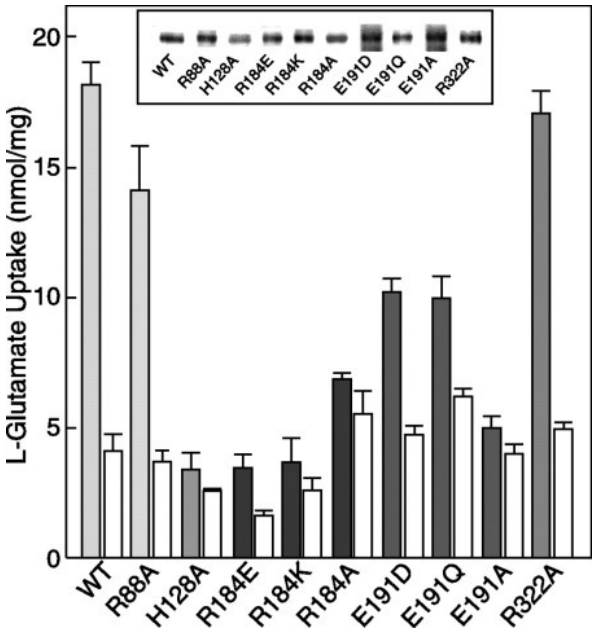

Figure 3.6 Effect of point-mutations in VGLUT2 on the glutamate uptake in reconstituted liposomes. *VGLUT2 was purified and reconstituted together with the bacterial F_oF_1-ATPase. Glutamate uptake was measured over a period of 5 min in the presence of 100 µM L-glutamate with (filled bars) and without ATP (open bars). From Juge et al., 2006.*

3.4.4 VGLUTs in health and disease

Glutamate is the most important neurotransmitter in the CNS and is involved in a variety of neurological and metabolic diseases due to its ubiquitous distribution. A direct link of genetically modified VGLUTs in diseases has so far only been found in VGLUT3. The p.A211V, found in two unrelated families, causes progressive, high-frequency nonsyndromic deafness [66]. Hearing could be restored in $VGLUT3^{-/-}$ mice using viral-mediated gene therapy [77].

In addition to the direct influence of genetic mutations on the VGLUT, the function can be impaired primarily through unbalances in cellular and intercellular ion concentrations. For example, overstimulation of the postsynapse by increased [$Glut^-$] in the synaptic cleft triggers epilepsy. Fasting naturally increases ketone bodies, which are among the natural inhibitors of VGLUT by competing with Cl^- at the allosteric activation site. Therefore, fasting has long been used as a therapeutic approach for epilepsy [52]. Excessive inhibition of glutamate transport by ketone bodies is also suspected in the neurological damage of genetic maple

syrup disease [52]. This disease causes apathy, muscle hypertonia and seizures in the first days of life and can cause severe brain damage or even death if left untreated. This disease affects the function of the branched-chain keto acid dehydrogenase complex, which is responsible for the breakdown of AA leucine, isoleucine and valine [78].

Ischemia and brain injury, where extracellular pH is reduced, could also tend to uncontrolled, non-vesicular glutamate release and thus also excitotoxicity [79–81]. The expression of VGLUT also plays a crucial role in healthy homeostasis. For example, altered expression of VGLUT1 in humans is associated with anxiety disorders [82] , Alzheimer's disease [83], or Parkinson's disease [83], with VGLUT2 playing a role in schizophrenia [84] or neuropathic pain [65]. In mouse models of amyotrophic lateral sclerosis, the expression of VGLUT2 is increased [85] and in mouse models of Alzheimer's disease, 40% increased glutamate release has been reported [86].

Treatments by influencing the glutamatergic signaling pathway have so far been rather difficult due to low efficacy or high side effects [87,88]. To date, VGLUT itself has not been considered as a target for pharmacological treatment due to its complex mode of action and localization. Pharmacologically, postsynaptic glutamate receptors are much more commonly used as targets for the modulation of excitatory signals. Examples include esketamine [89] and memantine [90] as NMDA receptor antagonists used in major depression or Alzheimer's disease.

3.5 Working hypothesis

This work aims to further decipher the complexity of VGLUTs. I focus primarily on the detection and characterization of the postulated channel activity of Cl^- conductance. This will be investigated using a combination of noise analysis, patch clamp, and fluorescence measurements. In addition, I am investigating the permeability of various large anions, including glutamate. The point mutation H120A in VGLUT1 was reported to inhibit the transport of glutamate [44]. In this work I characterize the effects of this mutation on the different transport processes of VGLUT and discuss its possible role as an initial proton acceptor to provide the binding of Cl^- for the activation of the transport [71]

.

4 Materials and Methods

4.1 Chemicals and materials

All chemicals and solutions were purchased in *pro analysis* quality at Sigma Aldrich or different companies as listed in chapter 4.7. Solutions and buffers were produced and diluted in bi distilled water and filtered with a 0.22 µm pore size filter (Millipore).

4.2 Molecular biology

Rat VGLUT1 was inserted into pcDNA3.1 vector and tagged with a green fluorescent protein (GFP) to the 5'-end (C-terminus) of the cDNA coding region. Targeting signals that direct rat VGLUT1 to SVs have been identified in N- and C-terminal regions and neutralized to alanines by Cora Hannack (2015) [91] as part of her bachelor thesis (N-terminal $E_6E_7L_{11}$ and C-terminal $E_{505}E_{506}F_{510}V_{511}$). These targeting signals were found in dileucin-like motifs, equal to the ones previously found in VGLUT1 [72] or VGLUT2 [49]. The mutations and the H120A point mutation were introduced using the Quick Change™ method and verified by restriction analysis and DNA sequencing. For the generation of stable, inducible $VGLUT1_{PM}$ cell lines in Flp-In T-Rex 293 cells, the constructs were subcloned into pcDNA5/FRT/TO vectors.

4.3 Cell culture

For hereterologous expression of $rVGLUT1_{PM}$, mammalian cell lines were transiently transfected or a stable cell line was generated.

4.3.1 Transient cell transfection

For a high heterologous expression and electrophysiological experiments, $rVGLUT1_{PM}$ was transiently transfected in HEK293T cells (human embryonic kidney cells, SV40 transformed). Cells were cultivated in DH10 medium (DMEM Medium (Dulbecco's Modified Eagle Serum; Gibco), 10% FBS (fetal bovine serum, Gibco) and 1% antobiotic/antimycotic (100X; Gibco)) at 37°C, 5% CO_2 and 95% humidity. The cells were passaged twice per week at a confluence ~90%, washed with PBS (phosphate buffered saline; 140 mM NaCl, 2,7 mM KCl, 10 mM NaH_2PO_4, 1,8 mM KH_2PO_4), detached from the culture dish with Trypsin/EDTA (0.05%; ThermoFisher) and seeded with a density of ~$1.5x10^5$ cells per Ø10cm dish.

HEK293T cells were transiently transfected with lipofectamine 2000 (ThermoFischer) 24 hours before experiments. For transfection in Ø5 cm dishes, cells were seeded to be 70-80% confluent. Two µg DNA and 6 µg lipofectamine were diluted in 250 µl Opti-MEM (Gibco) respectively and incubated at room temperature for 5 minutes. The diluted DNA was added to the diluted lipofectamine and incubated for 20-30 minutes at room temperature. The

DNA-lipid complex was added to the cells. After incubation for 8-10 hours at 37°C, cells were splitted into single cells for patch clamp experiments the day after. For confocal microscopy, cells were splitted on coverslips that have been coated with 0.1 mg/ml Poly-L-Lysin (PLL, Sigma Aldrich) for 20 minutes at room temperature and washed with PBS twice.

4.3.2 Stable cell lines

Flp-In T-REx 293 cells (Invitrogen) were used to generate stable, inducible cell lines. Cells were cultivated equal to HEK293T cells with additional 100 µg/ml zeocin (Gibco) and 10 µg/ml blasticidin (Gibco) in the medium before transfection. Forty-eight hours after transfection, zeocin was replaced by 100 µg/ml hygromycin (Gibco).

To use the Flp-In system, the inserted WT $VGLUT1_{PM}$ and H120A $VGLUT1_{PM}$ were subcloned into pcDNA5/FRT/TO vector. The vector admits insertions of the target gene to a specific region in the human genome by the Flp recombination target (FRT) site and the DNA recombinase system (Flp; [92,93]). The expression of the target gene can be induced and regulated 15-24 hours before experiments with 0.1-0.15 µg/ml tetracyclin (diluted in 70% Ethanol).

Twenty-four hours before transfection, Flp-In T-REx cells were seeded to 40% confluence in a Ø10 cm dish without selection antibiotics. Cells were transfected with the calciumphosphate-precipitation method referring to Chen and Okayama (1987). The pOG44 (Flp recombinase expression vector) was added to 6 µg of the circular plasmid-DNA in a ratio of 9:1 and was mixed with 372 µl H_2O, 123 µl $CaCl_2$ (1 M), and 495 µl 2x HEBS. After 20 minutes incubation at room temperature, the mixture was added to the cells and incubated at 37°C for 24 hours, washed with PBS and PBS/EDTA and incubated another 24 hours without selection antibiotics. Selection with blasticidin and hygromycin started 24 hours post transfection. The medium (DH10 with blasticidin and hygromycin) was changed at least every second day until single colonies grew. These colonies were cultivated and tested for their expression at the confocal microscope and functionality in patch clamp experiments.

4.4 Confocal microscopy

For confocal imaging, HEK293T cells were transfected as described in chapter 4.3.1. Cells were seeded on PLL coated cover slips and imaged at a TCS SP5 II confocal laserscanning setup (Leica Microsystems) with an inverse Leica DM6000 CFS microscope. The target protein was detected by the fused GFP that was excited with an argon-laser at 488 nm and detected between 508 to 541 nm with a scan frequency of 400 Hz and a 63x/1.32-0.6 oil immersion objective. Images were recorded with Leica Application Suite Advanced Fluorescence 2.6 software and processed with ImageJ.

4.5 Electrophysiology

4.5.1 Setup

The inverse microscope (Olympus IX71) and the micro manipulators (LN SM 6, Luigs & Neumann) were positioned on a vibration isolated optical table (TMC), surrounded by a faraday cage. Standard whole cell patch clamp recordings were performed using a HEKA EPC10 amplifier (HEKA Elektronik) with the Patchmaster software or dPatch® amplifier (Sutter Instrument) with the included SutterPatch® Software with a 50 kHz sampling frequency and filtered with a 10 kHz low pass Bessel filter. The series resistance has been compensated for at least 80%. Borosilicate pipettes (Harvard Apparatus, Ø1.2 mm, with inner filament) were pulled with resistances between 1.0 MΩ and 3.0 MΩ with a micropipette puller (Sutter Instruments) followed by fire polishing with a microforge (MF-830, Narishige). For noise experiments, pipettes were covered with dental wax (Moyco Technologies) to reduce their capacitance. For all recordings the Ag/AgCl internal electrode and reference electrode were covered with 0.5 M KCl agar bridges (2% agar).

Before experiments, cells were washed and kept in 3 ml bath solution in a Ø5 cm dish for experiments. After opening a cell to whole cell mode, various external conditions were applied locally by lifting the cell and guiding it into the solution stream of a self-made gravity driven perfusion system, without exchanging the bath solution. Liquid junction potentials (LJPs) were calculated using the Junction Potential calculator (pClamp, Molecular Devices) and corrected *a priori* after entering the whole cell mode. Recordings were done in voltage clamp mode with voltages between -160 mV and +100 mV and an inter-sweep interval of 4 seconds. The holding potential was set to -50 mV for internal glutamate ($glut^-$), aspartate (asp^-), gluconate ($gluc^-$), 2-(N-Morpholino)ethanesulfonic acid (MES^-), Methanesulfonic acid (MSA^-) and isethionate ($iset^-$) or 0 mV for all other internal anions.

For all experiments, activation of endogenous currents was checked in untransfected cells as a control.

4.5.2 Solutions

To avoid interactions of our protein of interest with other permeable ions and to avoid the activation of endogenous proteins at acidic pHs, all solutions were made in the absence of sodium or potassium. Instead, the impermeable cation choline (Chol) was used as shown in Eriksen et al. (2016). A clear presentation of all solutions used can be found in the following Table 4.1. The standard pipette solution contained (in mM): 140 mM CholAnionX, 5 EGTA, 5 MgOH, 30 HEPES, pH 7.4 with TMA-OH where AnionX was one of the following anions: Cl^-, NO_3^-, Br^- (as Choline Bromide; TCI), I^- (as Choline Iodide; TCI), HCO_3^-, $glut^-$, asp^-, $gluc^-$, MES^- (Serva), MSA^- or $iset^-$ (as Choline Isethionate; Forschungszentrum Jülich).

Table 4.1 Composition of patch clamp solutions. *Unless otherwise stated, the pH of external solutions was titrated with Chol-OH and the internal pH with TMA-OH. Solutions with pH 6.8-7.5 were buffered with 30 mM HEPES, solutions with pH 5.0-6.8 with 50 mM MES. All internal solutions also contained 5 mM EGTA. The osmolarity of external solutions was adjusted with glucose 15 mOsmol above that of the internal solution. All numbers give the ion concentration in mM.*

Experiment	Figure	Bath	Internal	Perfusion
Noise / pH dependence	Figure 5.2	145 CholCl, 2 $MgCl_2$ pH 7.4	100 CholCl, 45 TMA-Gluc, 5 $MgGluc_2$ pH 7.4	145 CholCl, 2 $MgCl_2$ pH 7.0, 6.5, 6.0, 5.75, 5.5, 5.25, 5.0
	Figure 5.4			
	Figure 5.7 A-D			
	Figure 8.2, 8.3, 8.7		100 CholNO3, 45 TMA-Gluc, 5 $MgGluc_2$ pH 7.4	
Proton binding	Figure 5.3	145 CholCl, 2 $MgCl_2$ pH 7.4	130 CholCl, 5 $MgCl_2$, 30 HEPES/50 MES pH 7.4/5.5	145 CholCl, 2 $MgCl_2$ pH 5.5
Permeability small anions	Figure 5.5 A-D	136 CholCl, 2 $MgCl_2$, pH 7.4	140 CholCl/Br/NO3/I, 5 $Mg(OH)_2$ pH 7.4	100 CholGluc, 36 CholCl, 2 $MgCl_2$ pH 5.5
	Figure 5.7 E, G			
	Figure 8.4, 8.5			
Permeability big anions	Figure 5.5 E-H	136 CholGluc, 2 $MgGluc_2$ pH 7.4	140 CholGlut/Asp/HCO_3/ MES/ MSA/Iset, 5 $Mg(OH)_2$ pH 7.4	100 CholGluc, 36 CholCl, 2 $MgCl_2$ pH 5.5
	Figure 5.7 F, H-J			
Noise Glut	Figure 8.6 A-D	145 CholCl, 2 $MgCl_2$ pH 7.4	100 CholGlut, 5 $MgGlut_2$ pH 7.4	145 CholCl, 2 $MgCl_2$ pH 7.0, 6.5, 6.0, 5.75, 5.5, 5.25, 5.0
Proton current	Figure 5.6	80 CholGlut, 30 CholCl, 5 $MgCl_2$, 0.5 EGTA pH 7.4	80 CholGlut, 30 CholCl, 5 $MgCl_2$, 0.5 EGTA, 30 HEPES/30 MES pH 7.4/5.5 with CholOH	80 CholGlut, 30 CholCl, 5 $MgCl_2$, 0.5 EGTA pH 5.5
Glutamate-block	Figure 5.8 left	145 CholGluc, 2 $MgGluc_2$ pH 7.4	130 CholCl, 5 $MgCl_2$, pH 7.4	100 CholGlut/Gluc, 36 CholCl, 2 $MgCl_2$ pH 5.5
	Figure 5.8 middle, right		100 CholGlut/Gluc, 30 CholCl, 5 $MgCl_2$ pH 7.4	
Temperature dependence	Figure 5.9 A, B,F	100 CholGluc, 36 CholCl, 2 $MgCl_2$ pH 5.5 CholOH	130 CholCl, 5 $MgCl_2$, pH 7.4	
	Figure 8.8			
	Figure 5.9 C,D,E,F		130 CholGlut/Gluc, 5 $MgGlut_2$, pH 7.4	

The Bicarbonate (HCO_3^-) solution was oxygenated with carbogen (5% CO_2 in O_2) until start of experiment. To allow a complete washout of the internal solution, after opening the cell, two minutes were waited until the start of the measurement. For some experiments the internal pH was set to 5.5 and the buffer HEPES was replaced by 50 mM MES. The standard bath solution contained (in mM) 136 CholCl, 30 HEPES and 2 $MgCl_2$ pH 7.4 with CholOH. The external osmolarity was adjusted to be 15 mOsm higher than the internal solution. For acidic perfusion solutions, 30 HEPES was replaced by 50 MES, following the capacity of the buffers. When the permeability of big anions was investigated, the chloride in the bath solution was replaced by gluconate and the perfusion solutions contained in total 40 mM chloride, the rest was gluconate.

4.5.3 Fluorescence normalization

Transiently transfected cells were detected with an ultrafast switching monochromator (Polychrome V, Till Photonics) at 470 nm. To compare current amplitudes of transiently transfected cells with different expression levels, a picture of the cell fluorescence was taken before every measurement with a camera directly connected to the microscope (NEO 5.5 sCMOS, ANDOR; Oxford Instruments) with an UAPON-340 objective (40x/ 1,15w, Olympus). In Fiji (ImageJ), the analyzed cell was surrounded by a ROI and the raw integrated density (the sum of the grey values of the pixels in the selection) was measured. An inevitable error arises here by also measuring fluorescence in intracellular compartments. However, it can be assumed that the ratio between different cells hardly changes. The background fluorescence for every cell was measured by placing the same ROI next to the fluorescent cell and was subtracted from the recording. It should be noted that direct comparisons of currents normalized to fluorescence cannot be made between different constructs because the ratio of expression in the plasma membrane and in intracellular compartments may change [95]. Here, only relative currents can be compared.

4.5.4 Whole cell recordings

Mean values of current amplitudes were always measured at steady state. If steady state was not reached, a biexponential function was fitted to the recordings and the extrapolated steady state current was used.

The dependence of VGLUT anion currents on the external pH was fitted with a standard dose-response curve in Origin with a hill coefficient n of 1:

eq. 1
$$\frac{\mathbf{E}}{\mathbf{E_{max}}} = \frac{\mathbf{1}}{\left(\mathbf{1}+\left(\frac{\mathbf{EC_{50}}}{\mathbf{[A]}}\right)^{\mathbf{n}}\right.}$$

A represents the proton concentration, E is the magnitude of the response, and EC_{50} is the concentration of protons with the half maximum response.

In experiments where the permeability (P) for different big anions was calculated, the background current at pH 7.4 was subtracted from the measured values at pH 5.5. The permeability was calculated according to Linsdell et al. (1997, 1998) using the Goldmann-Hodgkin-Katz equation:

eq. 2
$$\frac{P_X}{P_{Cl}} = \frac{[Cl^-]}{[X^-]} \exp^{-\Delta E_{rev} F/RT}$$

Where ΔE_{rev} is the difference of reversal potential of anion X^- and the reversal potential with Cl^-, F is the Faraday constant, R the gas constant, and T the temperature in Kelvin. Reversal potentials were determined either by voltage jumps between -160 and +80 mV and fitting a polynomial function to the current-voltage-relationship or by 100 ms ramps from -160 to +75 mV.

In current protocols where the fast deactivating Cl^- influx at positive potentials is analyzed by an activating voltage step to -160 mV, capacitive currents were eliminated by subtracting the currents of inactivated VGLUTs at pH 7.4 from currents at pH 5.5. These measurements were performed by Yannick Güthoff as part of his master thesis (not yet published).

4.5.5 Noise analysis

For noise analyses, currents were digitized with 100 kHz while the 10 kHz Bessel filter was inactive. Normalization of fluorescence was omitted to avoid unnecessary background noise. Power spectrum analysis was performed on the steady state current of 50 seconds long voltage jumps to -100 mV (46 seconds analyzed). Spectral density was determined using fast Fourier transform. The first data point was skipped for further analysis since it contains the DC offset that should not be part of the spectrum. Data were binned into 2300 data points, averaged over all measured cells and plotted with a combination of pink noise and a double Lorentzian function:

eq. 3
$$S = \frac{S(0)_1}{f^a} + \frac{S(0)_2}{1+f/fc_1} + \frac{S(0)_3}{1+f/fc_2}$$

where S denotes the spectral density, f the frequency, a the slope of the linear pink noise, and S(0) and fc the amplitude and the corner frequencies respectively. The corner frequencies are predicted to represent the time constants (τ_m) of macroscopic activation kinetics by the relation

eq. 4
$$f_c = \frac{1}{2\pi\tau_m}$$

The macroscopic currents seen in whole cell mode recordings result from the sum of many individual currents from ion channels. The noise in these macroscopic currents is thus the result of the sum of all random individual events. As a consequence, the macroscopic current (I) is the product of the single channel amplitude (i), the number of ion channels in the plasma membrane (N), and the open probability (p(0)).

eq. 5 $$\mathbf{I = i \cdot N \cdot p(0)}$$

Stationary noise analysis was used to determine the single channel amplitudes of the WT and H120A VGLUT1$_{PM}$. The analysis was performed on steady state currents at -160 mV at 5-8 different external pHs between pH 5.0 and 7.4. To prevent variances from being overestimated because the current has not fully reached the steady state, we isolated high frequency noise signals form slowly relaxing current traces by applying a butterworth high pass filter with a cut-off frequency at 200 Hz. The unitary current amplitude (i) was obtained by plotting the current variances (σ^2) against the mean current amplitude (I). To assess if the noise-current plot can best be described by a parabola or a linear function, we performed model selection using an F-test. The fit with a parabola was significantly better than the fit with the linear function. Consequently, we calculated single channel amplitudes from parabolic fits:

eq. 6 $$\mathbf{\frac{\sigma^2 - \sigma_{bg}^2}{I} = i - \frac{I}{N}}$$

The background variance σ_{bg} was obtained by fitting (eq. 6) to the data of each cell as a Y-axis intercept, subtracted from the data and fitted again. To obtain the single channel amplitude of all cells, a global fit with one single channel amplitude and N for each cell was individually fitted. To improve fit convergence and avoid unphysical results, we added a restrain on the variances of the individual number of channel parameters. The duration of single channel events in the current noise was investigated by examining the effect of filter dependence on the current variances [98]. A low pass Butterworth filter was used for this offline analysis. For noise analysis, Butterworth filters are preferred over Bessel filters because they have a sharp roll off and distort transient signals [99]. To determine mean open times of VGLUT1$_{PM}$ anion channels, we studied the effect of filtering on the unitary current amplitudes obtained by noise analysis with the filtered current recordings. We simulated current variances generated by channels with one open and one closed state [98,100]. We modified open times by changing opening and closing rates and investigated the effect of filtering on apparent unitary current amplitudes.

4.5.6 Deactivation times

To study the recovery (reactivation) of the anion currents, a double-pulse protocol [101–103] was used. Two activating pulses, first at -140 mV, then at -120 mV, were separated in time by a depolarizing pulse of variable length (2-60 ms, 30 sweeps) at +120 mV, thus changing the channel conformation from open to closed to open again. The increasing length of the depolarizing pulse raises the probability of the channel closure before it opens again (Figure 4.1). A double exponential function (blue) was fitted to the reactivating current of each sweep to determine the instantaneous current amplitudes at the time of the second negative voltage

jump. A mono exponential fit (red) to the instantaneous current amplitudes of all voltage jumps was used to obtain the deactivation time course of the channel.

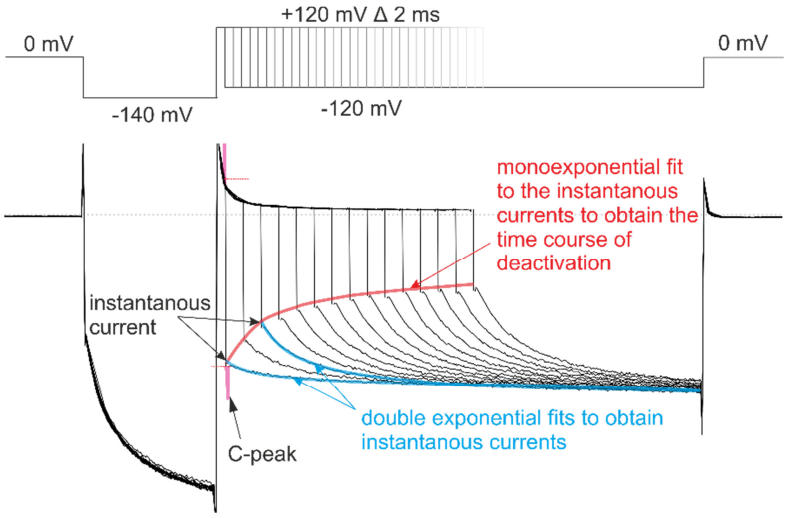

Figure 4.1 Analysis of deactivation time constants. *Representative recording of channel deactivation. The cell was stimulated within 30 sweeps to two negative voltages, separated by a hyperpolarizing pulse at various length (2-60 ms). Only every second recording is demonstrated and C-peaks (pink) were removed for better representation. A double exponential fit to the reactivating current was used to obtain the instantaneous currents at the time of the second voltage jump. A mono exponential function (red) was fitted to the instantaneous currents to determine time constant of channel deactivation.*

4.5.7 Temperature dependence

To measure the temperature dependence of $VGLUT1_{PM}$, the dual automatic temperature controller (TC-344C, Warner Instruments), in combination with the Single Inline Solution Heater (SH-27B, Warner Instruments) and the Quick change chamber (QE-2, multichannel systems) for 50 mm dishes were used. All measurements were started at room temperature and stepwise increased up to 40 °C. To avoid quenching of the GFP, fluorescence for normalization was always recorded *a priori* at room temperature. An Arrhenius plot was fitted by plotting the logarithmic value of the current amplitude or time constant (k) against the reciprocal value of the temperature (T in Kelvin) and fitted with the Arrhenius equation:

eq. 7
$$\mathbf{ln(k) = ln(A) - \frac{E_A}{R} \cdot \frac{1}{T}}$$

where A represents the pre-exponential factor, R the gas constant and E_A the activation energy. The temperature coefficient Q_{10} is a value for the relative change in 10°C of the analyzed parameter and was calculated by:

eq. 8
$$\mathbf{Q_{10} = \left(\frac{k_2}{k_1}\right)^{\frac{10K}{T_2 - T_1}}}$$

where T_2 is the higher temperature with k_2 as the parameter at this temperature and T_1 and k_1 at the lower temperature.

4.6 Data analysis and statistics

All data were analyzed using a combination of Fitmaster (HEKA Elektronik), Sigmaplot (version 12.5, Systat Software), Origin (Origin 2020, Electronic Arts), Excel (Excel 2010, Microsoft Corporation), and self-written scripts in Python (Anaconda 3, Continuum analytics; with the help of Daniel Kortzak and Claudia Alleva). Further image processing of the graphs was performed using CorelDRAW (CorelDRAW 2020, Corel Corporation). Figures of protein structures were generated using PyMOL [104].

Representative measurements were selected following the given mean values and filtered at 10 kHz for noise-free display. In some cases the capacitive peak was deleted for better representation. For presentation of currents measured with internal big anions, the background at pH 7.4 was fitted with a double exponential function and subtracted from the measurement at pH 5.5.

Unless otherwise stated, data are represented as mean ± 95% confidence interval (CI). For statistical analysis of two groups, t-test was performed when data were normally distributed and Mann-Whitney U-test was performed when data were not normally distributed. To compare more than one group for one variable one-way-ANOVA and for more than one variable two-way-ANOVA was performed after testing for normal distribution and homogeneity of variances. Data are considered significantly different if $p \leq 0.05$ (*), $p \leq 0.01$ (**), $p \leq 0.001$ (***) or $\chi 2 > 0.05$ (#) for Kruskal-Wallis one-way-ANOVA. Significant outliers were identified with the Grubbs test and excluded from the evaluation of mean values (specifically mentioned in the text). All data including outliers were also included in the Supplemental material.

Most data are presented as boxplots and include all single data and represent the mean value, median, upper and lower quartiles, and 95% CI as presented in Figure 4.2.

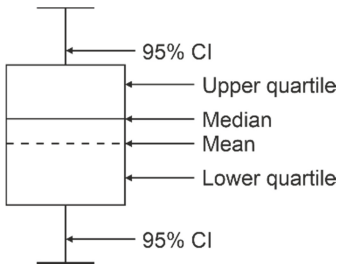

Figure 4.2 Composition of data representation in boxplots.

4.7 Manufacturers

Table 4.2 List of manufacturers

Company	Registered office
Continuum analytics	Austin, TX, USA
Corel Corporation	Ottawa, Canada
Electronic Arts	San Mateo, CA, USA
Forschungszentrum Jülich	Jülich, Germany
Gibco	Darmstadt, Germany
HEKA Elektronik	Lambrecht, Germany
Invitrogen	Carlsbad,CA, USA
Leica Microsystems	Wetzlar, Germany
Luigs & Neumann	Ratingen, Germany
Microsoft Corporation	Redmond, WA, USA
Molecular Devices	San José, CA, USA
Moyco Technologies	Montgomeryville, PA, USA
Multichannel systems	Reutlingen, Germany
Narishige	Amityville, NY, USA
SERVA	Heidelberg, Germany
Sigma Aldrich	Göttingen, Germany
Sutter Instrument	Novato, CA, USA
Systat Software	Frankfurt am Main, Germany
TCI- Tokyo Chemical Industry	Tokyo, Japan
ThermoFischer	Waltham, MA, USA
TMC	Peabody,MA, USA
Olympus Europa SE & Co. KG	Tokyo, Japan
Warner Instruments	Hamden, CT, USA

5 Results

5.1 VGLUT1$_{PM}$ exhibits an inward rectifying anion current that is allosterically activated by protons

VGLUT1 was inserted into the plasma membrane of transiently transfected HEK293T cells by neutralizing N- and C-terminal targeting signals in dileucine-like motifs [91] equal to Eriksen et al. (2016). The group additionally inserted a luminal hemagglutinin-tag (HA-tag) between TM one and two and identified the orientation of VGLUT$_{PM}$ with an antibody directed against HA-epitope. They showed that the physiological luminal facing part of the protein is oriented to the extracellular space as illustrated in Figure 5.1. In her bachelor thesis, Cora Hannack (2015) found in total seven amino acids (E_6,E_7,L_{11},E_{505},E_{506},F_{510},V_{511}) that she neutralized to alanines to robustly insert VGLUT to the plasma membrane [91] (in the following referred to as VGLUT1$_{PM}$; Suppl. Figure 8.1).

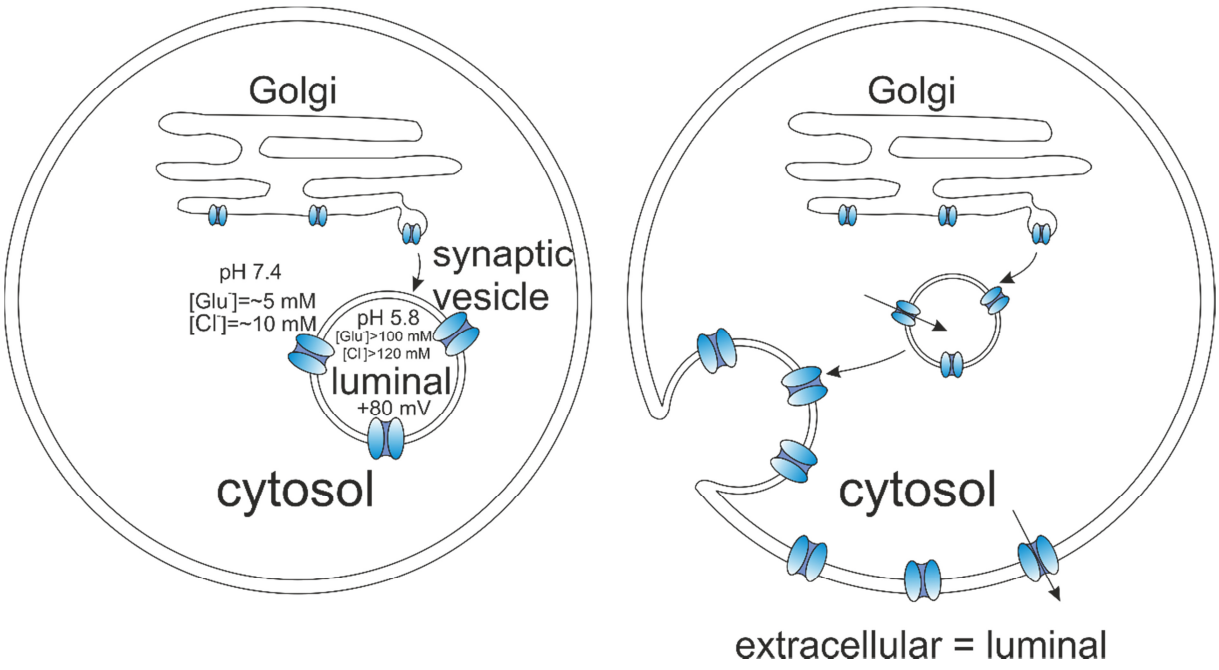

Figure 5.1 Orientation of VGLUTs. *Schematic presentation of the orientation of VGLUT under physiological conditions in the synaptic vesicle (left) and of VGLUT1$_{PM}$ in transiently transfected HEK293T cells (right). The fusion with the plasma membrane results in the luminal-directed side of the protein in VGLUT$_{PM}$ being exposed to the extracellular side.*

To verify the functionality and pH dependence of the VGLUT1$_{PM}$, cells were stimulated with voltages ranging from -160 to +20 mV and perfused externally with a Cl^--based solution at different pH's ranging from 7.4 to 5.0. Figure 5.2 A shows representative recordings at neutral pH 7.4 and at acidic pH 5.0 with Cl^- as internal permeable anion. The corresponding normalized current-voltage relationships are given in Figure 5.2 B. VGLUT1$_{PM}$ exhibits large inward rectifying anion currents that increase with more acidic external pH. Since the inward

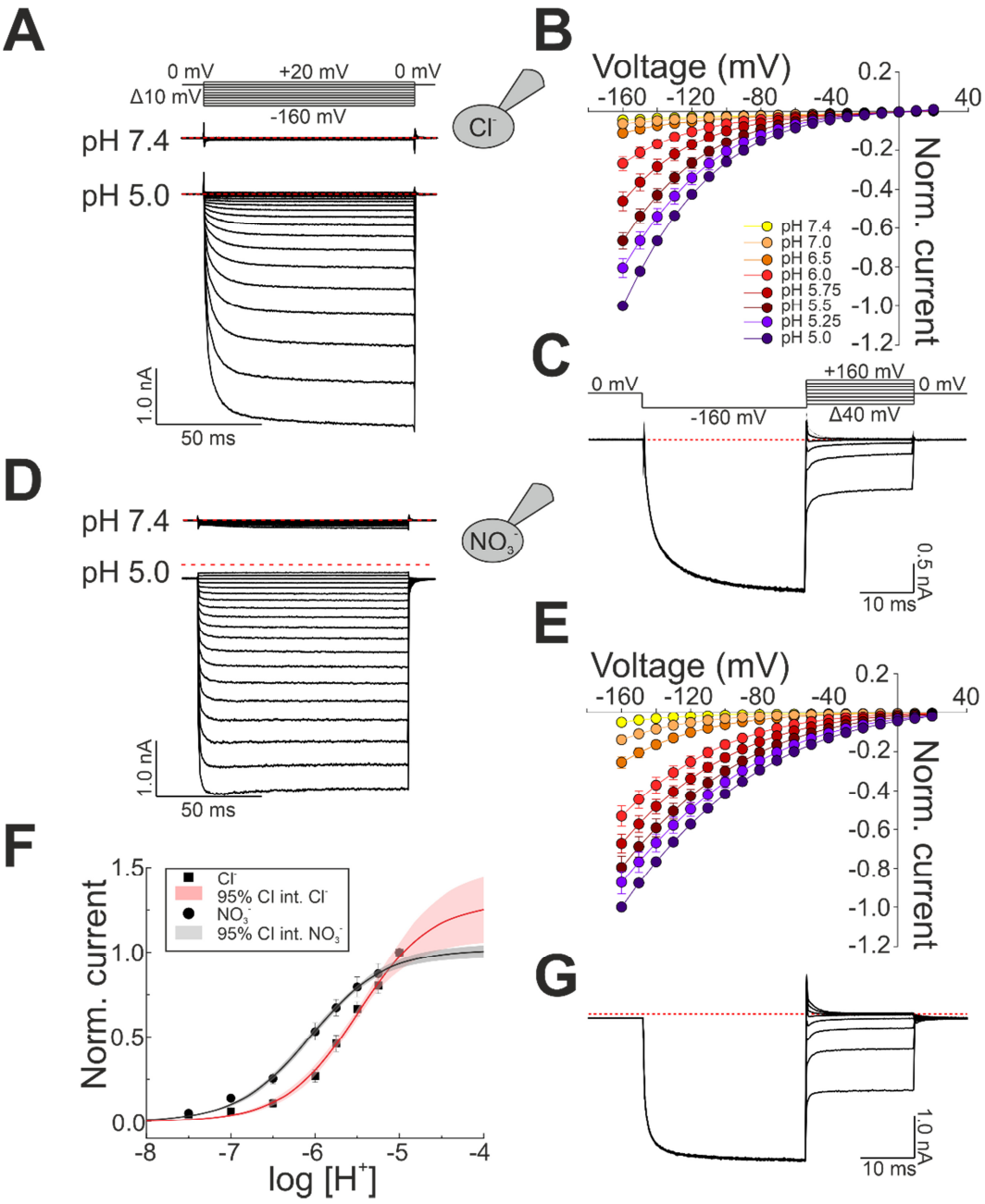

Figure 5.2 VGLUT1$_{PM}$ exhibits a strong inward rectifying anion current. ***A, D*** *Representative recordings clamped to voltages between -160 and +20 mV with Cl⁻ (**A**) or NO_3^- (**D**) as the permeable internal anion. Cells were exposed to Cl⁻-based solutions at different acidic pHs (red, dashed lines represent zero current).* ***B, E*** *Current-voltage relationship (IV) of VGLUT1$_{PM}$ to different extracellular pHs. Cells were normalized to pH 5.5 at -160 mV (n=27 for Cl⁻ (**B**) and n=12 for NO_3^- (**E**)).* ***C, G*** *Representative recordings of whole cell currents with internal Cl⁻ (**C**) or NO_3^- (**G**) that were stimulated between -160 and +160 mV with a prepulse at -160 mV (recorded by Yannick Güthoff).* ***D*** *Dose-Response curve at -160 mV for increasing $[H^+]_o$ for internal Cl⁻ (EC_{50}=5.49 ±0.06) or NO_3^- (EC_{50}=6.05 ± 0.02).*

rectifying currents correspond to the inward movement of cation/outward movement of anions by convention, these currents correspond to Cl^- diffusion from the cytoplasm to the extracellular space. The pH dependence of $VGLUT1_{PM}$ currents can be described by a dose-response relationship (Figure 5.2 F) that can be fit with an EC_{50} value of pH 5.49 ± 0.06 (Mean ± SD; n=27), similar to the data from Eriksen et al. (2016) for their membrane-bound VGLUT heterologously expressed in *Xenopus* oocytes. We did not observe anion currents when stepping from holding potential of 0 mV to positive voltages. Moreover, after an activating voltage step to -160 mV, currents quickly deactivate at depolarizing potentials (Figure 5.2 C,D; measured by Yannick Güthoff). In these recordings, capacitive currents were eliminated by subtracting the currents of inactivated VGLUTs at pH 7.4 from currents at pH 5.5.

In order to determine whether luminal protons activate VGLUT or if ΔpH serves as the driving force for the anion currents, we changed intracellular and extracellular pH to neutral or acidic values in Cl^--based solutions. Intracellular dialysis with acidic pH and extracellular perfusion of neutral solution fails to activate $VGLUT1_{PM}$, indicating that external (luminal) protons are necessary for the anion current. $VGLUT1_{PM}$ is tagged with a GFP at the C-terminus, allowing relative quantification of $VGLUT1_{PM}$ in cells by fluorescence measurements. To avoid a possible effect of quenching by intracellular anions, cells were imaged before entering the whole cell mode. Normalization to the fluorescence of the measured cells allows comparison of current amplitudes between cells with neutral and acidic internal pH. Figure 5.3 shows that luminal protons are required for activation of $VGLUT1_{PM}$, while cytoplasmic protons increase the amplitude by a factor of two (Table 5.1). The results suggest that at least one additional proton binding site on the cytoplasmic side exists next to the luminal binding side.

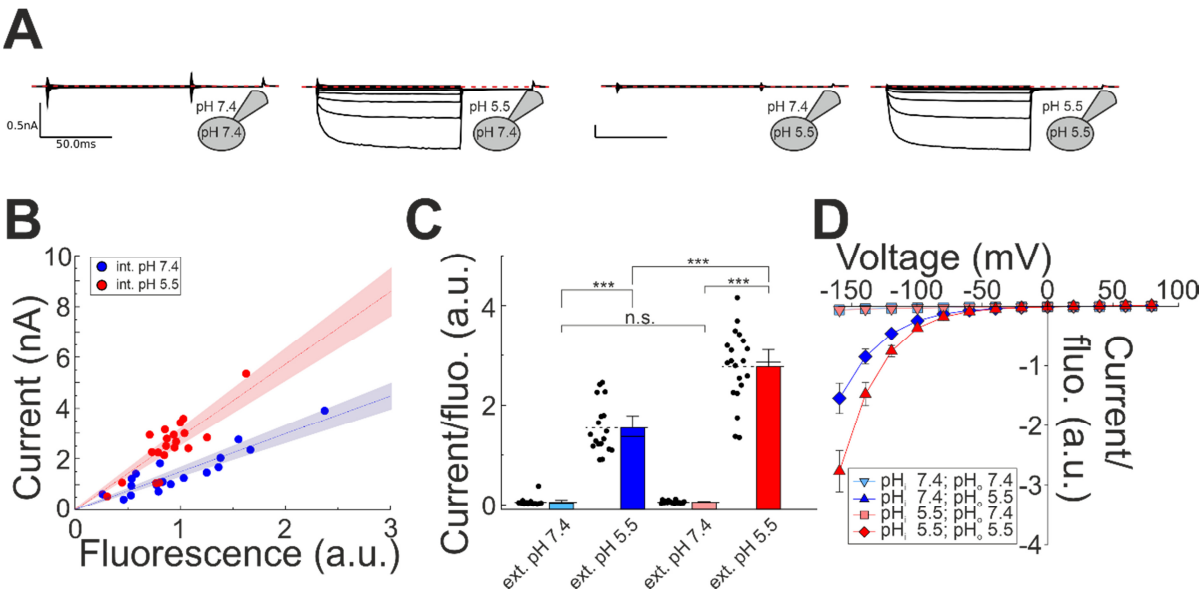

Figure 5.3 $VGLUT1_{PM}$ is activated by a luminal and stimulated by a cytoplasmic proton binding side. ***A*** *Representative whole cell recordings of HEK293T cells transiently transfected with WT*

VGLUT1$_{PM}$ at voltages between -160 and +20 mV. Cells were externally perfused and internally dialyzed with a Cl$^-$ based solution at pH 7.4 or 5.5. ***B*** *Whole cell fluorescence was measured for every recorded cell and plotted against its current amplitude at external pH 5.5. The light bars present the 95% CI. The fluorescence shows a linear correlation to the current amplitudes and can be used as a normalization factor for the data.* ***C*** *Comparison of current amplitudes normalized to fluorescence at -160 mV show significant differences between the individual conditions presented in (**A**). Luminal/external protons are mandatory to activate the channel but additional cytoplasmic protons modulate the current amplitude.* ***D*** *IV-relationships of the conditions shown in (**A**) (n=18-20).*

Table 5.1 Statistical analysis of the dependence of normalized current amplitudes on internal and external pH. *All pairwise comparisons are performed with the Holm-Sidak method.*

Statistical method	Condition pH	Norm. current	95% CI	n	Normality (Shapiro-Wilk)	Variance	p-value	Siginf.
Two-way-ANOVA	Int. 7.4 ext. 5.5	1540.3	254.7	18	Failed	Failed	<0.001	Yes ***
	Int. 7.4 ext. 7.4	53.3	40.8	18				
	Int 5.5 ext. 5.5	2769.3	344.3	20	Failed	Failed	<0.001	Yes ***
	Int. 5.5 ext. 7.4	53.9	11.7	20				
	Int. 7.4 ext 5.5	1540.3	254.7	18	Failed	Failed	<0.001	Yes ***
	Int. 5.5 ext. 5.5	2769.3	344.3	20				
	Int. 7.4 ext. 7.4	53.3	40.8	18	Failed	Failed	0.997	No
	Int. 5.5 ext. 7.4	53.9	11.7	20				

Anion channels are usually not selective for Cl$^-$ ions. There exist channels that prefer polyatomic anions (lyotropic selectivity sequence) and those that show the highest permeability to chloride. We replaced the internal anion Cl$^-$ by NO_3^- and observed that NO_3^- as an intracellular anion is also permeable to VGLUT1$_{PM}$ (Figure 5.2 D-G). NO_3^- current amplitudes were on average 4.4-times higher than in cells dialyzed with internal Cl$^-$ (more on this in chapter 5.2) and activated faster at hyperpolarizing voltages (Suppl. Figure 8.7). In addition, the EC_{50} with internal NO_3^- is shifted to pH 6.05 ± 0.02 (Mean ± SEM; n=12). Moreover, VGLUT1$_{PM}$ transfected cells already generate inward rectifying current at the holding potential of 0 mV, which was not present with internal Cl$^-$.

5.2 VGLUT1$_{PM}$ exhibits small unitary current amplitudes and short open times

Thus far, the transport mechanisms underlying the observed VGLUT anion currents have remained insufficiently understood. While it is suspected that VGLUT is a secondary active transporter, no clear evidence has been provided for coupled transport yet. In particular,

large current amplitudes and the absence of coupled proton transport for Cl^- suggest conduction through an aquous pore. A channel can be distinguished from a transporter by high single channel amplitudes. Single channel measurements provide a direct way to measure the amplitudes of individual proteins, but channels with low single channel amplitudes preclude such experiments because of background noises [99]. Noise analysis of macroscopic current amplitudes provides another possibility to differentiate transport processes. The noise in macroscopic currents conducted by ion channels arises from the random change between open and closed states of all ion channels. The power spectrum analysis allows to obtain the spectral density of these fluctuations, where ion channels show a power spectrum with a Lorentzian shape, compared to those of transporters which first increase and flatten at high frequencies [105,106].

Whole cell patch clamp measurements with Cl^- as the internal anion were used to investigate the transport mechanism of $VGLUT1_{PM}$ by noise analysis. The Fourier transform decomposes the anion currents into its frequencies and gives the power spectrum for $VGLUT1_{PM}$ at -100 mV. To account for background noise, the power spectrum at pH 7.4 was subtracted from that at pH 5.5 for 13 cells individually (Figure 5.4 A). The power spectrum could be fitted with eq. 3, a combination of pink noise and a double Lorentzian function. The pink noise with a slope of a=1.36 lies at the upper limit of the generally described 1/f noise [107,108]. The obtained corner frequencies (fc_1=265 Hz; fc_2=1456 Hz) predict very fast opening and closing of a channel. Upper bounds on the spectral density of transporter-mediated shot noise can be calculated using Schottky's theorem: S(f) = 2Iq, where I is the macroscopic current and q is the net charge transported per shot [108]. Calculated data for a uniporter ($S=3.7x10^{-29}$ A^2/Hz) are well below the spectral densities determined experimentally ($S_1=9.2x10^{-28}$ A^2/Hz; $S_2=6.2x10^{-28}$ A^2/Hz) and suggest a transport pathway through a channel. The power spectrum of untransfected HEK293T cells in acidic pH was mainly carried by the pink noise and resulted in indefinable scattering after subtraction of the spectrum in neutral pH (Suppl. Figure 8.2). The power spectrum results show that the current variances with internal Cl^- in $VGLUT1_{PM}$ results from the random opening and closing of ion channels, thus permitting noise analysis to study single channel amplitudes.

For stationary noise analysis, whole cell currents were measured with Cl^- as the internal permeable anion. The number of open channels was changed by stepwise perfusion of external solution with acidic pH's. The current variance was measured in the steady state from 100-500 ms long voltage steps and plotted against the current amplitude. Figure 5.4 B shows representative current-variance plots fitted with a parabola according to eq. 6. In order to minimize the least squares, eq. 6 was globally fitted to all 15 current-variance plots, keeping the single channel amplitude i constant while the number of channels between cells remained variable. The steady-state noise analysis yields a single-channel amplitude of

24.3 ± 2.4 fA (Mean ± SD) at -160 mV, which corresponds to a transport rate of ~150,000 anions per second. Similar rates could also be determined for ion channels [100,109] and exceed values for carriers or transporters [110,111].

According to eq. 5, the macroscopic amplitude, the single channel amplitude, and the number of transporters can be used to determine the probability of finding the channels in an open state. For WT VGLUT1$_{PM}$, we were able to determine an open probability of ~24%. Other secondary active transporters with anion channels, such as EAATs, exhibit much lower open probabilities of ~0.1% [109,112,113].

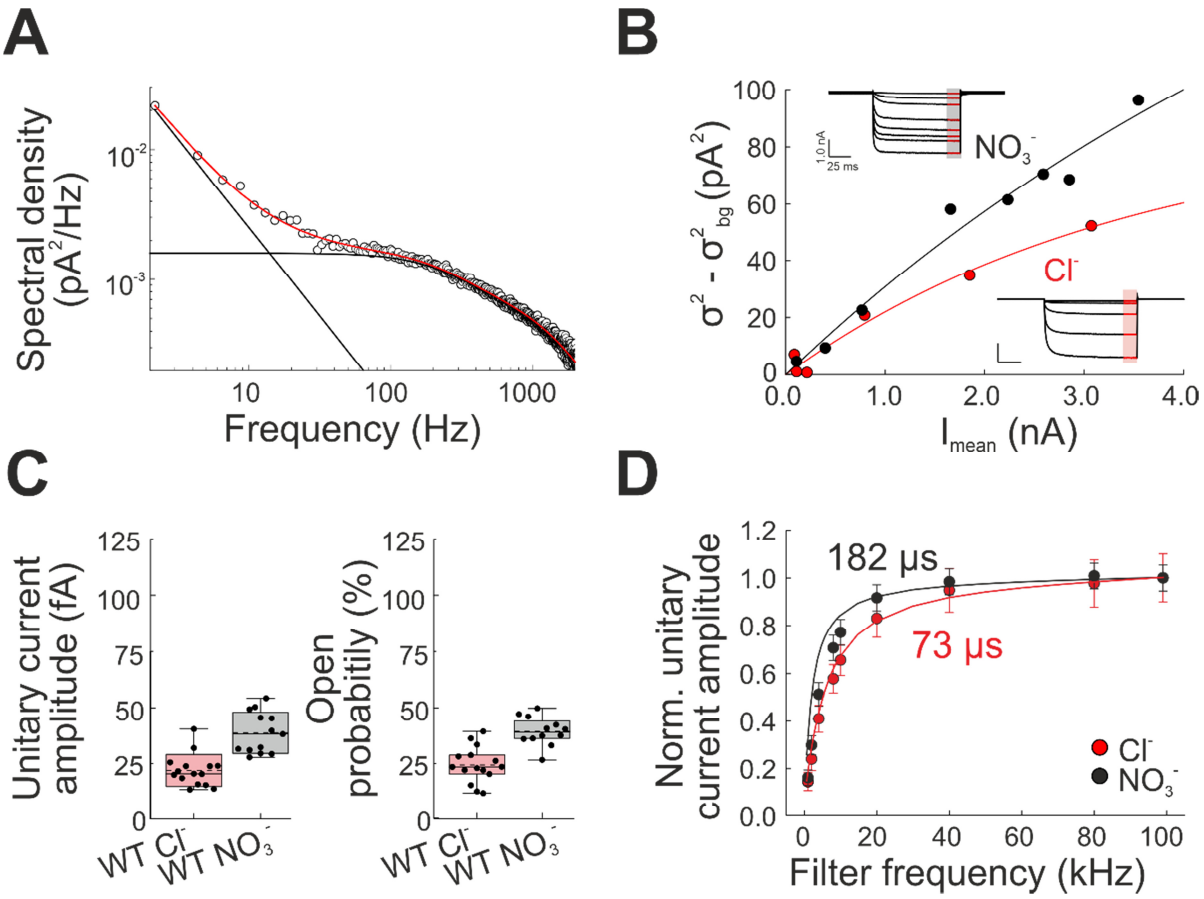

Figure 5.4 Unitary properties of VGLUT1$_{PM}$. ***A*** *Averaged power spectrum of the anion currents at -100 mV of 13 cells expressing VGLUT1$_{PM}$ with internal Cl^- at pH 5.5 after subtraction of the background at pH 7.4. The red line represents a combination of pink noise with a second-order Lorentzian function and the black lines the individual components of the fit.* ***B*** *Representative current variance plots of stationary noise analysis at -160 mV with internal Cl^- (red) or NO_3^- (black). The variance was measured at steady state current during perfusion of different pH's (insets).* ***C*** *Statistical analysis of the single channel amplitudes from the stationary noise analysis.* ***D*** *Dependence of the experimentally obtained individual amplitudes on the low-pass filter frequency. The curves represent simulated open times of unitary events.*

As previously discussed, significantly increased macroscopic currents were determined with NO_3^- as an internal anion. To investigate whether this difference was due to increased single

channel amplitude, the stationary noise analysis was performed under the same conditions with NO_3^- as the permeable anion. In order not to exceed the capacities of the used amplifier and to keep the macroscopic current below 10 nA, an inducible stable FlpIn cell line with $VGLUT1_{PM}$ was used for this experiment. Previous experiments have shown that HEK293T and FlpIn cells generate similar values in noise analysis for EAAT2 [109]. We observed slight but not significant increased single channel amplitudes (i=39 ± 2.1 fA; n=13) and open probabilities (39%) with NO_3^- (Figure 5.4 B,C). The 1.6-fold increased single channel amplitude, as well as the 1.6-fold increased open probability together cannot solely explain the more than four times increased macroscopic current.

Next, the filter dependence of $VGLUT1_{PM}$ noise analysis was investigated to estimate mean open times of $VGLUT1_{PM}$. When the channel opening lasts longer than 1/filter frequency, only small effects on the single channel amplitudes are expected, whereas a reduction of the low-pass filter frequency results in reduction of apparent i at lower values [98,100]. Figure 5.4 D shows the effect of the filter frequency on the apparent single channel amplitudes for Cl^- and NO_3^-. The curves represent simulated data where the open time is closest to the experimental data (simulated curves Cl^- = 72 µs; NO_3^- = 183 µs). The comparison of the experimental and simulated data shows that $VGLUT1_{PM}$ is an anion channel with a very short open time. It should be mentioned that the data for the stationary noise analysis were recorded with two different amplifiers (HEKA and SutterPatch). Suppl. Figure 8.3 shows the individual values for the unitary amplitudes with both amplifiers. Statistical tests show that the unitary amplitudes and the filter dependence are independent of the used amplifier.

5.3 $VGLUT1_{PM}$ has a broad selectivity filter with a lyotropic anion selectivity

In chapter 5.1 it has already been shown that $VGLUT1_{PM}$ anion channels exhibit a lyotropic anion selectivity. Anion selectivity can be analysed by the permeability of anions, calculated from the reversal potentials, or by comparing current amplitudes carried by different anions. Since the permeable anions in this work are intracellular and internal dialysis during an experiment is slow and not accurate, currents obtained on different cells were compared after normalization to whole cell fluorescence.

In addition to chloride (Cl^-) and nitrate (NO_3^-), bromide (Br^-) and iodide (I^-) were tested for permeability to $VGLUT1_{PM}$. Figure 5.5 A shows representative measurements at pH 5.5 and 40 mM external Cl^- for activation (residual gluconate). All cells were initially measured at neutral pH 7.4. The lack of activation by luminal/extracellular protons resulted in deactivation/closure of the anion channels and was subtracted from the current amplitudes at pH 5.5 as background current. Untransfected cells showed no currents under the experimental conditions (Figure 5.5 B). The fluorescence-current relationships in Figure

5.5 C show a linear increase in current with fluorescence, so it can be assumed that the ratio between internally localized proteins and proteins in the plasma membrane varies little in the experiments and can be used as a current normalization for all conditions (Figure 5.5 D). With internal NO_3^- or I^-, $VGLUT1_{PM}$ conducts negative currents at 0 mV, consistent with a lyotropic anion selectivity. All currents could also be activated without external perfusion of Cl^-, but the current amplitudes were significantly smaller (Suppl. Figure 8.4).

To characterize glutamate transport by $VGLUT1_{PM}$, the intracellular Cl^- was completely replaced by glutamate. Figure 5.5 E shows a representative HEK293T cell measured under these conditions. To avoid intracellular contamination with external Cl^-, cells were held at a holding potential of -50 mV between measurements. In addition, cells were kept in solutions without Cl^- and exposed to external Cl^- only for limited recording times. All measurements were performed first at neutral pH 7.4 and then at acidic pH 5.5. The background current at neutral pH was subtracted from the acidic pH after the measurements for all evaluations. Untransfected control cells showed no effect under these conditions (Figure 5.5 E, F, dashed lines). Equal to the Cl^--current in Figure 5.2, the amplitude of glutamate currents is depending on the luminal pH with an EC_{50} of 5.2 ± 0.12 (n=10; Suppl. Figure 8.6). An increase in external $[Cl^-]$ also indicates a concentration-induced increase in current across all voltages and suggests the presence of a Cl^--activated glutamate current (Suppl. Figure 8.6). While low Cl^- concentrations result in an increase in current amplitude, high $[Cl^-]$ above 40 mM appear to result in a decreased current amplitude. This biphasic activation by Cl^- is resembling the biphasic glutamate uptake in reconstituted vesicles [45,47]. Measurements with the stationary noise analysis under glutamate-transport-conditions show no correlation between variance and the current amplitude, possibly due to its low current amplitude (Suppl. Figure 8.6).

We also tested different polyatomic anions for their permeability in $VGLUT1_{PM}$. Surprisingly, currents could also be detected for aspartate (asp^-) as an internal anion, although earlier experiments indicate strong glutamate over aspartate selectivity for VGLUT1 transport [44,45]. Similar results can be seen in Figure 5.5 E-G also for the anions gluconate ($gluc^-$), bicarbonate (HCO_3^-), 2-(N-Morpholino)ethanesulfonic acid (MES^-), methanesulfonic acid (MSA^-), and isethionate ($Iset^-$). Current amplitudes at -160 mV normalized to their fluorescence decrease in the order HCO_3^->MSA^->$Iset^-$>MES^->Asp^->$Glut^-$>$Gluc^-$. HCO_3^- current amplitudes are in between the values of small anions such as Cl^- or Br^- and large anions such as glutamate or aspartate. Many of the anions also exhibit outward currents allowing the calculation of reversal potentials. This current represents the influx of Cl^- and is the electrophysiological counterpart of the recently proposed Cl^-/glutamate exchange during glutamate loading after endocytosis of synaptic vesicles [19]. Figure 5.5 H shows the reversal potentials of all measured cells. It is striking that glutamate (-6.0 ± 11.6 mV; n=25) and HCO_3^- (-13.5 ± 16.4 mV; n=11) show a significantly more positive E_{rev} than gluconate

(-73.8 ± 14.1 mV; n=12), aspartate (-59.5 ± 8.2 mV; n=11), MES (63.7 ± 7,8 mV; n=10), MSA (-56.7 ± 11.1 mV; n=9) or isethionate (-75.8 ± 5.0 mV; n=14). The results suggest that $VGLUT1_{PM}$ can transport glutamate and HCO_3^- into synaptic vesicles even at less positive potentials, whereas the other big anions are transported only at very positive potentials under physiological conditions.

Table 5.2 Statistical analysis of reversal potentials with big polyatomic anions. *Data passed Normality test (Shapiro-Wilk) and variance test. All pairwise comparisons were made with One-Way ANOVA with Holm-Sidak post hoc test.*

Comparison	**p**	**p<0.050**	**Comparison**	**p**	**p<0.050**
$Glut^-$ vs. $Iset^-$	<0.001	Yes	Asp^- vs. $Iset^-$	0.005	Yes
$Glut^-$ vs. $Gluc^-$	<0.001	Yes	Asp^- vs. $Gluc^-$	0.023	Yes
$Glut^-$ vs. MES^-	<0.001	Yes	Asp^- vs. MES^-	0.778	No
$Glut^-$ vs. Asp^-	<0.001	Yes	Asp^- vs. MSA^-	0.815	No
$Glut^-$ vs. MSA^-	<0.001	Yes	$Gluc^-$ vs. MSA^-	0.007	Yes
$Glut^-$ vs. HCO_3^-	0.296	No	$Gluc^-$ vs. MES^-	0.204	No
HCO_3^- vs. $Iset^-$	<0.001	Yes	$Gluc^-$ vs. $Iset^-$	0.653	No
HCO_3^- vs. $Gluc^-$	<0.001	Yes	MSA^- vs. $Iset^-$	0.001	Yes
HCO_3^- vs. MES^-	<0.001	Yes	MSA^- vs. MES^-	0.534	No
HCO_3^- vs. Asp^-	<0.001	Yes	MES^- vs. $Iset^-$	0.071	No
HCO_3^- vs. MSA^-	<0.001	Yes			

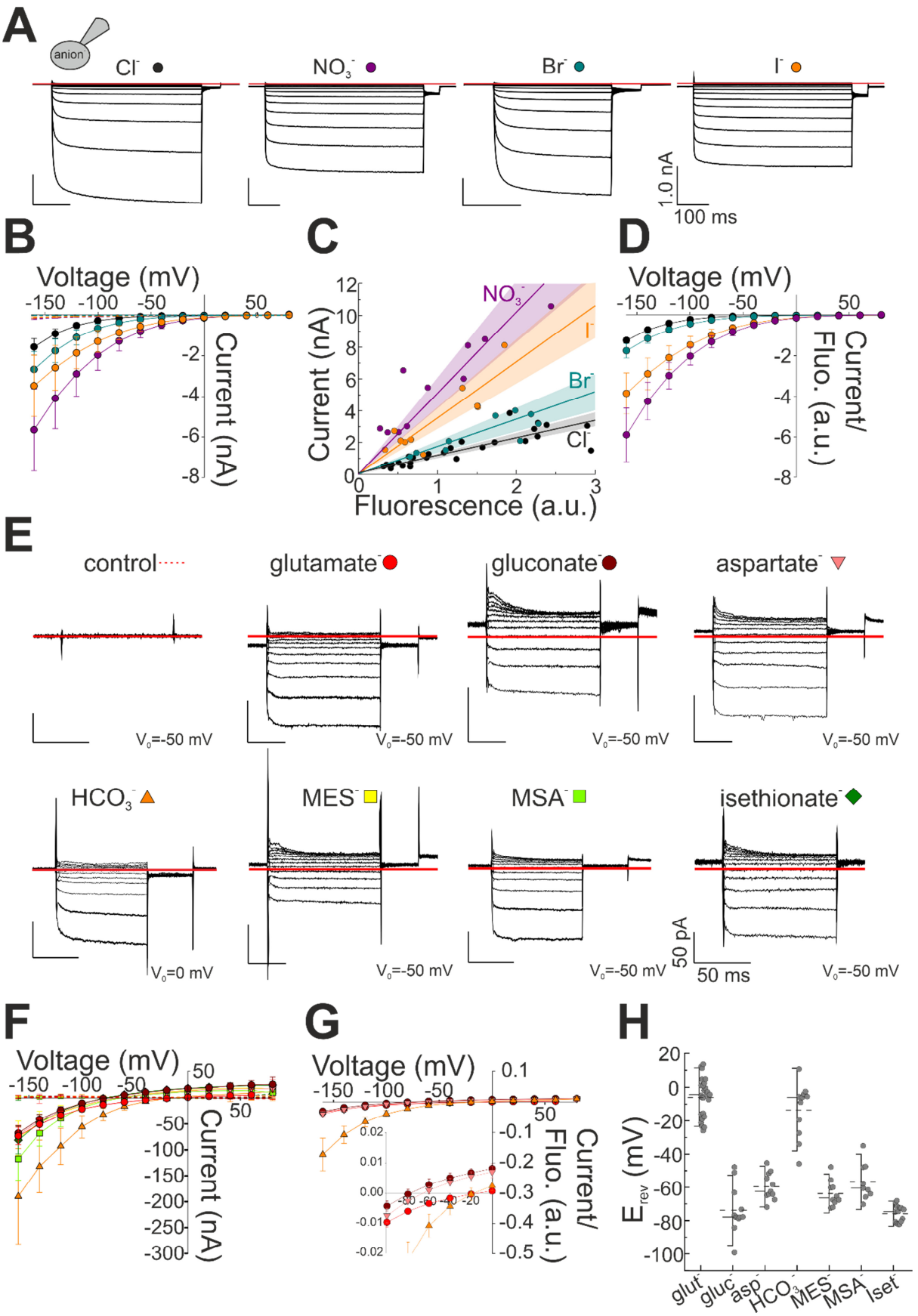

Figure 5.5 VGLUT1$_{PM}$ is permeable to several small and large anions. ***A*** *Representative recordings of various small internal anions between -160 and +80 mV at external pH 5.5 and 40 mM* Cl^-*. Background currents at neutral pH 7.4 were subtracted from all data.* ***B*** *IV-relationships of the*

*mean currents demonstrated in (**A**), error bars represent 95% CI. Dashed lines represent untransfected cells. **C** The whole cell fluorescence is linearly correlated with the current amplitude. **D** IV-ratio of data from (**B**) normalized to fluorescence in (**C**). **E** Representative measurements with different internal polyatomic anions. Control shows an untransfected cell with glutamate as internal anion. Absolute (**F**) and normalized (**G**) averaged IV-ratios of the anions from (**E**). **H** The inward and outward rectifying current allows the determination of the reversal potential (E_{rev}).*

5.4 VGLUT1$_{PM}$ does not mediate H^+-glutamate exchange

The more positive reversal potential of glutamate currents might be due to stoichiometric coupling of glutamate transport with another ion. Since many vesicular neurotransmitter transporters are coupled to the transport of H^+, this might be also the case for VGLUT. This theory has been discussed controversially in recent years [34,44,55,114]. Especially the channel function of VGLUT and its activation by H^+ and Cl^- pose experimental obstacles for the researchers.

To separate a potential H^+-coupled glutamate transport from currents conducted by VGLUT1$_{PM}$ anion channels, we used identical Cl^- and glutamate concentrations on both sides of the cell (80 mM glutamate, 30 mM Cl^-). Under these conditions, all possible current components, such as the glut$^-$/H^+ exchange, the anion channel, and also the leak current should be in equilibrium at 0 mV and pH 7.4 on both sides. By lowering the external pH from 7.4 to 5.5, a proton gradient is created that does not affect the reversal potential for anion and leak conductance, but generates coupled H^+/glutamate transport.

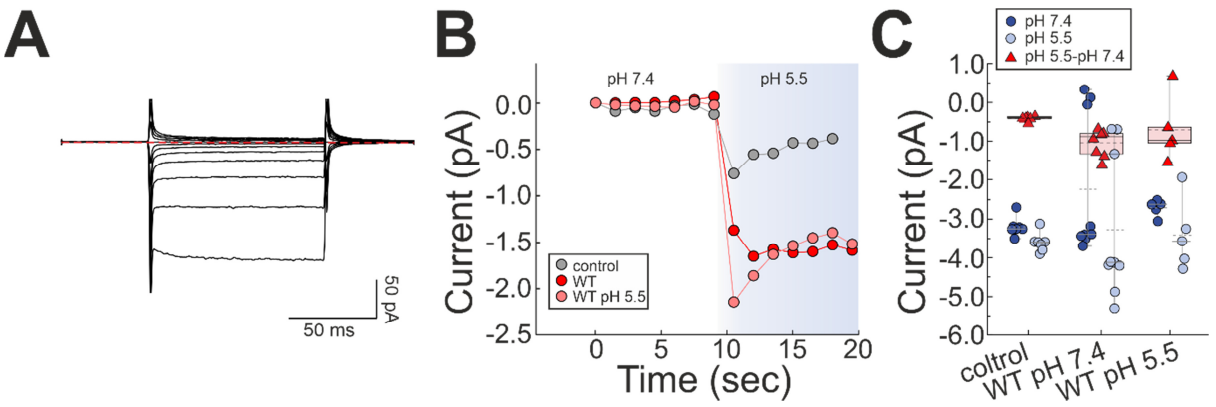

Figure 5.6 VGLUT1$_{PM}$ does not exhibit glut$^-$/H^+ exchange. *Equal ionic conditions were created on both sides of the membrane (80 mM Glut$^-$, 30 mM Cl$^-$).**A** Representative recording with internal pH 7.4 and external pH 5.5 at voltages between -160 and +80 mV serves as a control for proper perfusion. **B** Time courses of cells with internal pH 7.4 for untransfected cells (grey) and VGLUT1$_{PM}$ (red) or with internal pH 5.5 (pink). First, cells were perfused with neutral, followed by acidic solution. **C** Current amplitudes for the conditions shown in (**B**) with external pH 7.4 (dark blue), pH 5.5 (light blue) and pH 5.5 – pH 7.4 (red).*

To test for $VGLUT1_{PM}$ function under these conditions, cells were stimulated between -160 and +80 mV. All cells showed an activated current at external pH 5.5 (Figure 5.6 A). Figure 5.6 B, C show representative time courses and statistics for untransfected cells as control (n=7), and for cells transfected with $VGLUT1_{PM}$ with internal pH 7.4 (n=8) and internal pH 5.5 (n=5). We only observed extremely small currents (1.04 ± 0.3 pA) in $VGLUT1_{PM}$ transfected cells, however more than in untransfected cells (0.4 ± 0.06 pA). In experiments with internal acidic pH, i.e. without proton gradient after external acidification, similar current amplitudes were observed. These results suggest that coupled proton/glutamate currents are – if any – extremely small.

5.5 $VGLUT1_{PM}$ with point mutation H120A has impaired glutamate uptake ability and altered anion conductance

Juge et al. (2006) recently studied several point mutations with radioactive uptake assays with VGLUT2 reconstituted in lipid vesicles. A histidine at position 128, at the end of the second transmembrane domain, projects towards the central cavity (Suppl. Figure 8.1 C) and leads to an almost complete inhibition of VGLUT2 uptake when exchanged to alanine. We inserted the analogous mutation H120A into $VGLUT1_{PM}$ and investigated its effect on the experiments described above using whole cell patch clamp and fluorescence spectroscopy. Confocal images show that H120A does not prevent the expression of VGLUT in the plasma membrane (Suppl. Figure 8.1 B). Nevertheless, the mutation can alter the distribution between intracellular and plasma membrane expression, so that in the following whole cell current amplitudes cannot be directly compared with wild type (WT).

Figure 5.7 A shows representative currents, analogous to Figure 5.2 A with Cl^- at different external pH values. Like the WT $VGLUT1_{PM}$, the anion channel in H120A $VGLUT1_{PM}$ exhibits strong inward rectifying currents at luminal/extracellular acidic pH, although the EC_{50} for proton binding is shifted to more acidic values (EC_{50}=5.17 ± 0.08 for internal Cl^- and 5.78 ± 0.04 for internal NO_3^-; Figure 5.7 A). However, the time constants, i.e. the opening and closing of the channels are significantly slower in contrast to the WT (Suppl. Figure 8.7). The strongly inward rectifying anion conduction is also not affected by the mutation.

Next, the single channel amplitude of H120A $VGLUT1_{PM}$ was determined using the stationary noise analysis introduced in chapter 5.2. Figure 5.7 C shows the single channel amplitudes of all measured cells for WT and H120A with Cl^- and NO_3^- as internal anions. The single channel amplitude does not significantly change between Cl^- (52.4 ± 3.0 fA; n=13) and NO_3^- (62.8 ± 2.1 fA; n=15) within the mutated construct. However, the single channel amplitudes are almost twice as big as for WT. The open times for Cl^- and NO_3^- in H120A were similarly short as in WT, in agreement with a flickering mutant anion channel. In contrast to the WT, channel open times are higher for Cl^- than for NO_3^- (Figure 5.7 D).

Table 5.3 Statistical analysis of the data obtained by stationary noise analysis for WT and H120A VGLUT1$_{PM}$. *All pairwise comparisons are performed with Dunn's method.*

Statistical method	condition	Mean global fit	SD	Mean single fit	SD	n	Normality test (Shapiro-Wilk)	Variance	p-value	Sign.
Kruskal-Wallis One Way ANOVA	WT Cl^-	24.3	2.4	21.8	7.1	15	Passed	Failed	χ^2>0.05	No
	WT NO_3^-	39.0	2.1	38.7	9.3	13	p= 0.067			
	H120A Cl^-	52.4	3.0	53.6	13.7	13	Passed	Failed	χ^2>0.05	No
	H120A NO_3^-	62.8	2.1	63.1	19.5	15	p= 0.067			
	WT Cl^-	24.3	2.4	21.8	7.1	15	Passed	Failed	χ^2<0.05	Yes
	H120A Cl^-	52.4	3.0	53.6	13.7	13	p= 0.067			
	WT NO_3^-	39.0	2.1	38.7	9.3	13	Passed	Failed	χ^2<0.05	Yes
	H120A NO_3^-	62.8	2.1	63.1	19.5	15	p= 0.067			
	WT Cl^-	24.3	2.4	21.8	7.1	15	Passed	Failed	χ^2<0.05	Yes
	H120A NO_3^-	62.8	2.1	63.1	19.5	15	p= 0.067			
	WT NO_3^-	39.0	2.1	38.7	9.3	13	Passed	Failed	χ^2<0.05	Yes
	H120A Cl^-	52.4	3.0	53.6	13.7	13	p= 0.067			

Similar to the WT, the mutant transporter shows a strong inward rectification at depolarizing voltages towards Cl^-, NO_3^-, Br^- and I^- with a lyotropic anion selectivity. A quantitative comparison of the current amplitudes normalized to the fluorescence with the wild type is not possible due to the variation of the distribution of the proteins by the mutation (Suppl. Figure 8.1), but the relative currents can be compared. Thus, H120A VGLUT1$_{PM}$, unlike the WT, shows a strongly reduced amplitude for Iodide relative to other anions.

In the presence of polyatomic anions, currents could be observed in both directions, similar to WT (Figure 5.7 F, H). In contrast, all currents except HCO_3^- reverse at negative potentials (Figure 5.7 I). To statistically compare the reversal potentials for both constructs, significant outliers were tested with Grubbs test and excluded from the analysis (all data points are shown in Suppl. Figure 8.5).

Table 5.4 Statistical analysis of reversal potentials with big polyatomic anions for H120A VGLUT1$_{PM}$. *Data passed Normality test (Shapiro-Wilk) and failed variance test. All pairwise comparisons were made with One-Way ANOVA on Ranks with Dunn's post hoc test.*

Comparison	p<0.050
HCO_3^- vs. Asp^-	Yes
HCO_3^- vs. $Gluc^-$	Yes
HCO_3^- vs. $Glut^-$	Yes
$Glut^-$ vs. Asp^-	Yes
$Glut^-$ vs. $Gluc^-$	Yes
$Gluc^-$ vs. Asp^-	No

Table 5.5 Statistical analysis of reversal potentials with big polyatomic anions for WT and H120A VGLUT1$_{PM}$.

Condition	Test	Normality	Variance	p	p<0.050
$Glut^-$	MW-U test	passed	failed	<0.001	Yes
$Gluc^-$	t-test	passed	passed	0.268	No
Asp^-	t-test	passed	passed	<0.001	Yes
HCO_3^-	t-test	passed	passed	0.268	No

Figure 5.7 J shows relative permeability for various anions and for WT and H120A VGLUT1$_{PM}$ plotted against the anion size. The pore size of VGLUT must be at least the size of the smallest diameter of the largest anion. The ion diameters were adapted from Linsdell et al. (1997) and Linsdell and Hanrahan (1998) and the relative permeability was calculated with the Goldmann-Hodgkin-Katz equation. MES permeability indicates a minimum pore diameter of 6.5 Å for WT VGLUT1$_{PM}$, and aspartate permeability a minimum pore diameter of 6.2 Å for H120A VGLUT1$_{PM}$. MES was not measured in H120A VGLUT1$_{PM}$. We conclude that H120A, a point mutation that was reported to abolish glutamate transport, modifies multiple pore properties of VGLUT1$_{PM}$.

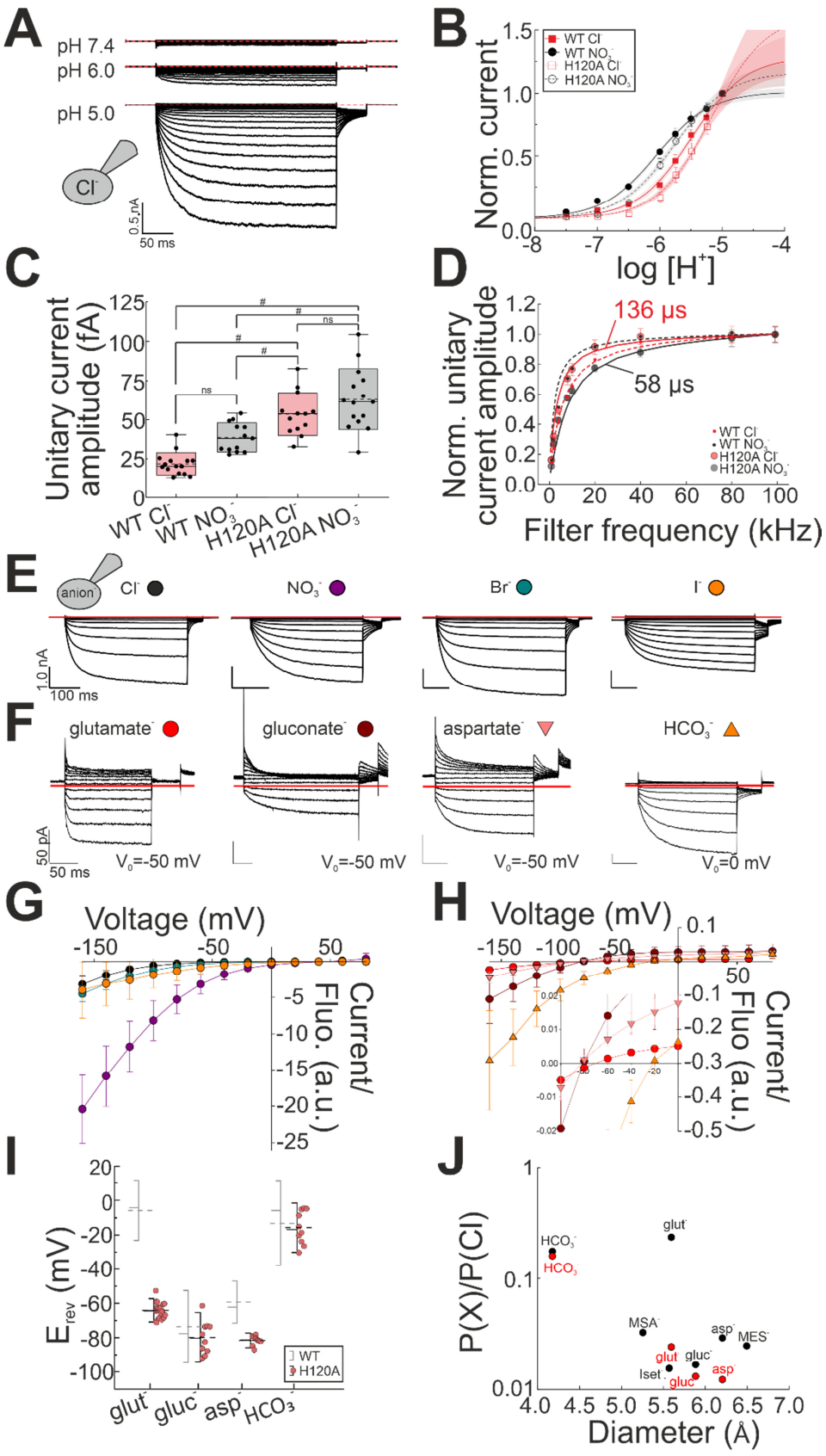

Figure 5.7 The point mutation H120A in VGLUT1$_{PM}$ alters anion channel properties and anion selectivity. ***A*** *Representative measurements of HEK293T cells transiently transfected with H120A VGLUT1$_{PM}$. Cl⁻ serves as an internal permeable anion and cells were perfused externally with a Cl⁻-based solution at different pHs.* ***B*** *Dose-response curve at -160 mV for increasing [H⁺] for internal Cl⁻*

or NO_3^- for WT (EC_{50}=5.5 ± 0.06 with Cl^- n=27; EC_{50}=6.1 ± 0.02 with NO_3^- n=12) or H120A VGLUT1 $_{PM}$ (EC_{50}=5.2 ± 0.08 with Cl^- n=17; EC_{50}=5.8 ± 0.04 with NO_3^- n=15). ***C*** *Single channel amplitudes from stationary noise analysis for Cl^- and NO_3^- for WT and H120A. # indicates statistical significance, tested by one-way ANOVA, ns denotes not significant.* ***D*** *Dependence of the experimentally determined unitary amplitudes on the low-pass filter frequency. The curves represent simulated open times of single events.* ***E*** *and* ***F*** *show respectively representative measurements of different small (**E**) and large (**F**) anions stimulated between -160 and +80 mV in 20 mV steps at pH 5.5. Background currents at pH 7.4 were subtracted from all data. Averaged IV-ratios of all small anions (**G**) shown in (**E**) or the large anions (**H**) shown in (**F**). The inset in (**H**) gives a magnification of the currents in the region of their reversal potentials, presented individually in (**I**) for H120A. Gray lines represent WT values shown in Figure 5.5 H.* ***J*** *Relative permeability of the large anions as a function of the mean ion diameter. The anion pore has a minimum diameter equal to the size of the largest permeable ion, which is 6.5 Å for WT (black) and 6.2 Å for H120A (red).*

5.6 Glutamate blocks anion currents from luminal and cytoplasmic side

Glutamate and Cl^- were suggested to compete for the same binding site and that glutamate blocks Cl^- currents [49].

We studied cells in the whole cell configuration perfused with 40 mM Cl^- to activate the channel together with 100 mM glutamate or gluconate at pH 5.5. Three intracellular conditions were used: Internal Cl^- only (left), Cl^- and gluconate (middle), and Cl^- and glutamate (right). The simultaneous measurement of fluorescence allowed normalization of whole cell currents to $VGLUT1_{PM}$ expression levels (Figure 5.8 A). For all internal solutions, external glutamate reduced amplitudes compared to cells perfused with gluconate for WT and also for H120A $VGLUT1_{PM}$.

Cells dialyzed with glutamate exhibit measureable currents at positive potentials, suggesting that glutamate might modify gating of $VGLUT1_{PM}$. We studied the time courses of channel deactivation (recovery) of the anion current using a double-pulse protocol [101–103] as described in chapter 4.5.6. Two activating pulses, first at -140 mV, then at -120 mV, were separated in time by a depolarizing pulse of variable length (2-60 ms) at +120 mV, thus changing the channel conformation from open to closed to open again. The increasing length of the depolarizing pulse raises the probability of the channel closure before it opens again. Figure 5.8 C and Table 5.6 and Table 5.7 show the time courses of the instantaneous current of all averaged cells at -120 mV for all conditions. The results show on the one hand that glutamate decreases the current amplitude but on the other hand also affects the deactivation of the channels at positive potentials dramatically.

But not only external glutamate showed a blocking effect of the current, also with internal glutamate the currents are significantly smaller in contrast to gluconate (Figure 5.8 right).

Deactivation by positive voltages was also almost completely blocked by glutamate on both sides, indicating that the channels were already open during the subsequent depolarization. Interestingly, the blocking effect of internal glutamate is much more pronounced in H120A than in WT (compare Figure 5.8 A middle and right). In contrast, the deactivation by depolarization is almost completely abolished in WT, whereas it still seems to be slightly active in H120A.

We conclude that external, but especially internal glutamate has a blocking effect on the Cl^- permeation of WT and H120A $VGLUT1_{PM}$ by binding to the same binding site and thereby occupying the pore. Gluconate and glutamate both appear to bind less tightly to H120A than to WT $VGLUT1_{PM}$.

Table 5.6 Statistical analysis of the blocking effect of glutamate on the anion channel amplitude and deactivation in WT $VGLUT1_{PM}$.

Int.	Ext.	n	slope	Test	Sign. Fluo	Tau (ms)	Sign. Tau
Cl^-	$Gluc^-$	10	0.0010	F-Test	p=0.14873 n.s	8.5	p<0 ***
Cl^-	$Glut^-$	10	0.0008			9.5	
$Gluc^-$	$Gluc^-$	11	0.0006	F-Test	p=0.00112 **	9.1	p<0 ***
$Gluc^-$	$Glut^-$	11	0.0005			6.9	
$Glut^-$	$Gluc^-$	11	0.0004	F-Test	p=0.037 *	11.4	p<0 ***
$Glut^-$	$Glut^-$	11	0.0003			31.0	

Table 5.7 Statistical analysis of the blocking effect of glutamate on the anion channel amplitude and deactivation in H120A $VGLUT1_{PM}$.

Int.	Ext.	n	slope	Test	Sign. Fluo	Tau (ms)	Sign. Tau
Cl^-	$Gluc^-$	11	0.0022	F-Test	p=0.0003 ***	5.5	p=0 ***
Cl^-	$Glut^-$	11	0.0013			5.1	
$Gluc^-$	$Gluc^-$	11	0.0017	F-Test	p=0.0011 **	5.2	p=0 ***
$Gluc^-$	$Glut^-$	11	0.0009			4.3	
$Glut^-$	$Gluc^-$	11	0.0003	F-Test	p=0.0098 **	7.2	p=0 ***
$Glut^-$	$Glut^-$	11	0.0002			28.4	

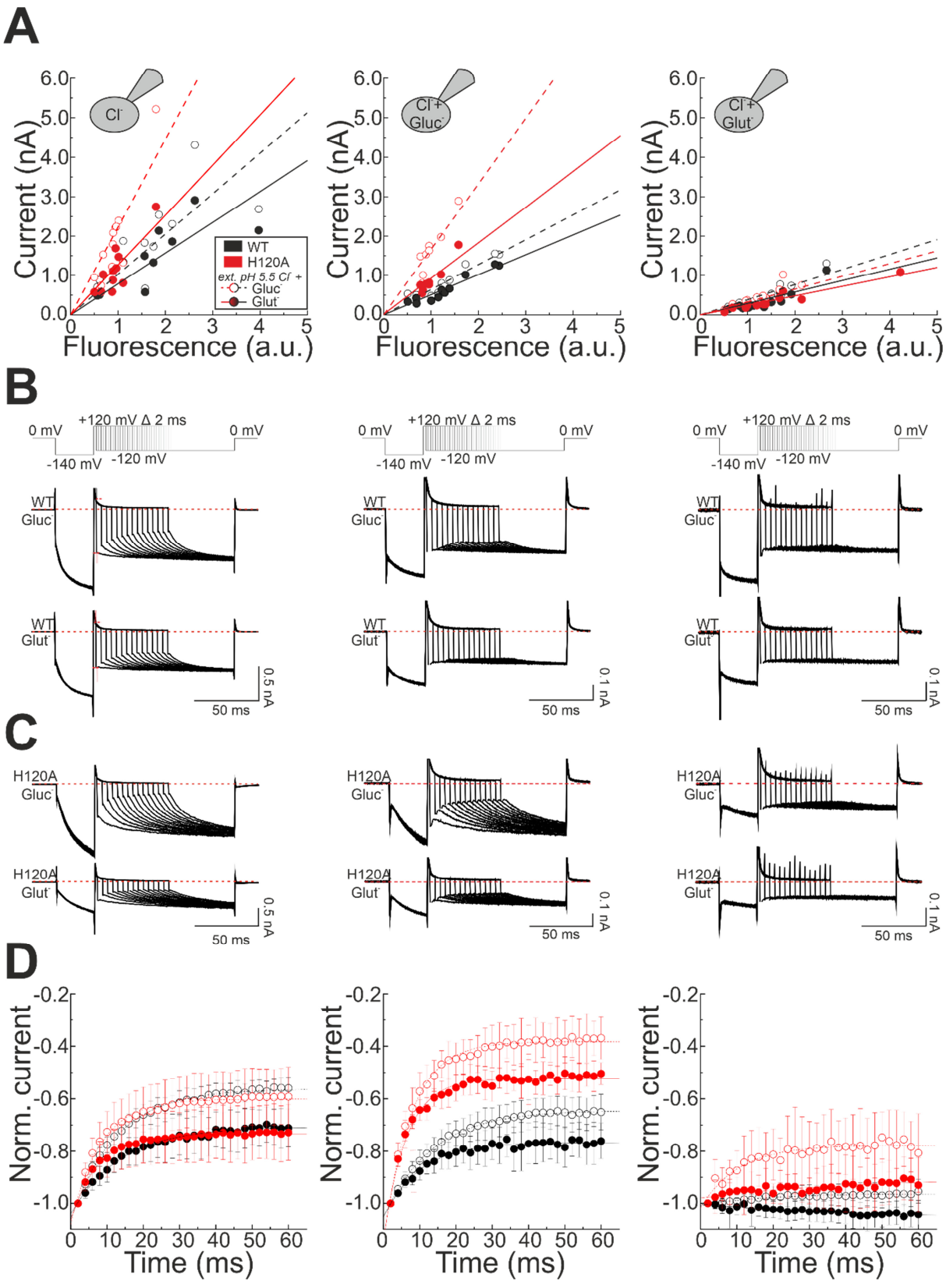

Figure 5.8 Glutamate blocks anion currents from luminal and cytoplasmic side. ***A*** *Current-Fluorescence plots of WT (black) and H120A (red) VGLUT1$_{PM}$ during perfusion of Cl⁻-based solutions with either glutamate (filled) or gluconate (unfilled) under three different internal conditions: 1. internal Cl⁻ (left), 2. internal Cl⁻ and gluconate (middle), 3. internal Cl⁻ and glutamate (right).* ***B,C*** *Representative recordings with the deactivation protocol under the mentioned conditions for WT*

*(**B**) or H120A (**C**). The depolarizing step at -120 mV was extended for 2 ms with each sweep. Only every second stimulus is shown. **D** Time courses of the instantaneous current amplitudes from the deactivation protocols shown in (**B**) and (**C**).*

5.7 The temperature dependence of the anion current

Ion channels form a permeation pathway via an aqueous pore through which ions can diffuse [115]. In contrast, ion transport by transporters relies on conformational changes, for example by shifting a protein domain. Transporters often have to overcome transition states with higher energies than channels and are thus more temperature dependent.

I therefore studied the temperature dependence of the Cl^-, glutamate and gluconate currents. The fluorescence of the individual cells again served as a factor for the quantitative comparison of the individual cells with each other. To ensure that the quenching of the GFP is not affected by different temperatures [116], all cells were recorded at room temperature and the temperatures were increased up to 40 °C only when entering the whole cell mode. Figure 5.9 A shows a representative recording with Cl^- as internal permeable anion at -160 and +80 mV. To ensure that the steady state current was reached, the current was extrapolated by a biexponential fit. The currents of all cells (n=11) showed no significant correlation between the temperature and the amplitude (Figure 5.8), whereas the first fast time constant changes linearly with temperature. To investigate the influence of channel deactivation at positive potentials, a stimulation protocol to measure the deactivation as described in chapter 4.5.6 and 5.6 was applied and the time constant of activation and deactivation were plotted in an Arrhenius diagram (Figure 5.9 B). We calculated activation energies from Arrhenius plots and obtained a low value for the activating time constant (E_A=35.8 kJ/mol) and high values for the deactivating time constant (E_A=105.5 kJ/mol). In case data do not exhibit a linear correlation, it may have several causes such as a temperature-dependent change in affinity to permeable anions, to the proton or Cl^- binding site, lipid phase transitions, or changes in the rate-limiting step during a transport mechanism [117].

In contrast to Cl^-, both glutamate and gluconate current amplitudes show a significant correlation between amplitude and temperature at de- and hyperpolarizing potentials. We calculated activation energies for all conditions using the slope of the Arrhenius plot (Table 5.8, Figure 5.9 C,D,E). The low activation energies with 28.2 kJ/mol for glutamate and 23.7 kJ/mol for gluconate at -160 mV and 47.6 kJ/mol for glutamate and 24.0 kJ/mol for gluconate at + 80 mV, are similar to those of transporters and also channels described in the literature [117–119]. Similar activation energies at -160 and +80 mV for glutamate and gluconate suggest a similar transport mechanism for glutamate efflux and Cl^- influx. The difference in E_A with glutamate at + 80 mV is difficult to interpret due to the low current amplitudes of ~13.2 pA, compared to ~36.6 pA with gluconate. A biphasic temperature dependence of

transport rates was observed for many proteins in the literature [117,118,120,121]. These could not be detected in the present measurements, which might be due to the limiting temperature range of the measurement system.

The temperature coefficient Q_{10} is a value for the relative change in 10°C of the analyzed parameter and was calculated from current-temperature or current-τ-plots between 20 and 30 °C (Figure 5.8, Suppl. Figure 8.8). It is generally accepted that permeability through channels, due to their low energy barrier for diffusion, is rather insensitive to temperature changes and the Q_{10} value is typically <1.5 [138.139]. We here show that most Q_{10} values are well within this range like the activating time constant of the Cl^--channel, the Cl^- influx at +80 mV with internal gluconate, but also the transport of gluconate or glutamate (Table 5.8). In accordance with the exceptionally high activation energy, the Q_{10} of the deactivation in the Cl^- current, in particular, was significantly higher with 3.5.

Reversal potentials were measured in these experiments for all conditions by a ramp protocol between -160 and +75 mV within 100 ms (Figure 5.9 C,D right panel). None of the conditions shown in Figure 5.9 F indicated a correlation of E_{rev} with the temperature. Thus, the permeability of the displayed anions is not changed by temperature or any conformational changes.

We showed that Cl^-, glutamate and gluconate permeation through WT $VGLUT1_{PM}$ is associated with low activation energies and low temperature coefficients. The deactivation of the Cl^- channel with its large E_A and high Q_{10} value appears to undermine stronger conformational changes.

Table 5.8 Temperature dependence of WT $VGLUT1_{PM}$. *Linear correlation between current amplitude and temperature was tested with Pearson correlation (n.c.=no correlation).*

internal	n	Voltage	Pearson correlation	E_A (kJ/mol)	Q_{10}
Cl^-	11	+80	0.25 n.c.		
		-160	0.19 n.c.		
		Activation	p<0.001 ***	35.8	1.5
		Deactivation	p<0.001 ***	105.5	3.5
$Glut^-$	11	-160	p<0.001 ***	28.2	1.5
		+80	p<0.001 ***	47.6	2.5
$Gluc^-$	10	-160	p<0.001 ***	23.7	1.5
		+80	p<0.001 ***	24.1	1.4
E_{rev}	11	Cl^-	0.21 n.c.		
	11	$Glut^-$	0.52 n.c.		
	10	$Gluc^-$	0.75 n.c.		

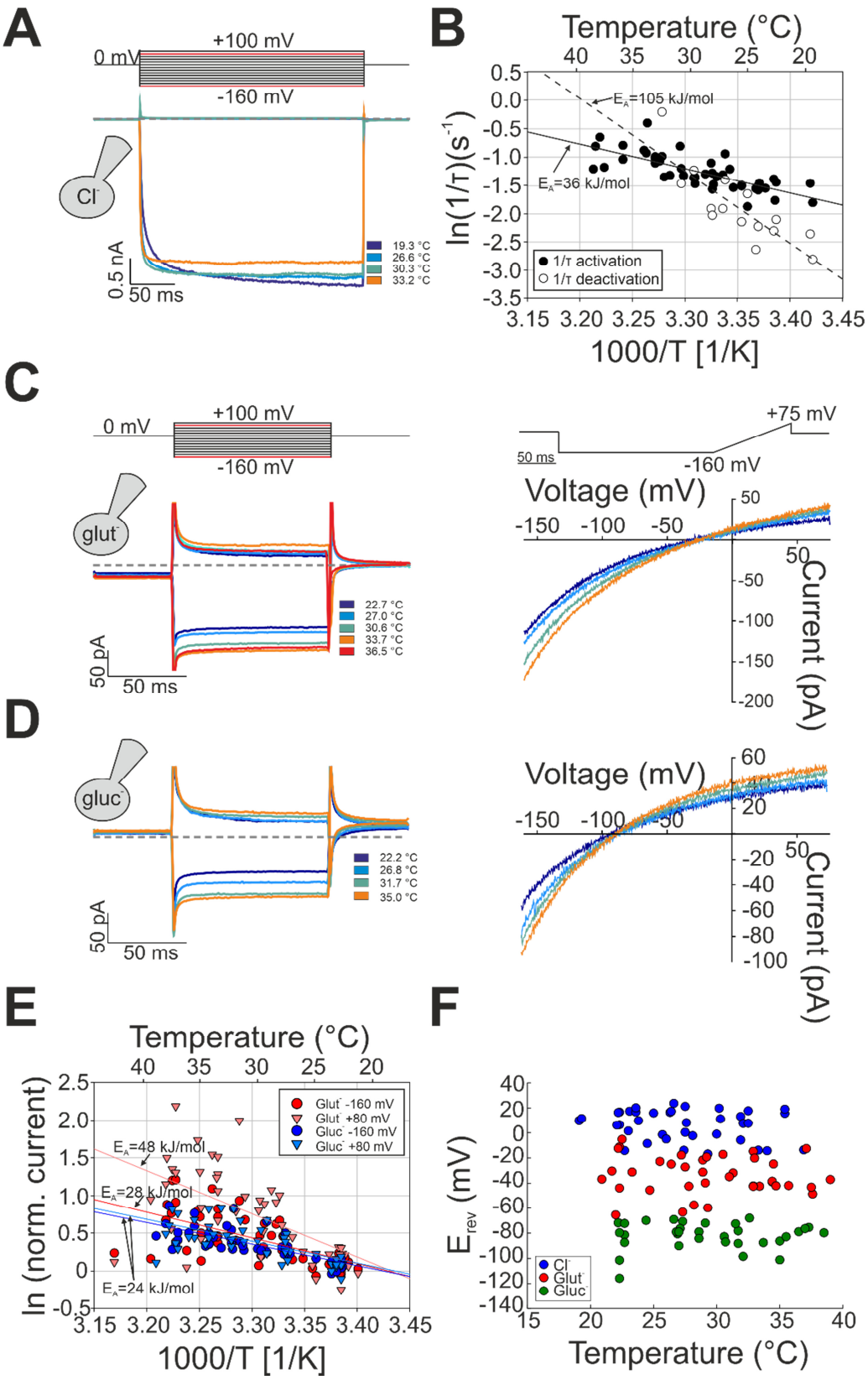

Figure 5.9 Temperature dependence of VGLUT1$_{PM}$ anion currents. *The cells were stimulated between -160 and +100 mV at temperatures between 20 and 40 °C.* ***A, C*** *and* ***D*** *show representative voltage jumps at -160 mV and +80 mV (left) or ramp protocols between -160 and +75 mV within 100 ms (**C,D** right) with internal Cl⁻ (**A**) glutamate (**C**) or gluconate (**D**) as permeable anions. The current amplitude for Cl⁻ does not correlate with the temperature in contrast to the time constant for the*

activation and deactivation of the channel. ***B*** *Arrhenius plot of time constants with internal Cl⁻. The slopes, determined by a linear regression, correspond with* E_A *values of 36 kJ/mol for the activation and 105 kJ/mol for the deactivation time constant of the channel.* ***E*** *Arrhenius plot of the conditions from (****C****) and (****D****). Glutamate and gluconate cause a significant increase in current amplitude with increasing temperature. The cells were normalized to the whole cell fluorescence and the current at 20 °C.* ***E*** *The reversal potentials from the measurements in (****A,C*** *and* ***D*** *right side) are unaffected by the temperature.*

6 Discussion

VGLUTs mediate the loading of the excitatory neurotransmitter glutamate into synaptic vesicles in the presynapse. Although these transporters are of high physiological importance, their transport mechanism is discussed controversially. VGLUTs are thought to be secondary active glutamate transporters, but can also function as anion channels or as Na^+-coupled phosphate transporters. Here I studied the anion permeation of VGLUT1 electrophysiologically using whole cell patch clamp, noise analysis and fluorescence intensity measurements in transiently transfected HEK293T cells.

6.1 $VGLUT1_{PM}$ whole cell currents are inward rectifying and pH dependent

The mechanism of VGLUT during vesicle loading remains very controversial in the literature. The physiological localization in synaptic vesicles or in the plasma membrane and the different activation properties and transport mechanisms complicate a direct measurement of physiological experiments. Presumably, several components may lead to the large discrepancy in experimental results. It has been reported that the composition of phospholipids in the membrane may be a crucial issue for the imbalance in the results [41,54]. For example, in measurements in reconstituted proteoliposomes, the composition of acidic phospholipids in liposomes and the strength of the membrane potential could influence the local [glutamate] near the membrane. It has been shown that the lipid composition can influence the function of integral proteins and the synaptic vesicle cycle [124–127]. We do not believe such an effect in our experiments because our rather unphysiological conditions allow the control on the ion concentrations, the localization, membrane potential and pH gradient. Nevertheless it must be noted that VGLUT might generate different results under more physiological conditions with dynamic ion concentrations within the vesicular loading process.

The currents obtained in whole cell patch clamp measurements could be activated extracellularly/luminal with a Cl^--containing solution at acidic pH values. They were opened at hyperpolarizing potentials with time constants in the ms range and closed at positive potentials. A half-maximal activation of the macroscopic currents could be achieved at pH 5.5. Similar results with an EC_{50}=5.53 were also found by Eriksen et al. (2016) for VGLUT2 and appears to be consistent with physiological pH in endosomes and also in synaptic vesicles [21,22]. Although Juge et al., (2010) could not detect uptake of radioactive Cl^- in proteoliposomes during glutamate transport, the conductance of Cl^- through VGLUT was demonstrated previously in reconstituted synaptic vesicles or in patch clamp measurements

in oocytes, transiently transfected HEK cells, or fused endosomes of transiently transfected HEK cells [49,50,53,54,75].

6.2 $VGLUT1_{PM}$ functions as an anion channel

Large $VGLUT1_{PM}$ currents suggest anion conduction through an anion channel. To further test this hypothesis, we determined single channel amplitudes with noise analysis. The double Lorentzian noise of the power spectrum supports a channel-mediated transport [100]. We obtained single channel amplitudes with Cl^- of 24.3 ± 2.4 fA in stationary noise analyses. This corresponds to a transport rate of ~150,000 ions/s, far more than previously determined for any transporters (e.g. Cl^-/HCO_3^- exchange in erythrocyte anion exchanger AE1 ~50.000 ions/s, Brahm (1977)) or pumps (e.g. V-ATPase ~100 ions/s, Murata et al. (2008)) and in a range consistent with values of other anion channels (e.g. EAAT2 ~155,.000 ions/s, Kolen et al. (2020); Winter et al. (2012)). With the mutated protein H120A $VGLUT1_{PM}$, transport rates were even increased up to 400,000 ions/s with internal NO_3^-. The values show that in $VGLUT1_{PM}$, anion conductance occurs via diffusion along an aqueous conductance pathway. After the finding that permeability was significantly increased with NO_3^- in exchange for Cl^- as a permeable anion, we also performed the noise analysis with internal NO_3^-. Again, the single channel amplitude of 39.0 ± 2.1 fA was in the range of channels, but the single channel amplitude itself does not explain the ~four-fold increased macroscopic current.

In addition to the single channel amplitude, the number of channels in the membrane and thus the open probability could also be determined in the noise analysis. This value is increased ~1.6-fold with NO_3^- compared to Cl^-. The combination of increased single channel amplitude and open probability cannot explain the increased transport of NO_3^- for $VGLUT1_{PM}$. It has already been shown in EAATs that a miscalculation of the absolute number of transporters can occur in the noise analysis [109]. This miscalculation of the number of channels/transporters occurs in case of transitions between different states that result in pseudoequilibria that reduce the apparent number of channels/transporters. Such an effect may explain the discrepancy between the macroscopic current amplitude and the unitary current amplitude with NO_3^-.

Single channel amplitudes can be underestimated for high frequency flickering channels that are too fast to be resolved [99]. By changing the filter frequency in the noise analysis, we could show that the VGLUT anion channel is a high-frequency flickering channel with single events of 50-180 µs durations, which could lead to a slight underestimation of the actual single channel amplitude in our analysis. Nevertheless, these slight deviations do not affect the main conclusion of this work that VGLUT1 can function as a Cl^- channel.

In addition to their main role as secondary active glutamate transporters, EAATs are also anion channels. The single channel amplitude with NO_3^- in EAATs (~25 fA [109,129]) is very similar to the amplitudes determined here in VGLUTs. Although VGLUTs and EAATs are both glutamate transporters, there are significant differences between these proteins [130]. The affinity for glutamate in VGLUT is 100-1000-fold lower than in EAATs. VGLUTs, unlike EAATs, do not transport aspartate. Moreover, transport of the EAATs is coupled to the movements of Na^+, K^+ and H^+, while VGLUTs are driven by an electrical gradient generated by V-ATPase.

ClC-4 is another dual function protein that can function as transporter and as channel. Alekov and Fahlke (2009) showed that there is a slippage mode in which proton and anion transport uncouple and result in passive anion flux through a channel. They exhibit similar single channel amplitudes and open times between 100 and 200 µs, which are very similar to ours in $VGLUT1_{PM}$ and represent a flickering channel. Such a process, switching between a coupled exchanger mode and a non-coupled anion channel, is also conceivable for VGLUT.

The additional Cl^- conductance besides the main task of transporting important neurotransmitters, has also been found in another member of the SLC17 family, the sodium/phosphate transporters (NaPi) [131,132]. As mentioned in chapter 3.4.1, VGLUT also has the ability to transport phosphate in exchange for two sodium ions [50]. The physiological relevance of the Cl^- channel in vesicle loading is still controversial. It has been suggested that VGLUTs can support synaptic vesicle acidification through their Cl^- conductance [39,53,54]. Another theory is that the additional conductivity of Cl^-, is used to remove the Cl^- trapped after endocytosis from the vesicles to make space for glutamate [19,49,54,75]. This might lead to the suggestion, that the channel would mainly conduct ions from the lumen into the cytoplasm and we could measure this as a positive current at depolarizing potentials. However, this was not the case in our measurements with internal chloride. Under our experimental conditions, the $VGLUT1_{PM}$ Cl^- channel exhibits a strongly inward rectifying current and hardly any outward rectifying current, which means that the channel closes or deactivates rapidly at depolarizing potentials. This fast mechanism could be initiated by the unbinding of Cl^- or H^+. However, it cannot be ruled out that Cl^- can also develop other transport mechanisms under physiological conditions that could lead to the above mentioned conductance. This is supported by our measurements of small outward rectifying currents with internal glutamate and external Cl^-.

6.3 $VGLUT1_{PM}$ anion channels exhibit a lyotropic anion selectivity

Recently, whole cell measurements have shown that VGLUT1 can be activated by luminal/extracellular binding of Cl^- and Br^- and suggest a conductance for these ions [49]. In contrast, I^-, NO_3^-, and SCN^- could not allosterically activate VGLUT2 [45,49,52]. By replacing the

internal permeable anion Cl^- with NO_3^-, I^- or Br^-, we demonstrated here that permeation through the anion channel is possible for other small anions. Cl^- and Br^- show similar time constants in their activation kinetics, whereas NO_3^- and I^- permeate much faster. Due to the low outward rectifying current amplitudes, the reversal potentials are very descriptive and reveal hardly any information about the mechanism. However, the negative currents at a holding potential of 0 mV, as with NO_3^-, as well as the different current amplitudes indicate the lyotropic anion selectivity.

To account for differences in transporter expression, we used a combination of whole cell fluorescence and whole cell current recordings. Here, macroscopic current amplitudes were corrected for differences in the number of ion channels in the recorded cells. Each $VGLUT1_{PM}$ is tagged with a GFP fusion protein. Thus, the fluorescence represents the number of transporters in each cell [95,133]. To avoid possible quenching of the tested anions, the fluorescence was recorded before the start of the experiment. Figure 5.5 shows the clear linear relationship between the transporters in the plasma membrane and the anion current, even if the localization of intracellular fluorescent proteins causes slight deviations. Thus, this technique is a suitable tool for comparing absolute and relative current amplitudes of $VGLUT1_{PM}$.

A lyotropic or Hofmeister anion selectivity has already been found in various channels [119.120]. In contrast to transporters, the interaction or binding between ion and channel is much lower. Channels form a pore filled with water that narrows towards the center, the so-called selectivity filter. To pass through this filter, the ions surrounded by water molecules must be dehydrated with the energy recovered from the interactions with the selectivity filter [136]. Consequently, anions with low free hydration energies (lyotropic) show higher permeabilities than those with high hydration energies, as they can more easily switch from ion-water to ion-channel bonds. Large, halide ions such as iodide or bromide can therefore often permeate channels better than small halide ions such as Cl^- [137].

6.4 $VGLUT1_{PM}$ can be activated by luminal and modulated by cytoplasmic protons

Luminal protons and Cl^- stimulate glutamate transport, a mechanism that prevents the non-vesicular efflux of glutamate from VGLUT in the plasma membrane under physiological conditions [49,50,75]. The role of the ΔpH has been discussed very controversial in recent years and remains unclear. On one hand, it has been shown that loss of the pH gradient leads to increased glutamate uptake in synaptic vesicles [1,60,138], while in other experiments it has been shown to inhibit glutamate transport [48,56]. Tabb et al. (1992) assume an allosteric activation of glutamate transport by luminal protons. To test whether ΔpH is the driving force for the independent Cl^- channel shown here, the $[H^+]$ was varied between pH 7.4 and pH 5.5 on the

extracellular (luminal) and cytoplasmic sides (Figure 5.3). The results show that ΔpH dissipation does not inhibit channel activity and a bilaterally acidic pH even doubles the permeation of Cl^- ions. On the other hand, cytoplasmic protons alone are not sufficient to activate the anion channel. If ΔpH would be the driving force for the Cl^- conductance, acidic pH on both sides should inhibit the Cl^- permeation. Since this is not the case, we thus postulate that VGLUT1 has at least two binding sites for protons, whereby the luminal binding of protons is absolutely necessary to activate the anion channel and the cytoplasmic binding site additionally modulates the channel capacity.

6.5 $VGLUT1_{PM}$ is permeable to glutamate and several large anions

To investigate glutamate currents in whole cell patch clamp measurements, internal anions were completely exchanged for glutamate and contamination of Cl^- was prevented by a negative holding potential. All $VGLUT1_{PM}$ measurements were checked for possible leakage currents with a measurement at pH 7.4 that precede each measurement at pH 5.5. The neutral external pH inactivates VGLUT and permits to separate leak currents from VGLUT currents. Leak currents are then subtracted as background current. We were able to measure inward rectifying currents, with small outward currents with glutamate. Inward current amplitudes were significantly smaller than with Cl^-. As a control, glutamate was replaced by presumedly impermeable anions such as aspartate, gluconate, MES, MSA, or isethionate. To our surprise, we could not identify any impermeable anion, which appears to contradict the well-studied glutamate selectivity of VGLUT [45,55]. Notably, aspartate has been studied in the past in radioactive uptake assays [44,45], but also in patch clamp measurements in endosomes [75]. Nevertheless, the transport of aspartate is not unlikely due to its similar structure to glutamate and is also recognized by other glutamate transporters such as EAATs [130] or sialin [139].

In our measurements, however, glutamate differs from other large anions mainly in a more positive reversal potential in measurements with external Cl^- and internal polyatomic anion. While glutamate currents reverse at a potential of -6 mV, all other anions have reversal potentials between -50 and -80 mV. One possible reason why the permeability for aspartate or gluconate has not been found in uptake assays so far might be that the membrane potential generated by the V-ATPase was not large enough to establish a sufficient driving force for anion uptake into vesicles. Even under physiological conditions, only a membrane potential of about +80 mV can be built up [24,140,141]. In our experiments a potential of -80 mV (inverse localization of $VGLUT1_{PM}$) would not be strong enough to build up a driving force for gluconate since it just reaches its reversal potential. Chang et al. (2018) also investigated the permeability of VGLUT in fused endosomes in patch clamp experiments. They concluded impermeability for both gluconate and aspartate. It could be that the stimulation up to

+100 mV and the [anion] were not large enough to generate a significant current. Nevertheless, an increase in aspartate and gluconate current was also observed with increasing activation by luminal Cl^- in their recordings, although this was lower compared to glutamate. This is supported by the fact that we (Suppl. Figure 8.4) and also Eriksen et al. (2016) detected an anion current under conditions of Cl^- transport (internally 140 mM Cl^-) without luminal/external activation of Cl^-. In Chang et al. (2018), however, the remaining current was similar to that with gluconate or aspartate. In addition, in our experiments we used non-physiological solutions with high anion concentrations that would not occur in the vesicle or cytoplasm, with voltages that vesicular membranes in living cells are not able to generate. This is an advantage of the patch clamp method. By controlling the ion concentrations, the membrane potential, as well as and the pH gradient, we can study transporters beyond physiological limits. We conclude that under physiological conditions $VGLUT1_{PM}$ acts as a highly selective glutamate transporter or channel, but the protein may transport other anions under other conditions. Based on the calculated permeabilities and the size of the permeable anions, the pore of $VGLUT1_{PM}$ must therefore be at least 6.5 Å in diameter. Equal values between 5.2 and 6.4 Å were also found other channels [137,142–144]. A channel that conducts glutamate was already discovered in association with glutamatergic neurotransmission. While VGLUT is localized in the presynapse, the volume-regulated anion channel (VRAC) is localized in the plasma membrane of adjacent astrocytes. Recently, its obligatory subunit Swell1 has been shown to cause tonic or cell swelling-induced glutamate release via a channel [145]. The pore diameter of VRAC was estimated to be ~1.1 nm [146], but in contrast to VGLUT, VRACS exhibit huge unitary current amplitudes of 2.3 pA [147]. Also the cystic fibrosis transmembrane conductance regulator chloride channel (CFTR) can conduct several lyotropic (weakly hydrated) anions (5.3 Å) and kosmotropic (strongly hydrated) anions (13.8 Å), but the unitary current amplitude with Cl^- is also ~20-time higher (0.55 pA) than for VGLUT [96,97].

Besides glutamate, the reversal potential for HCO_3^- was similarly positive as for glutamate. Bicarbonate is the second most abundant anion in the human body after Cl^- [134,148]. The magnitude of the current amplitudes could be classified between those of the small and large anions and we suspect that HCO_3^- is also conducted by the channel. Chloride channels that are also permeable to HCO_3^- have been reported several times [142,149], but also transporters that permeate HCO_3^- [148,150]. Bicarbonate performs two physiological roles in cells: first, it serves as an intracellular pH regulator and second, it controls the activity and stability of solute proteins in body fluids [148]. Thus, ClC proteins were also reported to exhibit a bicarbonate permeability (ClC-5 [151]; ClC-2 [152]), as do sodium-driven chloride/bicarbonate exchangers (NDCBE). Both families also appear to be present in synaptic vesicles and could play a role in HCO_3^- transport alongside VGLUT [133.134]. However, the role of ClCs in

bicarbonate transport is unlikely because only ClC-3 has been reported in synaptic vesicles [13] and, to our knowledge, has not been associated with bicarbonate permeability. In addition, Taoufiq et al. [14] recently used proteomics to show that the abundance of ClC-3 in synaptic vesicles is too small to be considered as major SV protein.

Influx of bicarbonate into the synaptic vesicles would buffer the proton-gradient that was actively established by the V-ATPase with the use of energy in the form of ATP. Why would VGLUT work against this gradient? One explanation would be that VGLUT limits the vesicular loading with the HCO_3^- permeation after glutamate transport and thus signalizes the termination of the filling. A mechanism outside synaptic vesicles, for example in the presynaptic membrane is rather unlikely due to the activation of VGLUT by acidic pH. The pH plays an important role in neuronal excitability [79] and also in the strength of synaptic transmission [154]. Even small changes can influence neurological functions. To what extent and especially how VGLUT plays a role in this has not yet been clarified and must continue to be investigated.

6.6 Glutamate conductance is activated by luminal chloride

There are different theories from which side Cl^- allosterically activates glutamate transport, from the cytosolic, luminal, or both sides of the protein [51,53,54]. Biphasic activation of glutamate transport in proteoliposomes by Cl^- has also often been measured, where transport was low in the absence of cytoplasmic Cl^-, increased with rising concentrations up to 4 mM Cl^-, and inhibited at higher concentrations [45,47,55]. However, this biphasic activation could also arise from the fact that high [Cl^-] dissolves the membrane potential, which seems to be the main driving force for VGLUT.

Unfortunately, we cannot test activation by cytoplasmic Cl^- in our experiments because its presence would be measured in a permeation through the Cl^- channel at hyperpolarizing potentials which would not be distinguishable from the glutamate current. However, Wolosker et al., (1996) showed that glutamate uptake occurs even in the absence of cytoplasmic Cl^-. Therefore, we examined activation by Cl^- from the luminal side and found an increase in glutamate current up to 40 mM and inhibition at higher concentrations. This activation is reminiscent of that described for the cytoplasmic side with the difference that maximal activation is driven at higher [Cl^-] and no current could be detected in the absence of Cl^-. Activation by low $[Cl^-]_{cyto}$ and high $[Cl^-]_{lumen}$ could regulate uptake after recycling of the vesicle, where high $[Cl^-]_{lumen}$ of >120 mM [53] were detected shortly after endocytosis. VGLUT or other proteins may be initially involved in the export of Cl^- from the vesicle lumen and thus makes space for glutamate. When $[Cl^-]_{lumen}$ decreases, VGLUT directs increasingly more glutamate into the vesicle. It was also proposed that the transport of glutamate occurs in an exchange mechanism with Cl^- [19]. The increase in synaptic glutamate concentration thus correlates with

the decease of $[Cl^-]_{lumen}$ and the coupling provides osmotic stability. However, this exchange would be stochiometrically uncoupled. The clearly inward rectifying currents in our experiments with glutamate exclude an electroneutral $Glut^-/Cl^-$ exchange.

6.7 Proton-coupling with glutamate in $VGLUT1_{PM}$

A coupled transport of glutamate together with H^+ or Cl^- has not yet been proven so far. There are three different theories on how the transport of glutamate could function in addition to the anion channel: 1. As $Glut^-/H^+$ exchanger [19,54], 2. As $Glut^-/Cl^-$ exchanger [54,56], or 3. As an electrogenic $Glut^-$ uniporter [25]. Martineau et al. (2017) proposed VGLUT to be a $Glut^-/H^+$ exchanger with an additional anion channel for the non-stochiometrical exchange for glutamate and Cl^-. We investigated whether proton currents can also be measured under our experimental conditions. For this purpose, equal ionic conditions were created on the cytoplasmic and extracellular side with a combination of Cl^- and glutamate. A pH gradient was established between inside and outside at 0 mV. We could not differentiate any significant H^+ currents under these conditions from the currents under control conditions. It is reasonable to assume that if protons can be transported by VGLUT, the transport would be Δψ-dependent similar to that of Cl^- and glutamate or they would be coupled to the transport of glutamate. A $Glut^-/H^+$ symporter would be electroneutral and would also transport both ions against their concentration gradients. In some cases, it is assumed that glutamate can be transported either with or without protons [53,54]. In first measurements with the ratiometric dye BCECF, we could not detect any changes of the internal $[H^+]$ so far (unpublished results). Based on the present results, we assume that protons are not effectively transported by $VGLUT1_{PM}$, but the luminal binding of protons is mandatory for the activation of VGLUT.

6.8 A point mutation that modifies the kinetics and the unitary conductance of $VGLUT1_{PM}$ anion channels

A histidine at position 128 in VGLUT2 is localized at the bottom of the central cavity (Suppl. Figure 8.1) and has recently been identified as an amino acid that appears to be required for glutamate transport. A point mutation of histidine to alanine causes prevention of glutamate transport in purified and reconstituted VGLUTs in proteoliposomes [44]. This histidine is conserved in all VGLUT isoforms but not in other members of the SLC family, suggesting an important function in glutamate selectivity. There is no histidine at this position in sialin (SLC17A5), another SLC family member that transports aspartate or glutamate in symport with a proton. This suggests a role for this histidine in distinguishing glutamate from aspartate [139]. We inserted the analogous mutation H120A into $VGLUT1_{PM}$ and performed electrophysiological experiments. The mutant transporter still shows strong inward rectifying conductance with small anions such as Cl^-, Br^-, I^-, and NO_3^-, but with slightly altered gating properties. In particular, the first time constant was significantly increased when the channels

opened or closed concluding that the mutation mainly influences the activation of the channel.

In addition, significantly higher macroscopic current amplitudes could also be detected in H120A. Even though the amplitudes of WT and H120A $VGLUT1_{PM}$ normalized to fluorescence cannot be directly compared, for many measurements the expression of H120A $VGLUT1_{PM}$ had to be reduced in the stable FlpIn cell line because the currents were >10 nA. With the stationary noise analysis we could determine that the increased current amplitudes are a result of a doubled single channel amplitude (52 fA with Cl^- and 63 fA with NO_3^-).

Histidine plays an important role in proton binding in channel pores [155]. It is thought that amino acid E191 in VGLUT2 binds the protons for activation [71]. Due to its deep location within the pore, AA H128, which is partially aligned in the luminal direction, could act as an initial proton acceptor that passes the proton to E191. Thus, H128 and E191 are connected by a water-filled tunnel with a minimum diameter of 1.8 Å [71]. Due to the mutation to alanine, this initial binding of the proton is no longer possible, which would explain the slower opening and closing of mutant channels. Also, the shift of the KD from pH 5.5 in WT to pH 5.2 in H120A fits the role of the amino acid as initial proton acceptor.

The lyotropic anion selectivity is also affected by the H120A mutation. In particular, the permeability of iodide is dramatically reduced compared to the other ions. This shows that histidine is also part of the selectivity filter of the anion channel in VGLUT and the dehydration of iodide is affected by the mutation. However, it is surprising that other large halide anions such as Br^- are not affected.

6.9 H120A $VGLUT1_{PM}$ does not conduct glutamate under physiological conditions

Previously we have shown that H120A affects anion channel function in $VGLUT1_{PM}$. Impaired glutamate uptake has been reported in uptake assays in reconstituted synaptic vesicles [44]. We planned to use the impaired glutamate transport as a control for our glutamate currents. Surprisingly, H120A $VGLUT1_{PM}$ also showed distinct inward rectifying currents with the major anions $glut^-$, $gluc^-$, asp^-, and HCO_3^-. However, the reversal potential for glutamate in the mutant is shifted ~60 mV to the left and now resembles that of gluconate. The reversal potential for aspartate has also shifted from -60 mV to -81 mV, indicating a reduction in permeability in both cases, while HCO_3^- permeability was unaffected by this mutation. The shift in the reversal potential for glutamate transport supports the theory that glutamate is permeable, but is not transported under physiological conditions of $\Delta\psi$ at +80 mV in synaptic vesicles. H120A reduces the electrostatic potential and thus anion binding. Cl^- therefore permeates better, accounting for the increased single channel amplitudes, but glutamate and gluconate bind and permeate less well. This is confirmed by our glutamate blocking

experiments. Here blocking of internal glutamate has a much more powerful effect in WT compared to H120A VGLUT1$_{PM}$. Interestingly, the H128A mutation has no effect on the Na^+-phosphate transport [34]. Until now, the assumption was that glutamate and phosphate are transported via two different pathways in VGLUT, since phosphate transport is neither Cl^- nor H^+-dependent.

It is also remarkable that the drosophila VGLUT (dVGLUT, also inserted into the plasma membrane) has a similar negative reversal potential as H120A and would therefore not transport glutamate under physiological conditions (unpublished results by Yannick Güthoff). In contrast to mammals, *Drosophila melanogaster* possesses only one isoform of VGLUT [156,157], where an analogous histidine is not conserved at mentioned position. In contrast, all other amino acids that presumably play an important role in glutamate transport (see chapter 3.4.3) are also found in dVGLUT. The sequence identity between the rat VGLUT studied in this work and that of drosophila is ~47%. The background of the shifted reversal potential will be further investigated by our group in future electrophysiological measurements and in measurements at the neuromuscular junction of drosophila.

6.10 Glutamate blocks Cl^--currents

Whereas no outward currents could be detected in cells exposed to symmetrical Cl^-, we were able to detect outward currents in the presence of intracellular glutamate. This current represents the influx of Cl^- into the cell. With internal Cl^-, cells stimulated between -160 and +160 mV showed a rapid closure of the channel at positive potentials (Figure 5.2 C, G), indicating that the influx of Cl^- depends on the internal anion composition. We here investigated the fast closure and found that the closing of the channel happens in at least two energetically different steps.

Eriksen et al., (2016) and other groups have already shown that glutamate, but not aspartate inhibits the inward rectifying Cl^- current [45,53]. In these studies, glutamate inhibits currents better at lower than at higher [Cl^-], which is the reason why Cl^- and glutamate are assumed to share a binding site, so that the ions compete for it. We here investigated the influence of glutamate on the Cl^- channel. For this, we used a protocol in which the channels are first opened at hyperpolarizing potentials, then closed at depolarizations of different lengths, and finally opened again at negative potentials. The instantaneous current at the second negative pulse gives the deactivation of the channels by the depolarization. We found that both internal and external glutamate significantly reduced the Cl^- currents in contrast to gluconate, but also that the deactivation of the channel was inhibited by glutamate. Bilateral glutamate even inhibited deactivation almost completely. Gluconate block cannot be estimated from these experiments because the concentrations of internal permeable anion is changed when gluconate is supplemented to the solution (compare Figure 5.8 left and middle). From these

results we conclude that glutamate and Cl^- at least partially, if not completely, share a common transport pathway with glutamate having a much stronger binding to the amino acids within the pore, thus blocking permeation for Cl^-.

However, the slow deactivation that we detected through this stimulation protocol differs from the rapid deactivation seen in Figure 5.2 C. We propose that channel opening and closing proceeds during multiple steps with two conformational changes (Figure 6.1). Since luminal as well as cytoplasmic glutamate inhibits the anion current, we conclude that two binding sites for glutamate could exist. Since only the presence of glutamate on both sides almost completely inhibits deactivation, we assume an interaction between the two binding sites. During synaptic vesicle filling, the presence of cytoplasmic glutamate could thus prevent the influx of Cl^- or other anions into the vesicles so that glutamate transport can be regulated. On the luminal side, glutamate could cause a negative feedback mechanism. If Cl^- serves as a stoichiometrically uncoupled counterion for glutamate [19], an increasing glutamate concentration would inhibit Cl^- permeation and thus further glutamate uptake. This mechanism could regulate the quantal size of the vesicle by achieving an equilibrium between ions.

Our results suggest a model with at least two conformational changes between the apo (1) and an open Cl^- and H^+ bound state (3) (Figure 6.1). We showed (Figure 5.3) that luminal protons are mandatory for the activation of the anion channel but also cytoplasmic protons modulate the channel amplitude. Therefore we inserted a luminal H^+-binding site but it is suggested that more than a single proton-binding site might be required. H120 was supposed to play a role as a proton acceptor. We showed that the mutation of this amino acid does not abolish channel or transport activation but changes the kinetic properties. These results do not rule out the role for H120 to act as an initial H^+-acceptor as other amino acids might also be involved in this process. We also inserted a luminal Cl^--binding site due to the results of the allosteric Cl^--activation from Eriksen et al., (2016). Moreover, a cytoplasmic mechanism cannot be ruled out by our experiments because a differentiation between activation and permeation due to higher $[Cl^-]$ is not possible. Li et al. (2020) proposed that H199 and H183 together form the gate for the anion channel in VGLUT2. In the closed state, this 2-His-gate forms a channel diameter of 2.4 Å, too small for the permeation of the 3.62 Å Cl^- ion. It is thought that the amino acids need to slightly reorient themselves for Cl^- permeation [71]. This could be initiated by the luminal binding of protons and Cl^-. Glutamate can block the pore for permeation by stronger binding to the protein and prevents the channel from deactivation. To proof this theory, more experiments and simulations need to be done in future.

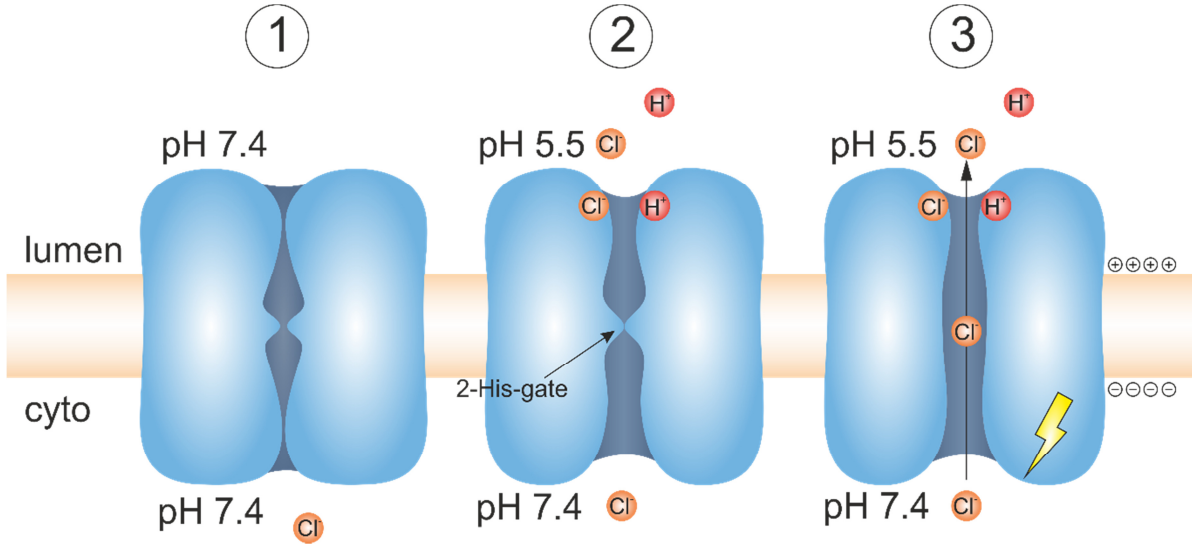

Figure 6.1 Theory for anion channel activation. *(**1**) Closed state (apo). (**2**) Deactivated state. Cl⁻ and H^+ bind to the luminal side of the protein and expose the 2-His-gate by conformational changes. (**3**) Open state. Δψ leads to small conformational changes in the 2-His-gate and increases the pore size.*

6.11 Temperature dependence of VGLUT1$_{PM}$

Ion permeation through channels is rather insensitive to temperature changes due to their low energy barrier for diffusion, with Q_{10} value typically <1.5 [122,123]. To test this also for VGLUT1$_{PM}$, cells were dialyzed with internal chloride, glutamate, or gluconate and stimulated at -160 mV and +80 mV, while cells were perfused externally with 40 mM Cl^- and pH 5.5. The bath temperature was gradually increased up to 40°C. It was statistically shown that the current amplitudes of the Cl^- currents are independent of the temperature, confirming permeation through the channel. In contrast, the time constants of activation (E_A=35.8 kJ/mol) and also deactivation (E_A= 105.5 kJ/mol) are strongly temperature dependent. The channels enter the open state more quickly at higher temperatures [120]. While temperature does not have an effect on the channel amplitude, it is known that the kinetics of activation and deactivation of the channels are strongly affected by temperature [102,121,123,158]. The high activation energy together with the high Q_{10} value for the deactivation indicates major structural changes within the protein. The results are in line with the theory of anion channel activation proposed in Figure 6.1. Therefore the channel activation is connected to a low energy consuming conformational change while the deactivation uses a high energy with bigger conformational changes.

In contrast, with internal glutamate and also with gluconate, a dependence of the current amplitudes on temperature could be observed. The activation energies with gluconate (E_A=23.7 kJ/mol) and glutamate (E_A=28.2 kJ/mol) are in ranges similar to those of various channels (54.4 kJ/mol for proton channels [120], 34.3 kJ/mol for K^+ channels [159], or 20.9 kJ/mol for EAAT anion channels [115]). On the other hand, the glycerol-3-phosphate transporter (GlpT)

transports glycerol-3-phosphate (G3P) in exchange with P_i into *Escherichia coli* cells with a relatively low activation energy of 34.7 kJ/mol [160]. The authors explained this rather low activation energy for a transporter by assuming that the substrate binding to the transporter (entropic contribution) lowers the energy barrier and thus enables substrate transport with little structural rearrangements, driven by Brownian motion (enthalpic contribution). They suggested that such a mechanism may also be present in other members of the MFS family, which includes VGLUTs. The mutated E325A lactose permease (LacY) exhibits equal activation energies of 38.9 kJ/mol and transports lactose without the stoichiometric coupling to H^+ [161]. GlpT and LacY are considered bacterial homologs for VGLUTs [73,74]. The controversial results for the temperature dependence of channels and transporters in the literature do not give a prove for VGLUT as a transporter or as a channel but also none of these transport mechanisms can be excluded.

7 Conclusion

In this work, I investigated two different transport processes in $VGLUT1_{PM}$, transiently transfected in HEK293T cells, using electrophysiological techniques. Under conditions of uncoupled and activated Cl^- transport, $VGLUT1_{PM}$ exhibited strongly inward rectifying currents at hyperpolarizing potentials, activated by luminal Cl^- and H^+ binding sites and modulated by a cytoplasmic H^+ binding site. The currents showed a Lorentzian noise above the resolution limit with a single channel amplitude equivalent to that of other channels. In addition to Cl^-, we also found permeabilities to several small and large anions with a lyotropic anion selectivity, with glutamate standing out from the other large anions due to its relatively positive reversal potential along with HCO_3^-. We concluded that $VGLUT1_{PM}$ functions as a highly selective glutamate transporter or channel only under physiological membrane potentials. The H120A $VGLUT1_{PM}$ point mutation confirmed this theory by altering lyotropic anion selectivity and providing a much more negative permeability to glutamate. It is assumed that this histidine acts as an initial proton acceptor. On the other hand, we could not find any indication for the coupled or uncoupled transport of glutamate and protons in our experiments. The competition for the binding site for Cl^- and glutamate, the permeability of various large anions, as well as the bilateral block of the Cl^- channel pore by glutamate, suggest at least a partly common transport pathway with a large pore for Cl^- and glutamate permeation, which can be modulated by different Cl^- and H^+ binding sites.

In summary we demonstrated the permeation of Cl^- by a channel that is transferred to an open state in multiple conformational steps. The mechanism of the glutamate transport, however, remains less clear. We cannot exclude permeation of this neurotransmitter through the same channel as Cl^-.

Due to the sensitivity to different anions and cations, it is not surprising that even the small changes in luminal, cytoplasmic or extracellular ion concentrations can lead to pathological changes in signal transmission and even excitotoxicity (chapter 3.4.4). In order to understand and treat various disease processes and their origins, it is of great importance to understand especially such important transporters as VGLUT on the molecular level and to consider them as possible targets for pharmacological treatments.

8 Supplemental Material

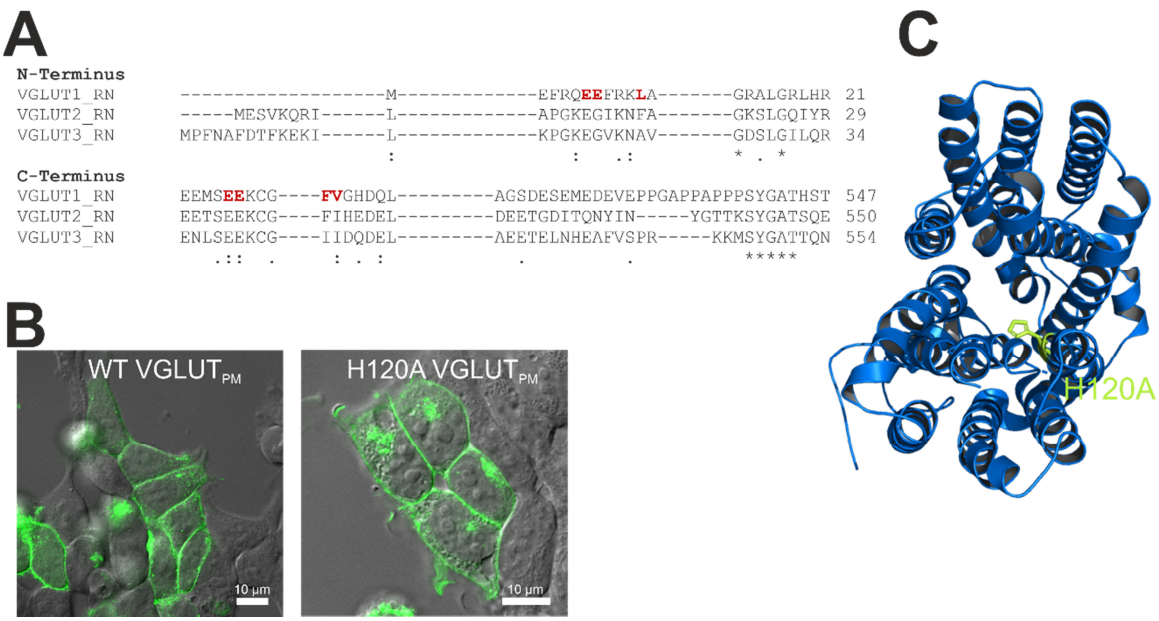

Suppl. Figure 8.1 Molecular modifications in VGLUT1. ***A*** *Our group identified seven AA in N- and C-terminal regions (red) that locate VGLUT1 to the vesicular membrane. We neutralized these AA to alanines and expressed VGLUT1$_{PM}$ as GFP fusion protein that is localized in the plasma membrane of transiently transfected HEK293T cells as seen in confocal images (**B**). **C** VGLUT1 contains 12 α-helices that build a pore. A Histidine at position 120 is located in the central cavity and supposed to play an essential role in glutamate uptake. The expression level of H120A VGLUT1$_{PM}$ is shown in (**B, right**).*

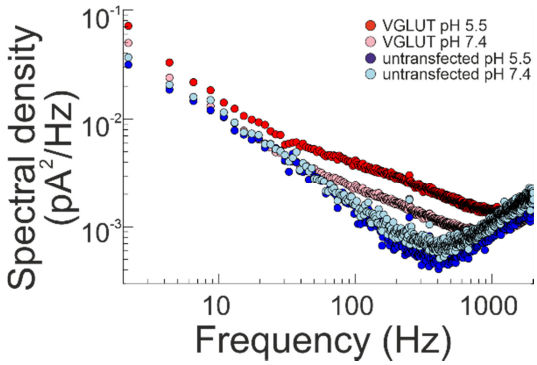

Suppl. Figure 8.2 Powerspectrum. *Spectral density of HEK293T cells transiently transfected with VGLUT1$_{PM}$ (red) or untransfected (blue) cells as control at -100 mV. Cells were measured in whole cell mode with internal and external Cl⁻. VGLUT1 currents were activated at external acidic pH 5.5 and inactivated at neutral pH 7.4. Untransfected cells show no difference in the spectral density between the conditions and are based on pink noise.*

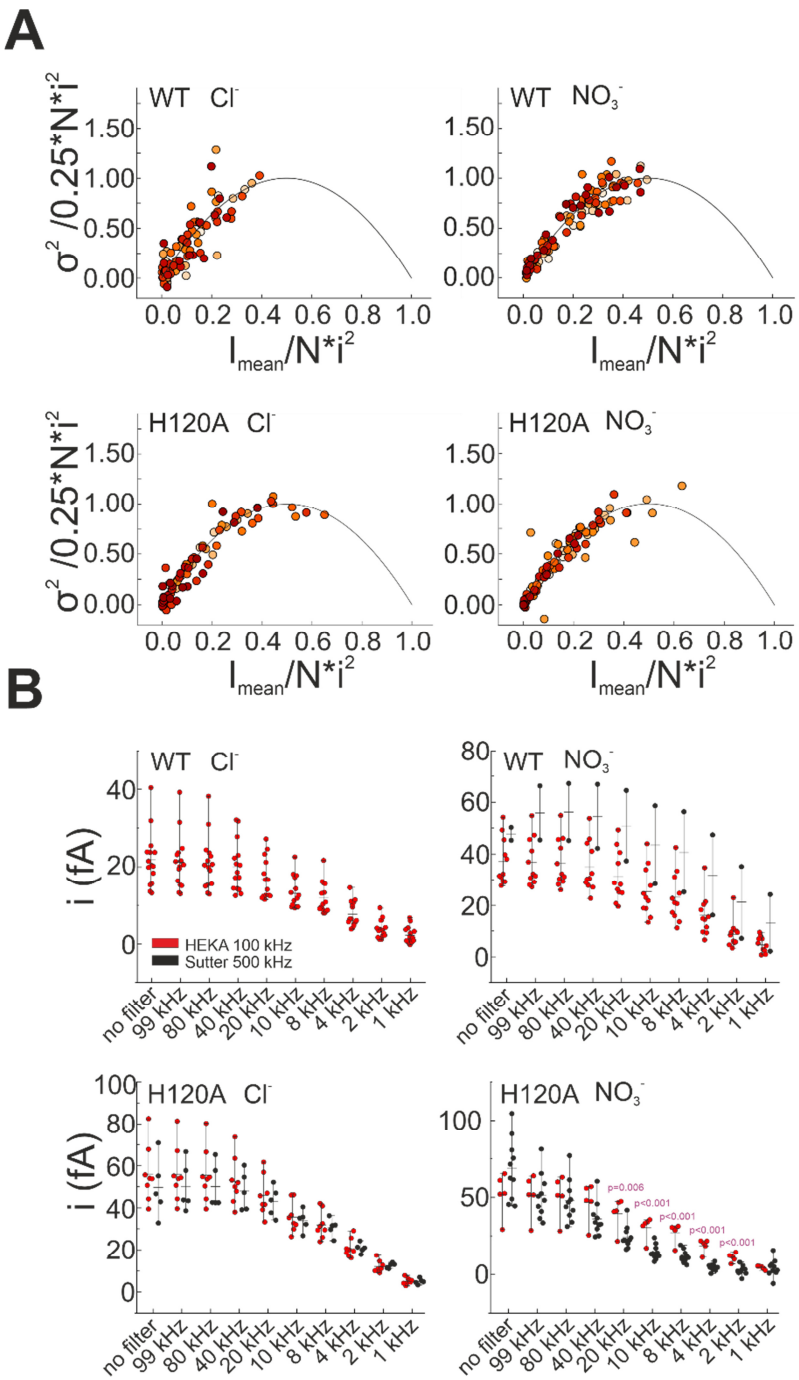

Suppl. Figure 8.3 Global analysis of stationary noise at -160 mV. ***A*** *Global fits with a parabolic function of all cells from stationary noise analysis for WT or H120A with internal* Cl^- *or* NO_3^-. ***B*** *Unitary current amplitudes of the conditions shown in (**A**). Experiments were done with HEKA amplifier with 100 kHz sampling frequency (red) and a SutterPatch amplifier (black) with 500 kHz sampling frequency. SutterPatch data were down sampled to 100 kHz before analysis. The data do not significantly differ from each other and can therefore be pooled.*

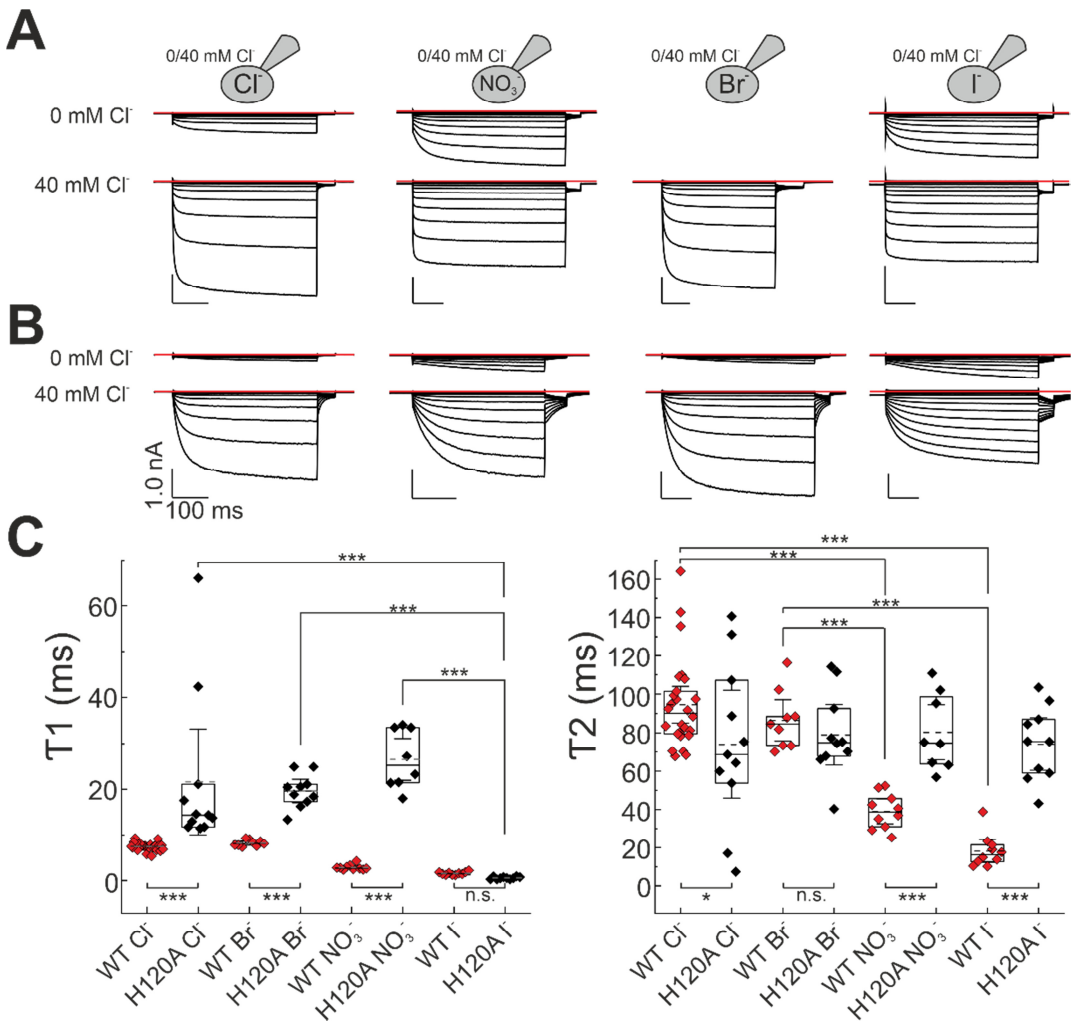

Suppl. Figure 8.4 Original anion currents with small internal anions. ***A,B*** *Cl^-, NO_3^-, Br^- or I^- serve as internal permeable anion. Cells expressing WT (**A**) or H120A (**B**) $VGLUT1_{PM}$ were perfused with gluconate based solution with or without 40 mM Cl^- at pH 5.5. Also in the absence of Cl^-, VGLUT exhibits an inward rectifying current.* ***C*** *Data shown in (**A** and **B**) with 40 mM external Cl^- were fitted with a double exponential function. The time constants differ significantly for WT and H120A.*

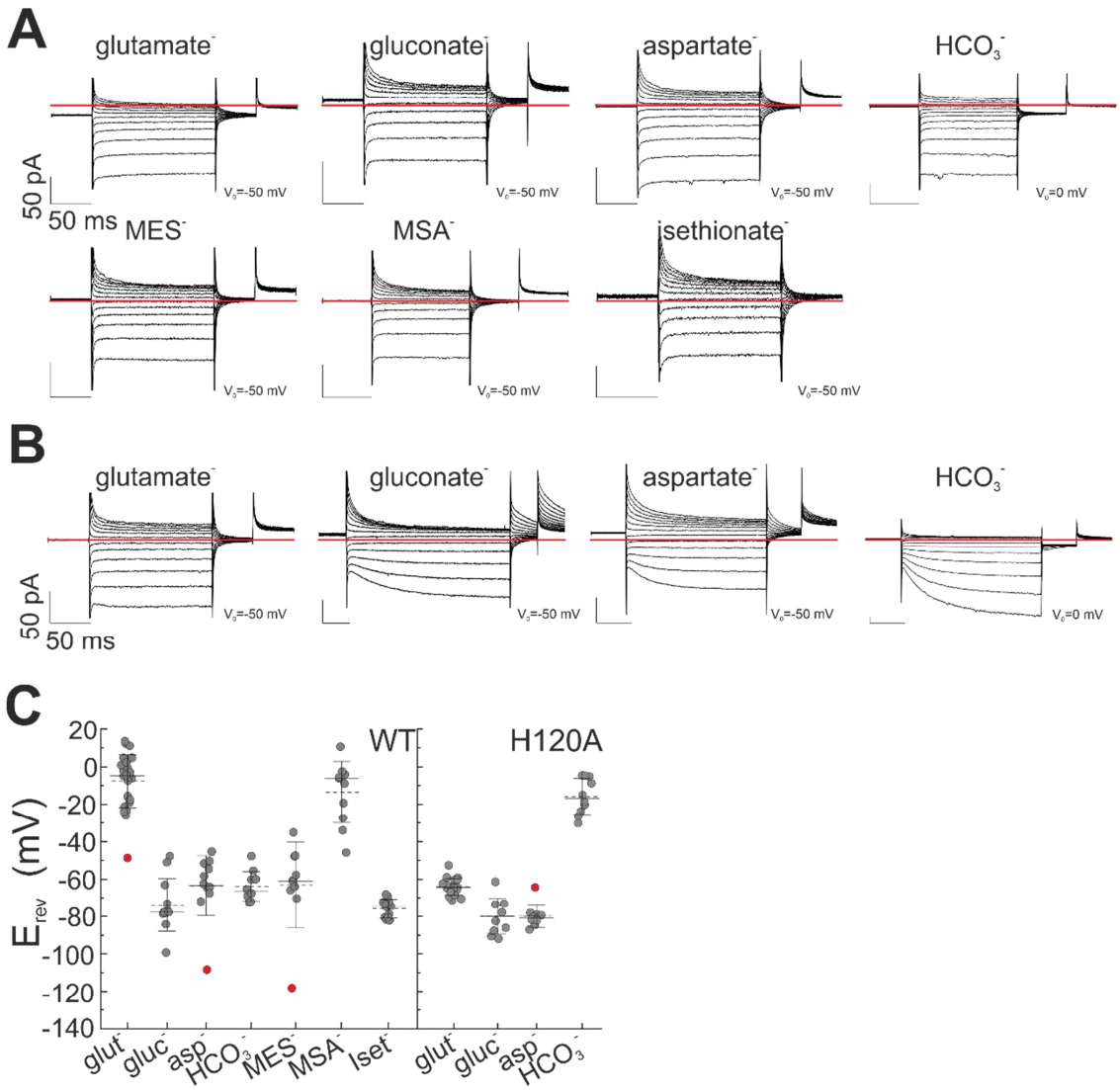

Suppl. Figure 8.5 Original anion currents with big internal anions. ***A*** *Cells transiently expressing WT (**A**) or H120A (**B**) VGLUT1$_{PM}$ were externally perfused with 40 mM Cl$^-$ at pH 5.5 and internally dialyzed with different big anions like glutamate$^-$, gluconate$^-$, aspartate$^-$, HCO$_3^-$, MES$^-$, MSA$^-$ or isethionate$^-$. The background currents at external pH 7.4 that inactivated VGLUT were not subtracted from the representative currents.* ***C*** *Reversal potentials of the conditions shown in (**A** and **B**) with subtracted background. Outliers were tested with Grubbs test (red) and were not included in the evaluation.*

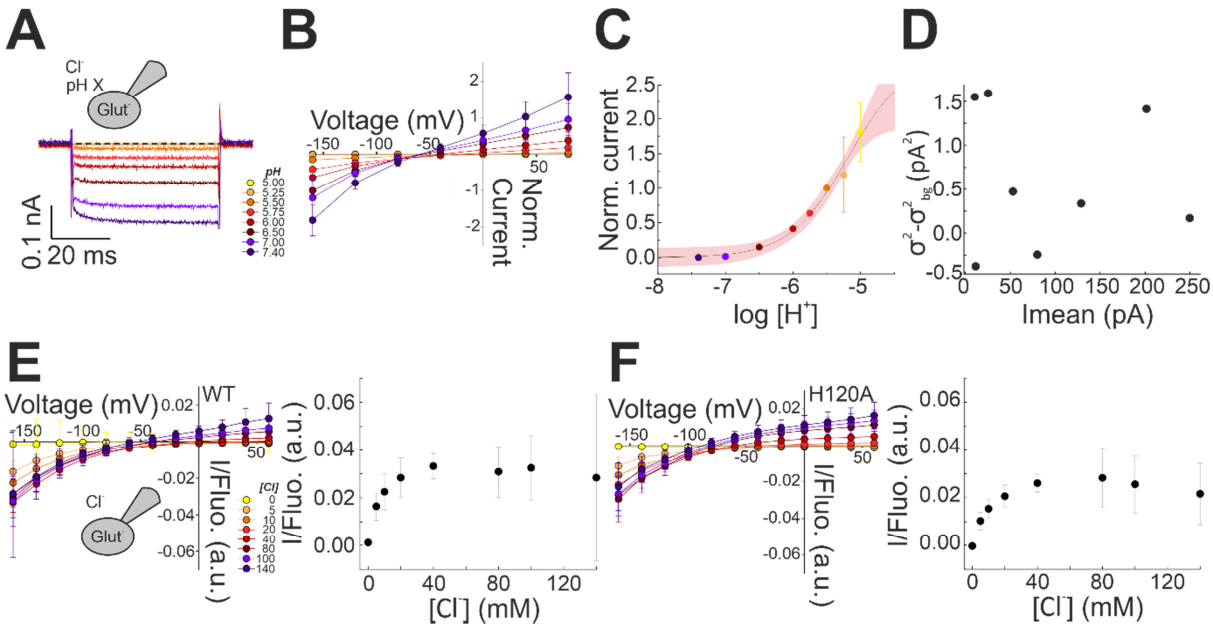

Suppl. Figure 8.6 PH dependence and Cl^- dependence of glutamate currents. *HEK293T cells transiently expressing WT VGLUT1$_{PM}$ were internally dialyzed with glutamate and externally perfused with a Cl^- based solution at different pH's. Cell were stimulated with voltage jumps between -160 and +80 mV.* ***A*** *Representative recordings at different pH's between 7.4 and 5.0 at -160 mV.* ***B*** *IV-relationships with varying external pH's.* ***C*** *Dose-response curve at -160 mV (EC_{50}=5.18 ± 0.12; n=10).* ***D*** *stationary noise analysis of currents shown in (**A**) reveals that the current variances cannot be distinguished from the background variance.* ***E, F*** *IV-relationship (left) and dose-response plots (right) of WT (**E**) or H120A (**F**) VGLUT1$_{PM}$ at rising $[Cl^-]_{ext.}$. Currents were maximally stimulated at 40 mM Cl^- while higher concentrations inhibit currents.*

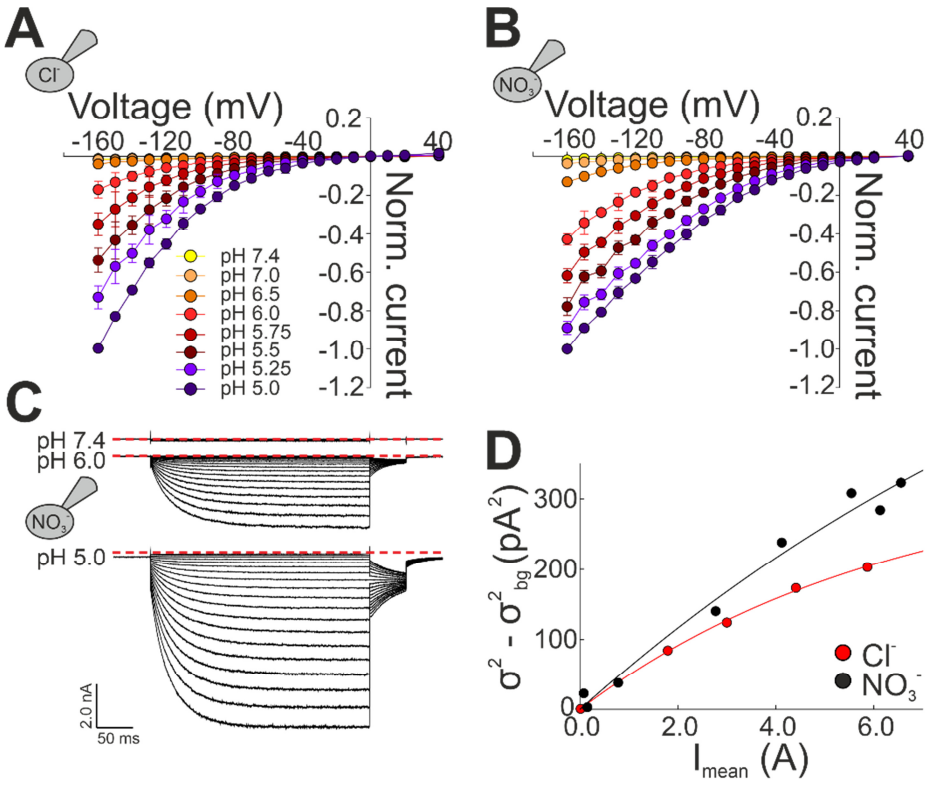

Suppl. Figure 8.7 Anion currents of H120A VGLUT1$_{PM}$. ***A, B*** *IV-relationships of steady state current amplitudes with internal Cl⁻ (**A**) or NO_3^- (**B**) at different external pH's.* ***C*** *Representative recordings with internal NO_3^-.* ***D*** *Representative fits of stationary noise analysis with internal Cl⁻ (red) or NO_3^- (black).*

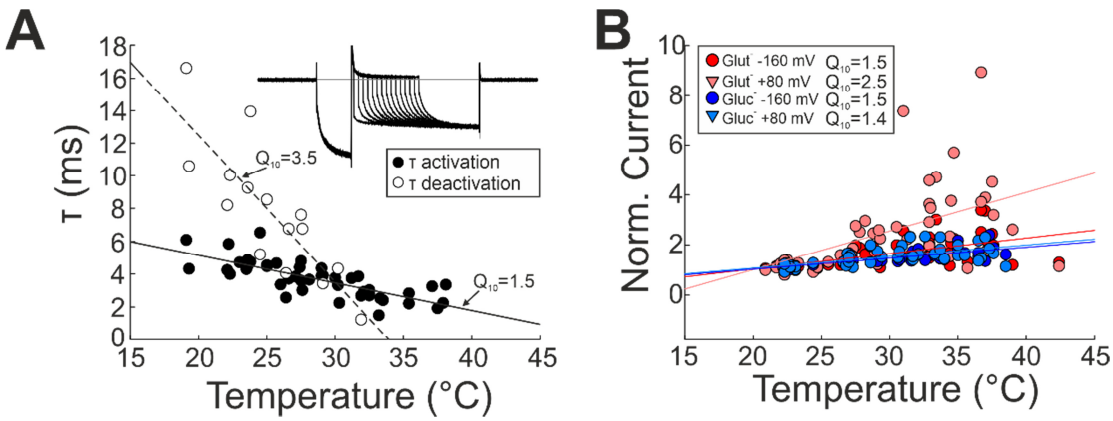

Suppl. Figure 8.8 Temperature dependence of WT VGLUT1$_{PM}$. ***A*** *Dependence of the time constants of the activating kinetics at -160 mV (filled) or deactivating kinetics (unfilled) at -120 mV with internal Cl⁻ on the temperature. The inset shows a representative recording of the deactivation protocol. Channels were first opened at -140 mV, then closed at +140 mV depolarizing voltages with variable length and then opened again at hyperpolarizing voltages at -120 mV.* ***B*** *Temperature dependence of current amplitudes with internal glutamate (red) or gluconate (blue) at -160 or +80 mV. Currents were normalized to whole cell fluorescence and to its amplitudes at 20 °C. All Q_{10} values were estimated between 20 and 30 °C.*

V Literature

1. Maycox, P. R., Hell, J. W. & Jahn, R. Amino acid neurotransmission: spotlight on synaptic vesicles. *Trends Neurosci.* 13, 83–87 (1990).

2. Collingridge, G. L. & Lester, R. A. Excitatory amino acid receptors in the vertebrate central nervous system. *Pharmacol. Rev.* 41, 143–210 (1989).

3. Fonnum, F. Glutamate: A Neurotransmitter in Mammalian Brain. *J. Neurochem.* 42, 1–11 (1984).

4. Headley, P. M. & Grillner, S. Excitatory amino acids and synaptic transmission: the evidence for a physiological function. *Trends Pharmacol. Sci.* 11, 205–211 (1990).

5. Lehmann, A., Isacsson, H. & Hamberger, A. Effects of In Vivo Administration of Kainic Acid on the Extracellular Amino Acid Pool in the Rabbit Hippocampus. *J. Neurochem.* 40, 1314–1320 (1983).

6. Choi, D. W. Ionic dependence of glutamate neurotoxicity. *J. Neurosci.* 7, 369–379 (1987).

7. Lehre, K. P. & Danbolt, N. C. The Number of Glutamate Transporter Subtype Molecules at Glutamatergic Synapses: Chemical and Stereological Quantification in Young Adult Rat Brain. *J. Neurosci.* 18, 8751–8757 (1998).

8. Rusakov, D. A. & Kullmann, D. M. Extrasynaptic Glutamate Diffusion in the Hippocampus: Ultrastructural Constraints, Uptake, and Receptor Activation. *J. Neurosci.* 18, 3158–3170 (1998).

9. Tong, G. & Jahr, C. E. Block of glutamate transporters potentiates postsynaptic excitation. *Neuron* 13, 1195–1203 (1994).

10. Martinez-Hernandez, A., Bell, K. P. & Norenberg, M. D. Glutamine synthetase: glial localization in brain. *Science* 195, 1356–1358 (1977).

11. Südhof, T. C. The synaptic vesicle cycle. *Annu. Rev. Neurosci.* 27, 509–547 (2004).

12. Ahnert-Hilger, G., Höltje, M., Pahner, I., Winter, S. & Brunk, I. Regulation of vesicular neurotransmitter transporters. *Rev. Physiol. Biochem. Pharmacol.* 140–160 (2003).

13. Takamori, S. *et al.* Molecular Anatomy of a Trafficking Organelle. *Cell* 127, 831–846 (2006).

14. Taoufiq, Z. *et al.* Hidden proteome of synaptic vesicles in the mammalian brain. *Proc. Natl. Acad. Sci.* 117, 33586–33596 (2020).

15. Goelz, S. E., Nestler, E. J., Chehrazi, B. & Greengard, P. Distribution of protein I in mammalian brain as determined by a detergent-based radioimmunoassay. *Proc. Natl. Acad. Sci.* 78, 2130–2134 (1981).

16. Walch-Solimena, C. *et al.* The t-SNAREs syntaxin 1 and SNAP-25 are present on organelles that participate in synaptic vesicle recycling. *J. Cell Biol.* 128, 637–645 (1995).

17. Burger, P. M. *et al.* Synaptic vesicles immunoisolated from rat cerebral cortex contain high levels of glutamate. *Neuron* 3, 715–720 (1989).

18. Takamori, S. Vesicular glutamate transporters as anion channels? *Pflüg. Arch. - Eur. J. Physiol.* 468, 513–518 (2016).

19. Martineau, M., Guzman, R. E., Fahlke, C. & Klingauf, J. VGLUT1 functions as a glutamate/proton exchanger with chloride channel activity in hippocampal glutamatergic synapses. *Nat. Commun.* 8, 2279 (2017).

20. Mestikawy, S. E., Wallén-Mackenzie, Å., Fortin, G. M., Descarries, L. & Trudeau, L.-E. From glutamate co-release to vesicular synergy: vesicular glutamate transporters. *Nat. Rev. Neurosci.* 12, 204–216 (2011).

21. Egashira, Y., Takase, M. & Takamori, S. Monitoring of Vacuolar-Type H+ ATPase-Mediated Proton Influx into Synaptic Vesicles. *J. Neurosci.* 35, 3701–3710 (2015).

22. Mitchell, S. J. & Ryan, T. A. Syntaxin-1A is excluded from recycling synaptic vesicles at nerve terminals. *J. Neurosci. Off. J. Soc. Neurosci.* 24, 4884–4888 (2004).

23. Chaudhry, F. A. *et al.* Glutamate transporters in glial plasma membranes: Highly differentiated localizations revealed by quantitative ultrastructural immunocytochemistry. *Neuron* 15, 711–720 (1995).

24. Omote, H., Miyaji, T., Juge, N. & Moriyama, Y. Vesicular Neurotransmitter Transporter: Bioenergetics and Regulation of Glutamate Transport. *Biochemistry* 50, 5558–5565 (2011).

25. Omote, H. & Moriyama, Y. Vesicular Neurotransmitter Transporters: An Approach for Studying Transporters With Purified Proteins. *Physiology* 28, 39–50 (2013).

26. He, L., Vasiliou, K. & Nebert, D. W. Analysis and update of the human solute carrier (SLC) gene superfamily. *Hum. Genomics* 3, 195–205 (2009).

27. Hediger, M. A. *et al.* The ABCs of solute carriers: physiological, pathological and therapeutic implications of human membrane transport proteins. *Pflüg. Arch.* 447, 465–468 (2004).

28. Reimer, R. J. SLC17: A functionally diverse family of organic anion transporters. *Mol. Aspects Med.* 34, 350–359 (2013).

29. Miesenböck, G., Angelis, D. A. D. & Rothman, J. E. Visualizing secretion and synaptic transmission with pH-sensitive green fluorescent proteins. *Nature* 394, 192–195 (1998).

30. Hell, J. W., Maycox, P. R. & Jahn, R. Energy dependence and functional reconstitution of the gamma-aminobutyric acid carrier from synaptic vesicles. *J. Biol. Chem.* 265, 2111–2117 (1990).

31. Johnson, R. G. Accumulation of biological amines into chromaffin granules: a model for hormone and neurotransmitter transport. *Physiol. Rev.* 68, 232–307 (1988).

32. Nguyen, M. L. & Parsons, S. M. Effects of internal pH on the acetylcholine transporter of synaptic vesicles. *J. Neurochem.* 64, 1137–1142 (1995).

33. Pietrancosta, N., Djibo, M., Daumas, S., El Mestikawy, S. & Erickson, J. D. Molecular, Structural, Functional, and Pharmacological Sites for Vesicular Glutamate Transporter Regulation. *Mol. Neurobiol.* 30, 1–25 (2020).

34. Omote, H., Miyaji, T., Hiasa, M., Juge, N. & Moriyama, Y. Structure, Function, and Drug Interactions of Neurotransmitter Transportersin the Postgenomic Era. *Annu. Rev. Pharmacol. Toxicol.* 56, 385–402 (2016).

35. Chaudhry, F. A., Boulland, J.-L., Jenstad, M., Bredahl, M. K. L. & Edwards, R. H. Pharmacology of neurotransmitter transport into secretory vesicles. *Handb. Exp. Pharmacol.* 184, 77–106 (2008).

36. Ni, B., Rosteck, P. R., Nadi, N. S. & Paul, S. M. Cloning and expression of a cDNA encoding a brain-specific Na(+)-dependent inorganic phosphate cotransporter. *Proc. Natl. Acad. Sci.* 91, 5607–5611 (1994).

37. Hisano, S. *et al.* Regional expression of a gene encoding a neuron-specific Na+-dependent inorganic phosphate cotransporter (DNPI) in the rat forebrain. *Mol. Brain Res.* 83, 34–43 (2000).

38. Bai, L., Xu, H., Collins, J. F. & Ghishan, F. K. Molecular and Functional Analysis of a Novel Neuronal Vesicular Glutamate Transporter. *J. Biol. Chem.* 276, 36764–36769 (2001).

39. Bellocchio, E. E., Reimer, R. J., Fremeau, R. T. & Edwards, R. H. Uptake of Glutamate into Synaptic Vesicles by an Inorganic Phosphate Transporter. *Science* 289, 957–960 (2000).

40. Takamori, S., Rhee, J. S., Rosenmund, C. & Jahn, R. Identification of a vesicular glutamate transporter that defines a glutamatergic phenotype in neurons. *Nature* 407, 189–194 (2000).

41. Fremeau, R. T. *et al.* The identification of vesicular glutamate transporter 3 suggests novel modes of signaling by glutamate. *Proc. Natl. Acad. Sci. U. S. A.* 99, 14488–14493 (2002).

42. Gras, C. *et al.* A third vesicular glutamate transporter expressed by cholinergic and serotoninergic neurons. *J. Neurosci. Off. J. Soc. Neurosci.* 22, 5442–5451 (2002).

43. Schäfer, M. K.-H., Varoqui, H., Defamie, N., Weihe, E. & Erickson, J. D. Molecular cloning and functional identification of mouse vesicular glutamate

transporter 3 and its expression in subsets of novel excitatory neurons. *J. Biol. Chem.* 277, 50734–50748 (2002).

44. Juge, N., Yoshida, Y., Yatsushiro, S., Omote, H. & Moriyama, Y. Vesicular Glutamate Transporter Contains Two Independent Transport Machineries. *J. Biol. Chem.* 281, 39499–39506 (2006).

45. Naito, S. & Ueda, T. Characterization of Glutamate Uptake into Synaptic Vesicles. *J. Neurochem.* 44, 99–109 (1985).

46. Hnasko, T. S. *et al.* Vesicular Glutamate Transport Promotes Dopamine Storage and Glutamate Corelease In Vivo. *Neuron* 65, 643–656 (2010).

47. Moriyama, Y. & Yamamoto, A. Vesicular L-glutamate transporter in microvesicles from bovine pineal glands. Driving force, mechanism of chloride anion activation, and substrate specificity. *J. Biol. Chem.* 270, 22314–22320 (1995).

48. Tabb, J. S., Kish, P. E., Dyke, R. V. & Ueda, T. Glutamate transport into synaptic vesicles. Roles of membrane potential, pH gradient, and intravesicular pH. *J. Biol. Chem.* 267, 15412–15418 (1992).

49. Eriksen, J. *et al.* Protons Regulate Vesicular Glutamate Transporters through an Allosteric Mechanism. *Neuron* 90, 768–780 (2016).

50. Preobraschenski, J. *et al.* Dual and Direction-Selective Mechanisms of Phosphate Transport by the Vesicular Glutamate Transporter. *Cell Rep.* 23, 535–545 (2018).

51. Hartinger, J. & Jahn, R. An anion binding site that regulates the glutamate transporter of synaptic vesicles. *J. Biol. Chem.* 268, 23122–23127 (1993).

52. Juge, N. *et al.* Metabolic Control of Vesicular Glutamate Transport and Release. *Neuron* 68, 99–112 (2010).

53. Preobraschenski, J., Zander, J.-F., Suzuki, T., Ahnert-Hilger, G. & Jahn, R. Vesicular Glutamate Transporters Use Flexible Anion and Cation Binding Sites for Efficient Accumulation of Neurotransmitter. *Neuron* 84, 1287–1301 (2014).

54. Schenck, S., Wojcik, S. M., Brose, N. & Takamori, S. A chloride conductance in VGLUT1 underlies maximal glutamate loading into synaptic vesicles. *Nat. Neurosci.* 12, 156–162 (2009).

55. Maycox, P. R., Deckwerth, T., Hell, J. W. & Jahn, R. Glutamate uptake by brain synaptic vesicles. Energy dependence of transport and functional reconstitution in proteoliposomes. *J. Biol. Chem.* 263, 15423–15428 (1988).

56. Wolosker, H., Souza, D. O. de & Meis, L. de. Regulation of Glutamate Transport into Synaptic Vesicles by Chloride and Proton Gradient. *J. Biol. Chem.* 271, 11726–11731 (1996).

57. Guzman, R. E., Grieschat, M., Fahlke, C. & Alekov, A. K. ClC-3 Is an Intracellular Chloride/Proton Exchanger with Large Voltage-Dependent Nonlinear Capacitance. *ACS Chem. Neurosci.* 4, 994–1003 (2013).

58. Graves, A. R., Curran, P. K., Smith, C. L. & Mindell, J. A. The Cl-/H+ antiporter ClC-7 is the primary chloride permeation pathway in lysosomes. *Nature* 453, 788–792 (2008).

59. Bellocchio, E. E. *et al.* The localization of the brain-specific inorganic phosphate transporter suggests a specific presynaptic role in glutamatergic transmission. *J. Neurosci. Off. J. Soc. Neurosci.* 18, 8648–8659 (1998).

60. Goh, G. Y. *et al.* Presynaptic regulation of quantal size: K+/H+ exchange stimulates vesicular glutamate transport. *Nat. Neurosci.* 14, 1285–1292 (2011).

61. Hayashi, M. *et al.* Secretory granule-mediated co-secretion of L-glutamate and glucagon triggers glutamatergic signal transmission in islets of Langerhans. *J. Biol. Chem.* 278, 1966–1974 (2003).

62. Morimoto, R. *et al.* Secretion of L-glutamate from osteoclasts through transcytosis. *EMBO J.* 25, 4175–4186 (2006).

63. Moriyama, Y. & Yamamoto, A. Glutamatergic Chemical Transmission: Look! Here, There, and Anywhere. *J. Biochem. (Tokyo)* 135, 155–163 (2004).

64. Herzog, E. *et al.* Localization of VGLUT3, the vesicular glutamate transporter type 3, in the rat brain. *Neuroscience* 123, 983–1002 (2004).

65. Moechars, D. *et al.* Vesicular Glutamate Transporter VGLUT2 Expression Levels Control Quantal Size and Neuropathic Pain. *J. Neurosci.* 26, 12055–12066 (2006).

66. Ruel, J. *et al.* Impairment of SLC17A8 Encoding Vesicular Glutamate Transporter-3, VGLUT3, Underlies Nonsyndromic Deafness DFNA25 and Inner Hair Cell Dysfunction in Null Mice. *Am. J. Hum. Genet.* 83, 278–292 (2008).

67. Peng, Z. *et al.* Temporospatial expression and cellular localization of VGLUT3 in the rat cochlea. *Brain Res.* 1537, 100–110 (2013).

68. Verma, P., Augustine, G. J., Ammar, M.-R., Tashiro, A. & Cohen, S. M. A neuroprotective role for microRNA miR-1000 mediated by limiting glutamate excitotoxicity. *Nat. Neurosci.* 18, 379–385 (2015).

69. Fremeau, R. T. *et al.* Vesicular glutamate transporters 1 and 2 target to functionally distinct synaptic release sites. *Science* 304, 1815–1819 (2004).

70. Leano, J. B. *et al.* Structures suggest a mechanism for energy coupling by a family of organic anion transporters. *PLOS Biol.* 17, e3000260 (2019).

71. Li, F. *et al.* Ion transport and regulation in a synaptic vesicle glutamate transporter. *Science* 368, 893–897 (2020).

72. Foss, S. M., Li, H., Santos, M. S., Edwards, R. H. & Voglmaier, S. M. Multiple Dileucine-like Motifs Direct VGLUT1 Trafficking. *J. Neurosci.* 33, 10647–10660 (2013).

73. Huang, Y., Lemieux, M. J., Song, J., Auer, M. & Wang, D.-N. Structure and mechanism of the glycerol-3-phosphate transporter from Escherichia coli. *Science* 301, 616–620 (2003).

74. Abramson, J. *et al.* The lactose permease of Escherichia coli: overall structure, the sugar-binding site and the alternating access model for transport. *FEBS Lett.* 555, 96–101 (2003).

75. Chang, R., Eriksen, J. & Edwards, R. H. The dual role of chloride in synaptic vesicle glutamate transport. *eLife* 7, e34896 (2018).

76. Almqvist, J., Huang, Y., Laaksonen, A., Wang, D.-N. & Hovmöller, S. Docking and homology modeling explain inhibition of the human vesicular glutamate transporters. *Protein Sci. Publ. Protein Soc.* 16, 1819–1829 (2007).

77. Akil, O. *et al.* Restoration of hearing in the VGLUT3 knockout mouse using virally mediated gene therapy. *Neuron* 75, 283–293 (2012).

78. Zinnanti, W. J. *et al.* Dual mechanism of brain injury and novel treatment strategy in maple syrup urine disease. *Brain* 132, 903–918 (2009).

79. Chesler, M. Regulation and modulation of pH in the brain. *Physiol. Rev.* 83, 1183–1221 (2003).

80. McDonald, J. W. *et al.* Extracellular Acidity Potentiates AMPA Receptor-Mediated Cortical Neuronal Death. *J. Neurosci.* 18, 6290–6299 (1998).

81. Timofeev, I., Nortje, J., Al-Rawi, P. G., Hutchinson, P. J. & Gupta, A. K. Extracellular brain pH with or without hypoxia is a marker of profound metabolic derangement and increased mortality after traumatic brain injury. *J. Cereb. Blood Flow Metab.* 33, 422–427 (2013).

82. Tordera, R. M. *et al.* Enhanced anxiety, depressive-like behaviour and impaired recognition memory in mice with reduced expression of the vesicular glutamate transporter 1 (VGLUT1). *Eur. J. Neurosci.* 25, 281–290 (2007).

83. Kashani, A. *et al.* Loss of VGLUT1 and VGLUT2 in the prefrontal cortex is correlated with cognitive decline in Alzheimer disease. *Neurobiol. Aging* 29, 1619–1630 (2008).

84. Oni-Orisan, A., Kristiansen, L. V., Haroutunian, V., Meador-Woodruff, J. H. & McCullumsmith, R. E. Altered vesicular glutamate transporter expression in the anterior cingulate cortex in schizophrenia. *Biol. Psychiatry* 63, 766–775 (2008).

85. Wootz, H., Enjin, A., Wallén-Mackenzie, A., Lindholm, D. & Kullander, K. Reduced VGLUT2 expression increases motor neuron viability in Sod1(G93A) mice. *Neurobiol. Dis.* 37, 58–66 (2010).

86. Hunsberger, H. C., Rudy, C. C., Batten, S. R., Gerhardt, G. A. & Reed, M. N. P301L tau expression affects glutamate release and clearance in the hippocampal trisynaptic pathway. *J. Neurochem.* 132, 169–182 (2015).

87. Lipton, S. A. Failures and Successes of NMDA Receptor Antagonists: Molecular Basis for the Use of Open-Channel Blockers like Memantine in the Treatment of Acute and Chronic Neurologic Insults. *NeuroRx* 1, 101–110 (2004).

88. Serafini, G. *et al.* Pharmacological properties of glutamatergic drugs targeting NMDA receptors and their application in major depression. *Curr. Pharm. Des.* 19, 1898–1922 (2013).

89. Swainson, J. *et al.* Esketamine for treatment resistant depression. *Expert Rev. Neurother.* 19, 899–911 (2019).

90. Robinson, D. M. & Keating, G. M. Memantine: A Review of its Use in Alzheimer's Disease. *Drugs* 66, 1515–1534 (2006).

91. Hannack, C. Identifizierung der Targeting-Signale in vesikulären Glutamat-Transportern. (Heinrich Heine Universität Düsseldorf, 2015).

92. Craig, N. L. The Mechanism of Conservative Site-Specific Recombination. *Annu. Rev. Genet.* 22, 77–105 (1988).

93. Sauer, B. Site-specific recombination: developments and applications. *Curr. Opin. Biotechnol.* 5, 521–527 (1994).

94. Chen, C. & Okayama, H. High-efficiency transformation of mammalian cells by plasmid DNA. *Mol. Cell. Biol.* 7, 2745–2752 (1987).

95. Ronstedt, K. *et al.* Impaired surface membrane insertion of homo- and heterodimeric human muscle chloride channels carrying amino-terminal myotonia-causing mutations. *Sci. Rep.* 5, 15382 (2015).

96. Linsdell, P. *et al.* Permeability of Wild-Type and Mutant Cystic Fibrosis Transmembrane Conductance Regulator Chloride Channels to Polyatomic Anions. *J. Gen. Physiol.* 110, 355–364 (1997).

97. Linsdell, P. & Hanrahan, J. W. Adenosine Triphosphate–dependent Asymmetry of Anion Permeation in the Cystic Fibrosis Transmembrane Conductance Regulator Chloride Channel. *J. Gen. Physiol.* 111, 601–614 (1998).

98. Silberberg, S. D. & Magleby, K. L. Preventing Errors When Estimating Single Channel Properties from the Analysis of Current Fluctuations. *Biophys. J.* 65, 1570–1584 (1993).

99. Gray, P. T. Analysis of whole cell currents to estimate the kinetics and amplitude of underlying unitary events: relaxation and 'noise' analysis. in *Microlelctrode techniques* 189–207 (The Company of Biologists Limited, 1999).

100. Alekov, A. K. & Fahlke, C. Channel-like slippage modes in the human anion/proton exchanger ClC-4. *J. Gen. Physiol.* 133, 485–496 (2009).

101. Oxford, G. S. Some kinetic and steady-state properties of sodium channels after removal of inactivation. *J. Gen. Physiol.* 77, 1–22 (1981).

102. Rodríguez, B. M. & Bezanilla, F. Transitions near the open state in Shaker K(+)-channel: probing with temperature. *Neuropharmacology* 35, 775–785 (1996).

103. White, M. M. & Bezanilla, F. Activation of squid axon K+ channels. Ionic and gating current studies. *J. Gen. Physiol.* 85, 539–554 (1985).

104. Schrödinger, L. *The PyMOL Molecular Graphics System*. (2021).

105. Kolb, H.-A. & Frehland, E. Noise-current generated by carrier-mediated ion transport at non-equilibrium. *Biophys. Chem.* 12, 21–34 (1980).

106. Kolb, H. A. & Läuger, P. Spectral analysis of current noise generated by carrier-mediated ion transport. *J. Membr. Biol.* (2005).

107. Neumcke, B. 1/f noise in membranes. *Biophys. Struct. Mech.* 4, 179–199 (1978).

108. DeFelice, L. J. *Introduction to membrane noise*. (Plenum Press, 1981).

109. Kolen, B., Kortzak, D., Franzen, A. & Fahlke, C. An amino-terminal point mutation increases EAAT2 anion currents without affecting glutamate transport rates. *J. Biol. Chem.* 295, 14936–14947 (2020).

110. Murata, T. *et al.* Ion binding and selectivity of the rotor ring of the Na+-transporting V-ATPase. *Proc. Natl. Acad. Sci.* 105, 8607–8612 (2008).

111. Brahm, J. Temperature-dependent changes of chloride transport kinetics in human red cells. *J. Gen. Physiol.* 70, 283–306 (1977).

112. Otis, T. S. & Kavanaugh, M. P. Isolation of Current Components and Partial Reaction Cycles in the Glial Glutamate Transporter EAAT2. *J. Neurosci.* 20, 2749–2757 (2000).

113. Fahlke, C., Kortzak, D. & Machtens, J.-P. Molecular physiology of EAAT anion channels. *Pflüg. Arch. - Eur. J. Physiol.* 468, 491–502 (2016).

114. Farsi, Z., Jahn, R. & Woehler, A. Proton electrochemical gradient: Driving and regulating neurotransmitter uptake. *BioEssays News Rev. Mol. Cell. Dev. Biol.* 39, (2017).

115. Wadiche, J. I. & Kavanaugh, M. P. Macroscopic and Microscopic Properties of a Cloned Glutamate Transporter/Chloride Channel. *J. Neurosci.* 18, 7650–7661 (1998).

116. Leiderman, P., Huppert, D. & Agmon, N. Transition in the Temperature-Dependence of GFP Fluorescence: From Proton Wires to Proton Exit. *Biophys. J.* 90, 1009–1018 (2006).

117. Bock, C., Zollmann, T., Lindt, K.-A., Tampé, R. & Abele, R. Peptide translocation by the lysosomal ABC transporter TAPL is regulated by coupling efficiency and activation energy. *Sci. Rep.* 9, 11884 (2019).

118. Lacko, L., Wittke, B. & Geck, P. The temperature dependence of the exchange transport of glucose in human erythrocytes. *J. Cell. Physiol.* 82, 213–218 (1973).

119. Schäfer, G., Heber, U. & Heldt, H. W. Glucose Transport into Spinach Chloroplasts. *Plant Physiol.* 60, 286–289 (1977).

120. DeCoursey, T. E. & Cherny, V. V. Temperature Dependence of Voltage-gated H+ Currents in Human Neutrophils, Rat Alveolar Epithelial Cells, and Mammalian Phagocytes. *J. Gen. Physiol.* 112, 503–522 (1998).

121. Rodríguez, B. M., Sigg, D. & Bezanilla, F. Voltage gating of Shaker K+ channels. The effect of temperature on ionic and gating currents. *J. Gen. Physiol.* 112, 223–242 (1998).

122. Hille, B. *Ionic Channels of Excitable Membranes*. vol. 3 (Sinauer Associates Inc., 1992).

123. Hodgkin, A. L., Huxley, A. F. & Katz, B. Measurement of current-voltage relations in the membrane of the giant axon of *Loligo*. *J. Physiol.* 116, 424–448 (1952).

124. Bernier, L.-P., Ase, A. & Seguela, P. Post-translational regulation of P2X receptor channels: modulation by phospholipids. *Front. Cell. Neurosci.* 7, 226 (2013).

125. Jensen, M. Ø. & Mouritsen, O. G. Lipids do influence protein function—the hydrophobic matching hypothesis revisited. *Biochim. Biophys. Acta BBA - Biomembr.* 1666, 205–226 (2004).

126. Lee, A. G. How lipids affect the activities of integral membrane proteins. *Biochim. Biophys. Acta* 1666, 62–87 (2004).

127. Rohrbough, J. & Broadie, K. Lipid regulation of the synaptic vesicle cycle. *Nat. Rev. Neurosci.* 6, 139–150 (2005).

128. Winter, N., Kovermann, P. & Fahlke, C. A point mutation associated with episodic ataxia 6 increases glutamate transporter anion currents. *Brain* 135, 3416–3425 (2012).

129. Schneider, N. *et al.* Functional Properties of the Retinal Glutamate Transporters GLT-1c and EAAT5. *J. Biol. Chem.* 289, 1815–1824 (2014).

130. Shigeri, Y., Seal, R. P. & Shimamoto, K. Molecular pharmacology of glutamate transporters, EAATs and VGLUTs. *Brain Res. Rev.* 45, 250–265 (2004).

131. Bröer, S. *et al.* Chloride conductance and Pi transport are separate functions induced by the expression of NaPi-1 in Xenopus oocytes. *J. Membr. Biol.* 164, 71–77 (1998).

132. Busch, A. E. *et al.* Expression of a renal type I sodium/phosphate transporter (NaPi-1) induces a conductance in Xenopus oocytes permeable for organic and inorganic anions. *Proc. Natl. Acad. Sci.* 93, 5347–5351 (1996).

133. Tan, H., Bungert-Plümke, S., Fahlke, C. & Stölting, G. Reduced Membrane Insertion of CLC-K by V33L Barttin Results in Loss of Hearing, but Leaves Kidney Function Intact. *Front. Physiol.* 8, (2017).

134. Jun, I. *et al.* Pore dilatation increases the bicarbonate permeability of CFTR, ANO1 and glycine receptor anion channels. *J. Physiol.* 594, 2929–2955 (2016).

135. Park, H. W. *et al.* Dynamic regulation of CFTR bicarbonate permeability by [Cl-]i and its role in pancreatic bicarbonate secretion. *Gastroenterology* 139, 620–631 (2010).

136. Dubyak, G. R. Ion homeostasis, channels, and transporters: an update on cellular mechanisms. *Adv. Physiol. Educ.* 28, 143–154 (2004).

137. Fatima-Shad, K., Barry, P. H. & Gage, P. W. Anion permeation in GABA- and glycine-gated channels of mammalian cultured hippocampal neurons. *Proc. R. Soc. Lond. B Biol. Sci.* 253, 69–75 (1993).

138. Shioi, J., Naito, S. & Ueda, T. Glutamate uptake into synaptic vesicles of bovine cerebral cortex and electrochemical potential difference of proton across the membrane. *Biochem. J.* 258, 499–504 (1989).

139. Miyaji, T. *et al.* Identification of a vesicular aspartate transporter. *Proc. Natl. Acad. Sci.* 105, 11720–11724 (2008).

140. Johnson, R. G. & Scarpa, A. Protonmotive force and catecholamine transport in isolated chromaffin granules. *J. Biol. Chem.* 254, 3750–3760 (1979).

141. Russell, J. T. Delta pH, H+ diffusion potentials, and Mg2+ ATPase in neurosecretory vesicles isolated from bovine neurohypophyses. *J. Biol. Chem.* 259, 9496–9507 (1984).

142. Bormann, J., Hamill, O. P. & Sakmann, B. Mechanism of anion permeation through channels gated by glycine and gamma-aminobutyric acid in mouse cultured spinal neurones. *J. Physiol.* 385, 243–286 (1987).

143. Franciolini, F. & Nonner, W. Anion and cation permeability of a chloride channel in rat hippocampal neurons. *J. Gen. Physiol.* 90, 453–478 (1987).

144. Arreola, J., Melvin, J. E. & Begenisich, T. Volume-activated chloride channels in rat parotid acinar cells. *J. Physiol.* 484, 677–687 (1995).

145. Yang, J. *et al.* Glutamate-Releasing SWELL1 Channel in Astrocytes Modulates Synaptic Transmission and Promotes Brain Damage in Stroke. *Neuron* 102, 813-827.e6 (2019).

146. Nilius, B., Eggermont, J. & Droogmans, G. The Endothelial Volume-Regulated Anion Channel, VRAC. *Cell. Physiol. Biochem.* 10, 313–320 (2000).

147. Sabirov, R. Z., Prenen, J., Tomita, T., Droogmans, G. & Nilius, B. Reduction of ionic strength activates single volume-regulated anion channels (VRAC) in endothelial cells. *Pflüg. Arch. - Eur. J. Physiol.* 439, 315–320 (2000).

148. Alka, K. & Casey, J. R. Bicarbonate transport in health and disease. *IUBMB Life* 66, 596–615 (2014).

149. Poulsen, J. H., Fischer, H., Illek, B. & Machen, T. E. Bicarbonate conductance and pH regulatory capability of cystic fibrosis transmembrane conductance regulator. *Proc. Natl. Acad. Sci. U. S. A.* 91, 5340–5344 (1994).

150. Shin, D. H. *et al.* Bicarbonate permeation through anion channels: its role in health and disease. *Pflugers Arch.* 472, 1003–1018 (2020).

151. Mo, L. *et al.* Comparison of Amphibian and Human ClC-5: Similarity of Functional Properties and Inhibition by External pH. *J. Membr. Biol.* 168, 253–264 (1999).

152. Catalán, M., Niemeyer, M. I., Cid, L. P. & Sepúlveda, F. V. Basolateral ClC-2 chloride channels in surface colon epithelium: regulation by a direct effect of intracellular chloride. *Gastroenterology* 126, 1104–1114 (2004).

153. Burette, A. C. *et al.* The sodium-driven chloride/bicarbonate exchanger in presynaptic terminals. *J. Comp. Neurol.* 520, 1481–1492 (2012).

154. Makani, S. & Chesler, M. Endogenous Alkaline Transients Boost Postsynaptic NMDA Receptor Responses in Hippocampal CA1 Pyramidal Neurons. *J. Neurosci.* 27, 7438–7446 (2007).

155. Pinto, L. H. & Lamb, R. A. Influenza virus proton channels. *Photochem. Photobiol. Sci.* 5, 629–632 (2006).

156. Daniels, R. W. *et al.* A Single Vesicular Glutamate Transporter Is Sufficient to Fill a Synaptic Vesicle. *Neuron* 49, 11–16 (2006).

157. Daniels, R. W. *et al.* Increased Expression of the Drosophila Vesicular Glutamate Transporter Leads to Excess Glutamate Release and a Compensatory Decrease in Quantal Content. *J. Neurosci.* 24, 10466–10474 (2004).

158. Keynes, R. D. & Rojas, E. Kinetics and steady-state properties of the charged system controlling sodium conductance in the squid giant axon. *J. Physiol.* 239, 393–434 (1974).

159. Lee, S. C. & Deutsch, C. Temperature dependence of K(+)-channel properties in human T lymphocytes. *Biophys. J.* 57, 49–62 (1990).

160. Law, C. J., Yang, Q., Soudant, C., Maloney, P. C. & Wang, D.-N. Kinetic evidence is consistent with the rocker-switch mechanism of membrane transport by GlpT. *Biochemistry* 46, 12190–12197 (2007).

161. Zhang, W. & Kaback, H. R. Effect of the Lipid Phase Transition on the Lactose Permease from Escherichia coli. *Biochemistry* 39, 14538–14542 (2000).

VI Danksagung

An dieser Stelle möchte ich mich bei allen nachstehenden Personen von Herzen bedanken, die mich während meiner Promotionszeit begleitet und unterstützt haben.

Ein besonderer Dank gilt meinem Doktorvater Prof. Dr. Christoph Fahlke, für die Chance in seinem Institut in einem so interessanten Themengebiet zu promovieren und dadurch meine Hingabe für das Patchen ausleben zu dürfen. Vor allem danke ich ihm für die intensive Betreuung, die konstruktive Kritik, die vielen Diskussionen und die Fähigkeit mich an schlechten experimentellen Tagen zu motivieren.

Prof. Dr. Christine R. Rose danke ich herzlich für die Übernahme des Zweitgutachtens und für die experimentellen Anregungen nach meinem ersten Jahr, die ich im weiteren Verlauf dieser Arbeit umsetzen konnte.

Des Weiteren möchte ich mich bei Dr. Daniel Kortzak für die Betreuung meiner Arbeit und der Hilfe beim Programmieren bedanken.

Ich bedanke mich bei allen aktuellen und ehemaligen Mitarbeitern des IBI-1, insbesondere bei Prof. Dr. Arnd Baumann, Prof. Dr. Frank Müller, Arne Franzen, Maike Berndt, Petra Thelen, Juan Sierra Marquez, Dr. Peter Kovermann, Daniel Portz, Dr. Gabriel Stölting, Dr. Stefanie Bungert und Dr. Claudia Alleva für Hilfestellungen und Anregungen jeglicher Art.

Mein außerordentlicher Dank gilt meinen lieben Kollegen Jana, Rachel und Lisa. Ihr hattet immer ein offenes Ohr für mich, habt mir mit Rat und Tat zur Seite gestanden und habt mir gezeigt, dass aus Kollegen wahre Freunde werden können. Danke Lisa, dass du kurz vor Ende meine Arbeit nochmal korrigiert hast.

Ein besonderer Dank gilt meinen Eltern für die uneingeschränkte Liebe und Unterstützung, die mich schon mein ganzes Leben begleitet und stärkt.

Zuletzt möchte ich mich bei meinem Mann Marcel bedanken. Während der Schulzeit, des Studiums und vor allem auch während der Promotion warst du immer mein Fels in der Brandung, hast mich unterstützt, aufgemuntert und bedingungslos geliebt. Ohne dich wäre ich heute sicherlich nicht da, wo ich jetzt bin.

VII Eidesstattliche Erklärung/Declaration

Ich versichere an Eides Statt, dass die Dissertation von mir selbstständig und ohne unzulässige fremde Hilfe unter Beachtung der „Grundsätze zur Sicherung guter wissenschaftlicher Praxis an der Heinrich-Heine-Universität Düsseldorf“ erstellt worden ist.

Ort, Datum

Bettina Kolen